

Packet Loss in Terrestrial Wireless and Hybrid Networks

Barsocchi Paolo

February 26, 2007

Dedications

I would like to thank my advisor Ing. Francesco Potorti for his guidance and unlimited support at the professional and personal level during the years that we have been working together. My research would have never reached this level without his contribution.

I would also like to thank the people that cooperated with me to address some of the research topics: Nedo Celandroni, Erina Ferro and Gabriele Oligeri. I am grateful to all people of Laboratory of Wireless Networks, where I worked these years.

Finally, I would like to thank my family for their permanent support. Especially, I would to express my love to Valentina who has always been there to help me when the work did not progress as expected.

Contents

1	Introduction	1
	References	4
2	Hybrid network	5
2.1	Performance evaluation	5
2.1.1	Testbed configuration	6
2.1.2	The Measurements	7
2.1.3	Conclusions	19
2.2	Forward Erasure Correction and Real Video Streaming	19
2.2.1	The Real Case Study	20
2.2.2	Experimental Results	21
	References	28
3	The multipath fading channel	30
3.1	The environment	30
3.2	Fading types	33
3.3	Large-scale fading	33
3.4	Small-scale fading	37
3.5	Conclusion	42
3.6	Parameters of the mobile multipath channel	44
3.6.1	Time dispersion	44
3.6.2	Coherence bandwidth	46
3.6.3	Doppler spread and coherence time	47
	References	48
4	Propagation models	50
4.1	Outdoor path-loss models	50
4.1.1	Most popular statistical outdoor path-loss models	51

VIII Contents

4.1.2	Most popular outdoor path-loss deterministic models	55
4.1.3	State of Art of the path loss models	56
4.2	Indoor Propagation Models	57
4.2.1	Log-distance Path Loss Model	58
4.2.2	Attenuation Factor Model	58
4.2.3	Deterministic models	58
	References	60
5	Frame error models	64
5.1	Bernoullian	65
5.2	Two state Markov model	65
5.3	Two-state Markov-modulated Bernoullian process	66
5.4	State of Art on the utilization of frame loss models	69
	References	72
6	Measurement campaign	74
6.1	The measurement methodology	75
6.1.1	Timing considerations	75
6.1.2	Software	76
	References	78
7	Outdoor	79
7.1	Measurement setup	80
7.2	Two-ray propagation model	81
7.2.1	Slow fading	85
7.3	Loss probability versus power level	85
7.3.1	Frame error process	85
7.4	Modelling frame errors as a Bernoulli process	87
7.4.1	AWGN model	89
7.4.2	Practical usage	90
7.5	Recommendations for simulation practitioners	92
	References	93
8	Indoor	95
8.1	Frame level statistics	96
8.2	Bit level statistics	100
	References	103

Contents IX

9	Packet loss model for TCP hybrid wireless networks	104
9.1	Link Characteristics	105
9.1.1	Satellite link	105
9.1.2	Wi-Fi link	106
9.2	Measurements environment	106
9.3	Commonly used packet error models	107
9.4	TCP on synthetic versus measured packet loss	108
9.5	Conclusion	112
	References	114

List of Figures

2.1	Testbed environment.	6
2.2	Typical trend of packet delay for the satellite channel in 45 minutes of transmission.	10
2.3	CDF of packet delay for data in 2.2.	11
2.4	Details of firsts 40 seconds of 2.2.	11
2.5	Details of a delay peak of 2.2.	12
2.6	Typical trend of packet delay for the WLAN channel with Retry 0 in 45 minutes of transmission.	12
2.7	Lost packets for WLAN transmission with Retry 0 of 2.6.	13
2.8	Details of firsts 20 seconds of 2.7.	13
2.9	Typical trend of packet delay for the WLAN channel with Retry 7 in 45 minutes of transmission.	14
2.10	Lost packets for WLAN transmission with Retry 7 of 2.9.	14
2.11	CDF of packet delay for WLAN transmissions.	15
2.12	PMF of the size of packet error bursts for WLAN transmissions.	15
2.13	CDF of packet delay for the WLAN channel with Retry 7, and for the first MAC try only.	16
2.14	Packet delay for the full path in 45 minutes of real video streaming.	17
2.15	CDF of packet delay for data in Fig. 2.14.	17
2.16	Packet jitter for the full path video stream.	18
2.17	Lost packets for the full path video stream.	18
2.18	The test-bed network topology.	21
2.19	Plant of the building.	22
2.20	Redundancy and error correction performance vs. coding ratio for client A.	23
2.21	Redundancy and error correction performance vs. coding ratio for the client B.	24
2.22	MOS of received video by client A.	26
2.23	Samples of the streamed video trailer at different coding and bit rates.	27

3.1	A typical scenario of mobile radio communications.	31
3.2	Angle of arrival of the n^{th} incident wave.	32
3.3	Channel fading types.	34
3.4	Small-scale fading (grey line) and large-scale fading (black line).	35
3.5	Path loss vs. distance measured in several German cities [7].	37
3.6	Flat-fading case: B_s is the signal bandwidth, and B_c is the coherence bandwidth.	39
3.7	Flat-fading channel characteristics.	39
3.8	Frequency selective fading case: B_s is the signal bandwidth, and B_c is the coherence bandwidth.	40
3.9	Frequency selective fading channel characteristics.	41
3.10	Type of small fading.	42
3.11	Type of small-scale fading types of experienced by a signal from the viewpoint of (a) symbol period, (b) baseband signal bandwidth.	43
3.12	Types of small-scale fading for the IEEE802.11 signal.	44
3.13	Maximum excess delay.	46
4.1	2-ray ground reflection model.	54
5.1	Channel model based on a two-state Markov chain.	66
5.2	Error gap distribution for the Gilbert model.	67
5.3	Error bursts distribution for the Gilbert model.	68
6.1	Error of packet intervals at the receiver.	76
6.2	Transmitted frame.	77
7.1	Comparison between 2-ray propagation models at Wi-Fi and GSM frequencies for $h_t = h_r = 1$ m.	82
7.2	Measured signal level, double regression model and two-ray model with sensitivity thresholds for $\Delta L = 0$. Error bars indicate 0.05, 0.50 and 0.95 quantiles of observed values.	83
7.3	Horizontal radiation pattern for two PCMCIA cards (vertical polarisation).	84
7.4	Frame errors and signal levels for each transmission rate.	86
7.5	Probability mass function of burst lengths.	87
7.6	Probability mass function of gaps lengths.	88
7.7	Chi-square test results.	89
7.8	Fit of Equation 7.10 with measured values.	90
8.1	Plant of the building where the measurements have been taken; T and R are the transmitter and receiver laptops used for the measurements.	96
8.2	Average of received, lost and corrupted frames during the first week.	97

List of Figures XIII

8.3	Average of received, lost and corrupted frames during the second week.	97
8.4	Average of received, lost and corrupted frames during the third week.	98
8.5	Probability mass function of burst length at frame level.	99
8.6	Probability mass function of gap length at frame level.	99
8.7	Probability mass function of gap length at bit level.	100
8.8	Probability mass function of burst length at bit level.	101
8.9	Probability mass function of number of errored bits per frame.	102
9.1	Plant of the building where the measurements have been taken; T and R are the transmitter and receiver laptops used for the measurements.	107
9.2	Error gap length distributions for one observed frame error trace and a synthetically generated Bernoulli trace with the same average frame error rate.	109
9.3	Goodput as computed with Padhie's formula and with a trace with Bernoullian frame error.	110
9.4	TCP goodput versus frame error rate of real traces for different error models.	111

List of Tables

2.1	Packet loss, packet delay and packet jitter statistics of the satellite and WLAN transmissions, relative to 45 minutes of CBR traffic presented in Fig. 2, 6 and 9.	9
2.2	Statistics of the full path transmission, relative to 45 minutes of a real video streaming.	19
2.3	Maximum, mean and variance of delivery delay for client A.	25
2.4	Maximum, mean and variance of delivery delay for client B.	25
2.5	Acceptability of received video by client A.	25
3.1	Path loss exponents for different environments.	36
3.2	Typical values of mean delay spread and maximum delay spread.	45
4.1	Characteristics of the considered outdoor propagation models.	56
7.1	Rate-dependent parameters in Equation 7.10.	91
9.1	Traces used in the simulation experiment.	111

1

Introduction

The presence of both a geostationary satellite link and a terrestrial local wireless link on the same path of a given network connection is becoming increasingly common, thanks to the popularity of the IEEE 802.11 protocol [1]. In the following, we will refer to this ubiquitous wireless terrestrial protocol as Wi-Fi, the popular trademark of the association founded to set interoperability standards for it. The most common situation where a hybrid network comes into play is having a Wi-Fi link at the network edge and the satellite link somewhere in the network core. Example of scenarios where this can happen are ships or airplanes where Internet connection on board is provided through a Wi-Fi access point and a satellite link with a geostationary satellite; a small office located in remote or isolated area without cabled Internet access; a rescue team using a mobile ad hoc Wi-Fi network connected to the Internet or to a command centre through a mobile gateway using a satellite link [2, 3]. The serialisation of terrestrial and satellite wireless links is problematic from the point of view of a number of applications, be they based on video streaming, interactive audio or TCP. The reason is the combination of high latency, caused by the geostationary satellite link, and frequent, correlated packet losses caused by the local wireless terrestrial link. In fact, GEO satellites are placed in equatorial orbit at 36,000 km altitude, which takes the radio signal about 250 ms to travel up and down. Satellite systems exhibit low packet loss most of the time, with typical project constraints of 10^{-8} bit error rate 99% of the time, which translates into a packet error rate of 10^{-4} , except for a few days a year. Wi-Fi links, on the other hand, have quite different characteristics. While the delay introduced by the MAC level is in the order of the milliseconds, and is consequently too small to affect most applications, its packet loss characteristics are generally far from negligible. In fact, multipath fading, interference and collisions affect most environments, causing correlated packet losses: this means that often more than one packet at a time is lost for a single fading event [3].

In chapter 2 we describe the hybrid wireless network; in fact natural and man-made disasters, like earthquakes, floods, storms, structural collapses, etc.,

pose a challenge to public emergency services. In order to cope with such disasters in a fast and coordinated manner, communications between rescue squads, both among themselves and outside the assisted zone, play a critical role. This chapter is subdivided in two main sections; in section 2.1 we evaluated the performance in terms of packet loss, delay and jitter for the satellite path, wireless path and finally for the full path, while in section 2.2 we study how to improve the QoS (Quality of Service) requirements of the multimedia flows. This portion of the study offers an subjective assessment of video quality as a function of channel error characteristics, together with explanations for the performance degradations based on network-level effects.

From a user's perspective, the details of the wireless technology used are generally unimportant: it's the performance of the final wireless-based application that counts. We distinguish two basic types of user applications: real-time datagram applications, with various quality of service constraints, and TCP-based applications, whose main performance indicator is the connection throughput. Analysing the performance of these applications on a wireless channel is challenging, because of the highly variable characteristics of the channel and the number of different causes that influence them. The aim of this dissertation is to analyse the behaviour of a wireless channel at the packet level in order to build a model able to capture the channel's main characteristics. In order to validate this model, we will resort to simulation and real-world measurements. A good knowledge of physical layer and the fundamental limitations in the performance of mobile communications system are necessary tools for engineers as well as for research scientists that wish to gain to a deeper understanding of a possible channel modelling. Therefore, in chapter 3 we describe a typical scenario for terrestrial mobile radio channel and the principal cause of the information loss (multipath fading). In fact, multipath propagation caused by reflections and the scattering of radio waves lead to a situation in which the signal phase is shifted depending on the length of each of the paths between transmitter and receiver, where signals carried over different paths are superimposed. This interference can strengthen, distort or even eliminate the received signal. Conditions that cause fading are illustrated in the third chapter. We will examine the fading effects that characterize mobile communications: large-scale fading and small-scale fading. Large-scale fading represents the average signal power attenuation, also called path loss, due to motion over large areas, while the small-scale fading refers to the sometimes dramatic changes in signal amplitude and phase that can be experienced as the result of small changes in the spatial separation between receiver and transmitter.

Knowledge of the properties of the time-varying frequency and space dispersive mobile radio channel is necessary for a good understanding of the phenomena that occur in wireless communications and for the design of mobile communication systems and networks. In chapter 4, an overview of state of the art in the modeling of the mobile radio channel is given.

Channel models are of particular interest for radio communication systems and network technologies like UMTS (Universal Mobile Telecommunications System) and WLAN (Wireless Local Area Networks). Thus, this work focuses on mobile terrestrial channel modelling, in general, and, in particular, on the modeling of radio wave propagation in urban and suburban areas. We will investigate the propagation models that characterize signal strength over large transmitter-receiver separation distances (large-scale propagation models) and models that characterize the rapid fluctuations of the received signal strength over short distances (small-scale models), both in outdoor and indoor scenarios. Chapter 4 is divided in two main sections: Section 4.1 addresses the outdoor models, while Section 4.2 focuses on the indoor models.

In Chapter 5, we describe the traditional approach to modelling packet losses through the use of a classical network model, such as Bernoulli, Gilbert-Elliott. In order to choose the best model, we must consider the statistical properties of them. For example, the Bernoulli model is based on a memoryless process. Thus, output values will be uncorrelated.

In Chapter 6, we will describe a complex and articulated campaign of measurements, together with tools used to generate and analyze the data. The campaign of measurements is conducted in outdoor and in indoor environments. The packet loss and the throughput are directly measured using a traffic generator and a receiver inserted at MAC layer.

Our goal would be to obtain a certain number of models, derived from real measurements, according to the environment characteristics; this argument is dealt in chapter 7 for the outdoor model.

In chapter 8 we describe the results obtained during the indoor measurement campaign, with are especially focused on burst length and gap length distributions. This chapter is subdivided in two main section; Section 8.1 address the main frame level statistics, while section 8.2 focuses on presents the results obtained at bit level.

Finally in chapter 9 we concentrate on frame error models in indoor environment targeted to TCP-based applications, for which the combination of high, correlated packet loss and high latency may cause very bad performance. Since TCP interprets packet loss as a sign of congestion, thus slowing its pace to avoid worsening the network conditions, frame errors due to corruption causes decreased throughput, even in the absence of network congestion.

References

1. IEEE Std 802.15.1-2002 IEEE Std 802.15.1 IEEE Standard for Information technology - Telecommunications and information exchange between systems - Local and metropolitan area networks - Specific requirements Part 15.1: Wireless Medium Access Control (MAC) and Physical Layer (PHY) Specifications for Wireless Personal Area Networks (WPANs).
2. A. Annesse, P. Barsocchi, N. Celandroni, and E. Ferro, "Performance evaluation of UDP multimedia traffic flows in satellite-WLAN integrated paths", proceedings of 11th Ka Band Utilization Conference, Rome, September 2005.
3. F. Davoli, E. Ferro, H. Mouftah, "Wireless access to the global Internet: mobile radio networks and satellite systems", guest editorial, *Int. Journal of Communication Systems*, vol. 16, no. 1, 2003.
4. Gabriele Oligeri, "Misura e caratterizzazione di un canale Wi-Fi", <http://fly.isti.cnr.it/didattica/tesi/Oligeri-Finotti/Oligeri.pdf>.

Hybrid network

Natural and man-made disasters, like earthquakes, floods, storms, structural collapses, etc., pose a challenge to public emergency services. In order to cope with such disasters in a fast and coordinated manner, communications between rescue squads, both among themselves and outside the assisted zone, play a critical role. In the hours and even days following these events, communication is often limited, due to the damages caused by the disaster to land connections or because the event occurred in an area without infrastructures.

Wireless communications are the reply to these needs; wireless networks are the easy, fast, and intuitive way for providing the first communications means for the depicted scenarios. In particular, MANET (Mobile Ad hoc NETWORKS) [1] is the topology generally contemplated in these situations, in which handheld devices or notebooks use wireless ad-hoc networks for communications between each other and with a special node, which is a gateway for outside communications, through a satellite link.

Given such a network, we assume that user data are flows derived from multimedia and real-time applications, like voice calls, video streaming, and video conferencing, which make use of UDP (User Datagram Protocol) transport protocol.

2.1 Performance evaluation

In this chapter, we present a set of experimental results, which show the behaviour of UDP traffic flows in a basic MANET testbed developed at ISTI. The testbed is constituted by a set of portable computers and handsets, interconnected among them in wireless mode, and a Skyplex Data satellite link [2, 5]. The portable computer that acts as a gateway between the ad-hoc network and the Skyplex box is a Debian Linux box (kernel 2.6.8, Celeron 1.133 GHz with 256 MB of RAM).

Wireless LANs [6, 7] have the advantage of low delivery delays, but they have drawbacks such as the high channel errors due to multiple paths and

data collisions. Satellite links have an inherent broadcast facility, but they suffer from high delivery delays and atmospheric adverse conditions which may worsen the Signal to Noise Ratio (SNR). Thus, the whole network, made up of WLAN nodes and the satellite link, is not a trivial environment for QoS (Quality of Service) requirements of the multimedia flows.

The packet loss, the data jitter and delay are separately measured in both the WLAN and the satellite link; then, these three parameters are evaluated as total, combined effects on the hybrid wireless network considered. The traffic flows used are both a simple CBR (Constant Bit Rate) generator, characterized by the size of the IP datagram packets and the packet generation time interval, and a multimedia and real-world video application. The investigation aims at evaluating the QoS performance of traffic flows, both in unicast and in broadcast/multicast transmission mode. Delivery delays, from the application layer's point of view, are finally calculated, which are useful for estimating the buffer's sizes of the receiving applications.

2.1.1 Testbed configuration

The testbed of transmission experiments is depicted in 9.1.



Fig. 2.1. Testbed environment.

The wireless path at ISTI is made up of notebooks (Celeron 1.133 GHz with 256 MB of RAM) equipped with a Debian Linux operating system (kernel 2.6.8) and with wireless PCMCIA network cards of different manufacturers (CNet CNWLC-811 IEEE802.11b for transmission, Conceptronic C54RC IEEE802.11g for reception), always operating with the standard DCF (Distributed Contention Function) [7] contention access mode at a rate of 11 Mbps,

and acting as traffic sources. An host acts as a gateway between the WLAN network and the Skyplex box, and forwards packets towards the satellite.

The satellite link is a Ka channel of Eutelsat HotBird 6 which uses the technology known as Skyplex Data [2, 3, 5]. This is an IP-based satellite network derived from the DVB-RCS [4] and it is used here in a standard point-to-point (for unicast traffic) and point-to-multi-point (for multicast traffic) topology.

We have used remote Linux hosts in Bari and in Genoa as traffic sinks on the other side of the satellite link.

In unicast transmissions, WLAN cards use standard IEEE802.11 settings; in particular, the DCF Retry Limit value is set to 7 for every outgoing MAC frame, i.e. up to 7 transmission retries are performed in case of unacknowledged frames. In multicast transmissions, the value of the Retry Limit is 0, i.e. the frame is transmitted only one time, regardless its good reception.

2.1.2 The Measurements

In the first step, UDP packets have been transmitted through a simple CBR generator written in C, in order to testing the single WLAN or satellite links and investigating their basic performance; about 24 hours of measures has been performed both on the satellite channel and on the WLAN channel, with single tests of 45 minutes each; then a real-world MPEG-4 video stream has been transmitted with the software VLC (Video Lan Client) on the full WLAN and satellite path.

A software in C has been developed with the purpose of tracking and collecting packets in the cardinal points of the path, i.e. at the WLAN source, the satellite gateway and the remote sink. This software runs on Linux in user mode, so the collected statistics refer to the application's layer; all the time measures (the end-to-end jitter and delay) have the precision of the Linux kernel clock. The `gettimeofday()` system call has been used; it returns microseconds-figure time from the Linux System Time.

We have gathered our measurements with notebooks located in fixed indoor positions at about 10 meters apart from the satellite gateway, separated by thin walls and doors, and with people working around involved in the common activities of an office environment.

Several measurement campaigns have been carried out, with CBR traffic at different transmission rates, varying both the packet lengths and their inter-generation time. It is well known that WLAN communication's performances widely change according to environment, people's presence and movements; thus, we here present only the most representative tests of the common situation observed, and we introduce a way for deriving Retry 0 transmission performances from the Retry 7 ones, so that a direct comparison is possible between the two WLAN operating modes.

Every test presented in this work lasts 45 minutes; every packet generated has its own sequence number; for all packets that travel through the three

cardinal points of observation of the network, the software sniffs pieces of information like the sequence number, the packet length and the transit time.

Each packet may experience a different transmission delay, so a jitter, defined as the difference between two transmission delays, is induced on the packet arrival time [8, 9]. By definition, in every single hop, the first packet received has a null jitter, while the n th packet (transmitted at the time $t_{TX,n}$ and received at the time $t_{RX,n}$) has the jitter $j_{n,1}$ given by

$$j_{n,1} = (t_{RX,n} - t_{RX,1}) - (t_{TX,n} - t_{TX,1}) \quad (2.1)$$

i.e. the jitter $j_{n,1}$ is referred to the transmission delay of the first packet, because this is comfortable for the delay calculation.

Since it's difficult to synchronize the clocks of the observation points and every clock has its own drift, we assumed linear clocks' drift. A linear correction has thus been adopted along with every interval of 12 consecutive hours of measures. In short, the slope of the linear part of the jitter drift, caused by the different clock drift of the transmitting and receiving side, has been calculated for such intervals, and a linear correction proportional to the time was applied at every $j_{n,1}$. Then, an offset O is added to the jitters so calculated in order to obtain the packet delays D_n given by

$$D_n = j_{n,1} + O \quad D_{hop} = \min \{D_n\} \quad (2.2)$$

so that the minimum delay obtained is equal to the minimum delay of the hop D_{hop} , measured as the half of the minimum round trip time of 1000 ping packets sent with the same size and inter-generation time of the analyzed packets.

Furthermore, continuous jitter calculation, as specified by RTP protocol in [10], is evaluated as

$$J_n = J_{n-1} + \frac{|j_{n,n-1}| - J_{n-1}}{16} \quad (2.3)$$

where the difference between transmission delays $j_{n,n-1}$ is referred to consecutive packets. From this point, when we speak of packet jitter, we are referring to this J_n .

The satellite path

Fig. 2.2 shows the packet delay of the typical satellite transmission test, for a CBR traffic with UDP packets of 1000 bytes (IP header included) and packet inter-generation time of 20 ms, following a generated rate of 400 kbps. The figure shows a packet delay quite regular and concentrated, except for rare peaks, in which the system seems to recover after a sort of bad situation. It is worth pointing out that the satellite used performs on board processing, and is shared in TDMA (Time Division Multiple Access) mode with other users. Fig. 2.4 and 2.5 show the details of the regular band and of the peaks

of the packet delay, respectively. In particular Fig. 2.5 shows what happens when, for a less than 1 second time interval, packets are not transmitted in the satellite path: when transmission resumes the delay has piled up but the situation restores in about 5 seconds. This phenomenon has been observed in all the satellite transmission tests and the recovery speed is due to the channel available bandwidth, that is 2 Mbps. Fig. 2.3 presents the CDF (Cumulative Distribution Function) for the packet delay.

The satellite channel has resulted to be almost error-free; very few losses have been observed so that is not possible to give a precision value of the packet loss. No single packet errors have been registered and this is probably due to the peculiarity of Skyplex architecture; error bursts of 2 or 3 consecutive packets have rather been seen.

The minimum delay measured on the satellite path has been 0.284619 s; table 2.1 shows the mean and standard deviation of the packet delay and the mean packet jitter.

Table 2.1. Packet loss, packet delay and packet jitter statistics of the satellite and WLAN transmissions, relative to 45 minutes of CBR traffic presented in Fig. 2, 6 and 9.

	Packet loss probability	Packet delay [s]		Mean jitter [s]
		Mean	Standard deviation	
Satellite	-	0.334329	0.104579	0.0133456
WLAN Retry 0	$3.33 \cdot 10^{-1}$	0.000912	0.000094	0.000028
WLAN Retry 7	$4.82 \cdot 10^{-4}$	0.001379	0.001080	0.000669
WLAN "Retry 0" emulated	$2.12 \cdot 10^{-1}$	0.000978	0.000091	0.000022

The WLAN path

Fig. 2.6 shows the packet delay of the typical WLAN transmission test with Retry 0 (suitable for multicast and broadcast transmission), for a CBR traffic with UDP packets of 1000 bytes and packet inter-generation time of 20 ms. The delay is quite constant and delimited within a narrow band. Fig. 2.7 and 2.8 show the size of packet error bursts during the test. The packet loss, the mean packet delay, its standard deviation and the mean packet jitter for this test are shown in table 2.1.

Fig. 2.9 shows the packet delay of a WLAN transmission test like the previous one, but with Retry 7 (suitable for unicast transmission). It's plain that the different bands in which the delays of the packets are gathered correspond with the retries the WLAN MAC layer operates. As shown in table 2.1, the mean and standard deviation of packet delay for WLAN Retry 7 test is greater than the WLAN Retry 0, but the packet loss benefits of the retries. This is plain visible in Fig. 2.10, that shows the size of packet error bursts

for the Retry 7 test, and in Fig. 2.12, that show a comparison of the PMF (Probability Mass Function) of the size of packet error bursts for the Retry 0 and Retry 7 tests. In Fig.2.11 the CDF for the packet delay of Retry 0 and Retry 7 tests are compared.

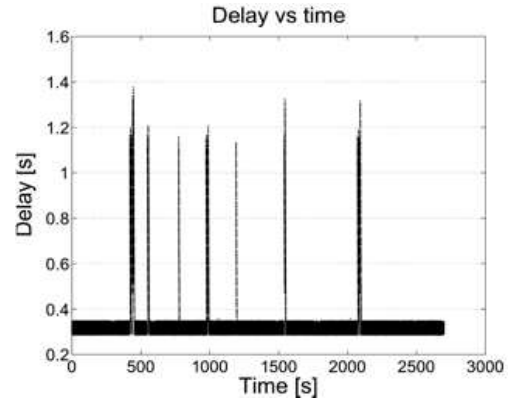


Fig. 2.2. Typical trend of packet delay for the satellite channel in 45 minutes of transmission.

It's important to notice that WLAN channel's performances widely change due to radio multipaths and environment variations, and the two WLAN tests shown before are not really comparable. In fact in other Retry 7 tests very heavy packet losses have been found too.

Instead it's easy to discriminate for the most part of the packets of the Retry 7 test, the ones received at the first MAC try from that received at subsequent retries, simply watching the delay accused by each packet. If the Retry would be set to 0 all packets transmitted with MAC retries would have been lost. So it's possible for the Retry 7 test to go back and to achieve roughly what's would be happened in the same situation if the Retry would be set to 0. Fig. 2.13 show the CDF of packet delay for the WLAN channel with Retry 7 compared to the one obtained for the first MAC try only of the same transmission (for the purpose packets with delay less or equal to 0.0026s have been considered first MAC try packets). Table 2.1 show the packet loss, the mean packet delay, its standard deviation and the mean packet jitter for this comparable "Retry 0" emulated transmission.

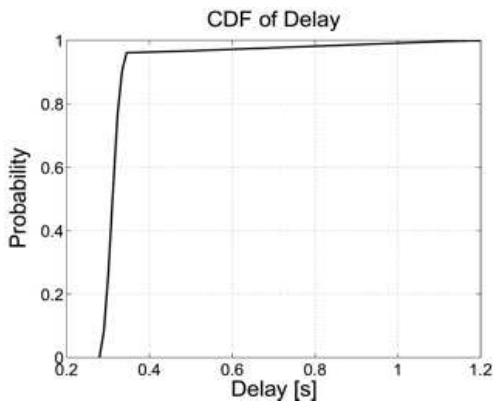


Fig. 2.3. CDF of packet delay for data in 2.2.

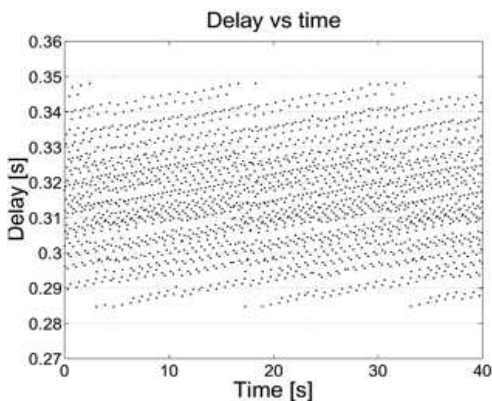


Fig. 2.4. Details of firsts 40 seconds of 2.2.

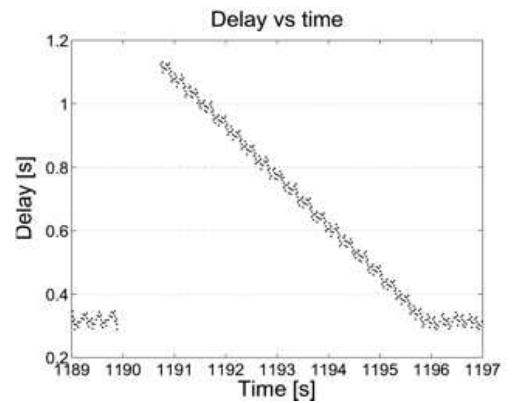


Fig. 2.5. Details of a delay peak of 2.2.

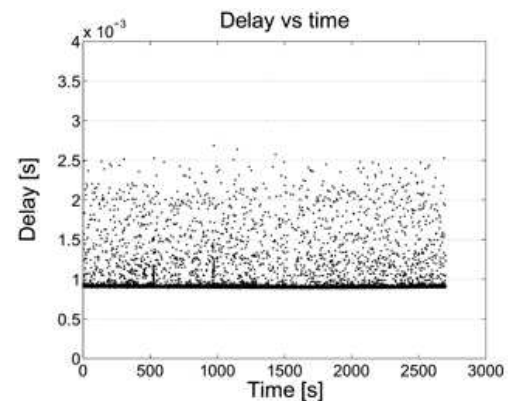


Fig. 2.6. Typical trend of packet delay for the WLAN channel with Retry 0 in 45 minutes of transmission.

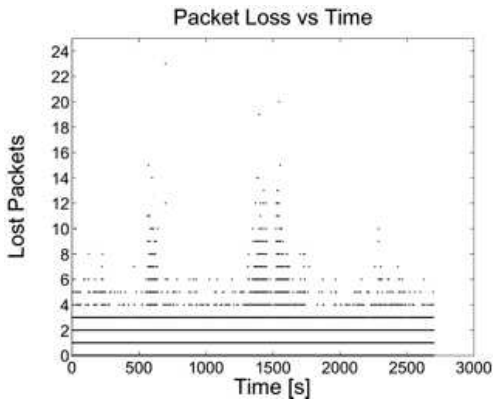


Fig. 2.7. Lost packets for WLAN transmission with Retry 0 of 2.6.

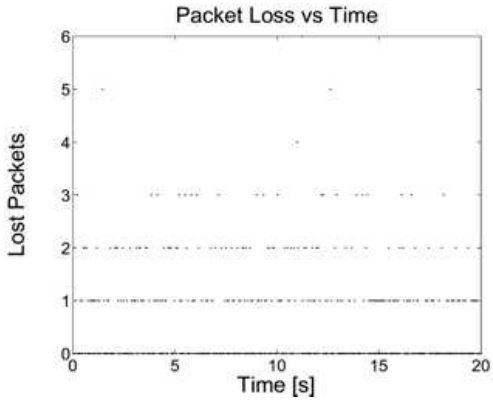


Fig. 2.8. Details of firsts 20 seconds of 2.7.

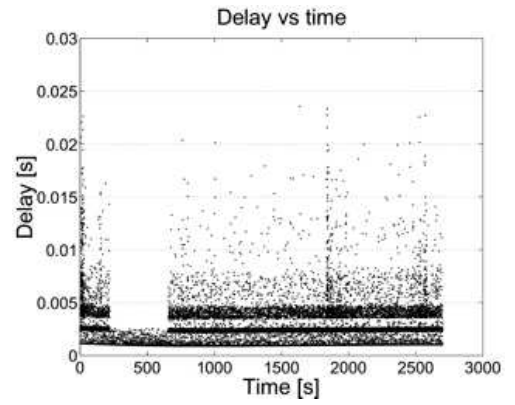


Fig. 2.9. Typical trend of packet delay for the WLAN channel with Retry 7 in 45 minutes of transmission.

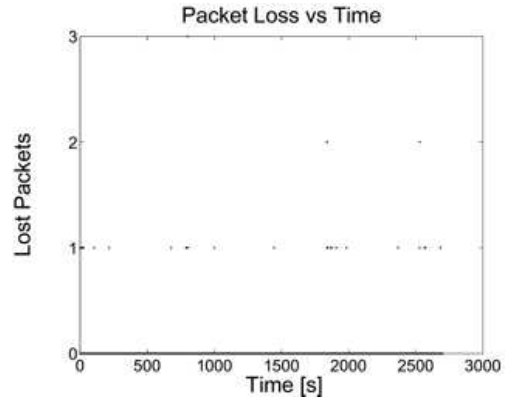


Fig. 2.10. Lost packets for WLAN transmission with Retry 7 of 2.9.

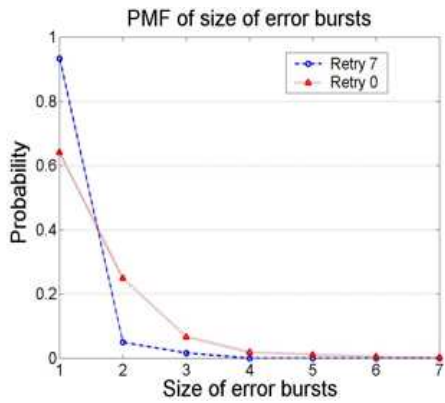


Fig. 2.11. CDF of packet delay for WLAN transmissions.

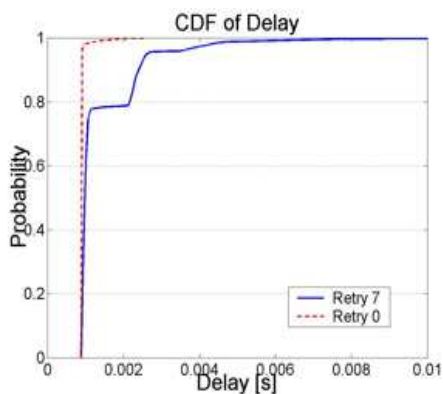


Fig. 2.12. PMF of the size of packet error bursts for WLAN transmissions.

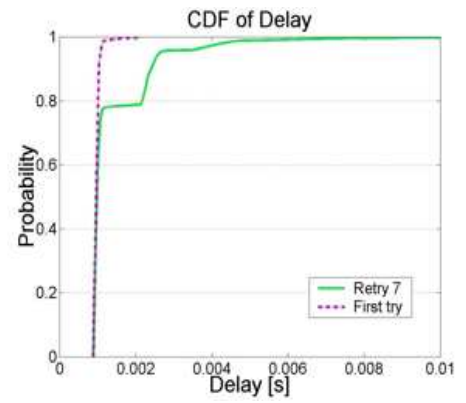


Fig. 2.13. CDF of packet delay for the WLAN channel with Retry 7, and for the first MAC try only.

The minimum delay measured on the WLAN path has been 0.000883s.

Full path behaviour

A transmission of a real MPEG-4 video stream has been performed over the full WLAN and satellite path. The software VLC [11] has been used as source: it generates UDP packets of a fixed size of 1344 bytes (IP header included) with a variable inter-generation time. Further 4 bytes has been added to each of that packets, for tracking purposes. The transmission has lasted 45 minutes, and 160402 packets has been generated, achieving a mean throughput of 640.7 kbps. The WLAN hop has operated in the Retry 0 mode, emulating a multicast or broadcast transmission, within a quite clear channel.

Table 2.2 shows the packet loss, the mean packet delay, its standard deviation and the smoothed mean jitter measured in each hop, and the ones resulted in the total full path.

Fig. 2.14, 2.15 and 2.16 show the trend of the packet delay, the CDF of the packet delay, and the packet jitter, for the full path streaming, respectively. Most of that are due to the satellite hop. Fig. 2.17 shows the lost packets in the full path, but they are fully due to the WLAN hop.

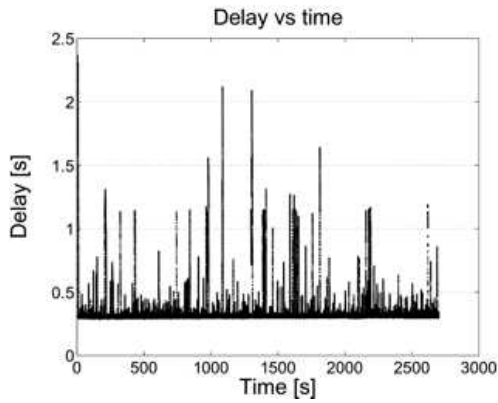


Fig. 2.14. Packet delay for the full path in 45 minutes of real video streaming.

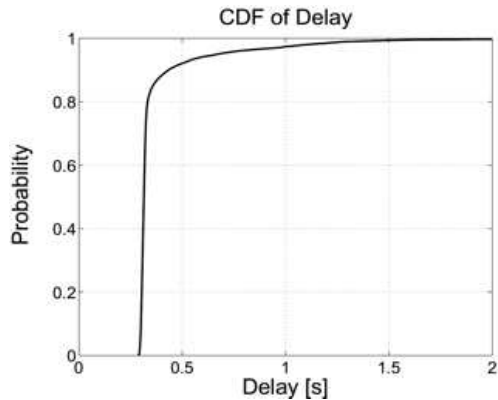


Fig. 2.15. CDF of packet delay for data in Fig. 2.14.

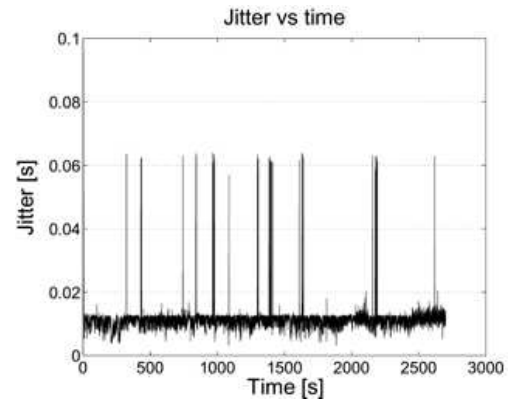


Fig. 2.16. Packet jitter for the full path video stream.

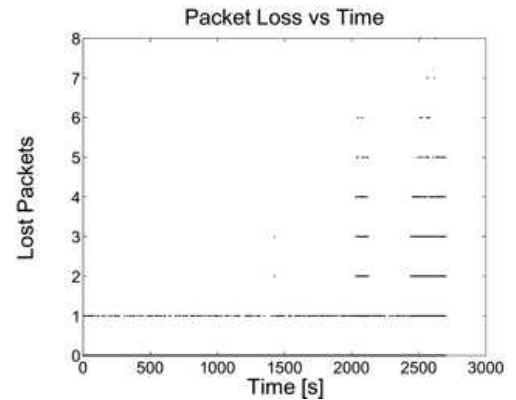


Fig. 2.17. Lost packets for the full path video stream.

Table 2.2. Statistics of the full path transmission, relative to 45 minutes of a real video streaming.

	Packet loss probability	Packet delay [s]		Mean jitter [s]
		Mean	Standard deviation	
WLAN (Retry 0)	$4 \cdot 10^{-2}$	0.000940	0.000231	0.000021
Satellite	-	0.367103	0.196004	0.010863
Full path	$4 \cdot 10^{-2}$	0.367946	0.196004	0.010864

2.1.3 Conclusions

A WLAN cum satellite testbed has been developed, and UDP transmissions have been performed both with CBR traffic and with a real video stream. The packet loss, the packet delay and the packet jitter have been experimented.

In the end the resulting packet loss of this hybrid network topology is fully due to the losses in the WLAN hops, while most of the delay and the jitter comes from the satellite hop.

The Quality of Service of multimedia and real-time transmissions over this kind of network topology is severely tried, and the negative effects of each hop are summed in the full path.

A buffer of few seconds located at the receive application, according to the experimental results found, could assure the quality of multimedia non real-time streams. It would be better to implement in the WLAN hops a stronger loss recovery strategy, because the Retry 7 mode improve the safety of transmitted packets but it's not suitable for multicast and broadcast transmissions. Adaptive Forward Error Correction (FEC) techniques could be used instead in the WLAN hops: they could improve the packet safety with the trade-off of a little increase of the delivery time of the packets. This topic could be investigated in future research. Nothing could be done for the minimum delay introduced by the satellite channel, and this could be the biggest problem for real-time interactive applications.

The investigation of TCP flows within the hybrid topology described is another interesting topic: the optimization of the goodput of TCP flows is a challenging problem to be investigated as well; this issue is currently argument of ongoing research.

2.2 Forward Erasure Correction and Real Video Streaming

In a heterogeneous MANET, based on wireless LANs linked together by via satellite, the overall channel efficiency is impaired by multiple effects, because of multipath fading in the terrestrial segment and atmospheric fading on the satellite link. In this paper, we address this issue by applying forward erasure

correction codes (FZC) to MPEG-4 video sequences exchanged by the hosts of a hybrid network. The network is made of a satellite link and a wireless LAN that uses 802.11b devices. The stream is FZC encoded at the streamer and decoded at the individual receivers. Encoding and decoding operations occur just above the transport layer. This approach has the advantage of being independent of the equipment, the operating system and the end-user application. It performing performs as middleware between the application and the underlying operating system services, and thus allows allowing the employing use of standard streaming applications both at the sender and the receiver. This work aims at demonstrating the improvement in quality of service of the video transmitted in the hybrid network. The main parameters measured are the packet loss, the delivery delay, and the overhead in bandwidth occupancy imposed by the use of FZC. The received video is then evaluated by using a MOS (Mean Opinion Score) procedure. While the concept of using FZC has been widely studied for several years [12, 13], the literature is lacking in experimental results in a hybrid wireless environment. In the following, we first describe our test scenario and then we present measurements obtained in the described environment.

2.2.1 The Real Case Study

The forward error correction technique employed in our experiments a class of linear block codes based on Vandermonde matrices [14]. Basically, k blocks of source data are encoded to produce n blocks of encoded data, such that any subset of k encoded blocks suffices to reconstruct all source data (with $n > k$). Let x be the vector of source blocks and y the vector of encoded blocks. Then, the problem is to find an appropriate nk coding matrix C such that $y = Cx$ and $x = C'^{-1}y'$, for any subset y' of k blocks in y , where C' is the corresponding row-wise sub-matrix in C (a linear block code is said to be systematic if I is a row-wise sub-matrix in C). As indicated in [14], of special interest are the FZCs derived from Vandermonde coding matrices are of special interest; they employ efficient field arithmetic.

The video stream used in the experiment is coded using MPEG-4. MPEG-4 is the first standard that describes multimedia contents as a set of audio-visual objects to be presented, manipulated and transported individually. The high compression ratio and error resilience offered by MPEG-4 has driven an explosion of its popularity. The evaluation of FZC performance in MPEG-4 stream delivery on the single wireless path is not new. For example, in [15] the joint usage of FZCs and MPEG-4's Fine Granularity Scalability (FGS) – a highly suitable technique for IEEE 802.11 – is studied, while [16] studies the behavior of FZCs when applied to MPEG-4 streaming via 3G networks. Anyway, there is a lack of experimental results in hybrid wireless environment. In order to provide such results, our target scenario is composed of a video-streaming server interconnected to an ad hoc wireless network through an OBP (On Board Processing) satellite. The satellite link is carried by the

Eutelsat HotBird6 satellite in Ka band, and uses the technology known as Skyplex Data [5, 6], which is, an IP-based satellite network, derived from DVB-RCS. We used it this satellite technology in a point-to-multipoint topology, by using a single multicast receiver. The Skyplex link we used has a bandwidth of 2 Mb/s. Figure 2.18 depicts the scenario of our experiment. The video streamer transmits a FZC encoded multicast stream on the satellite; the local gateway receives the traffic from the satellite multicast receiver and broadcasts forwards it to the wireless clients. The ad-hoc wireless LAN uses the IEEE 802.11b standard [5].

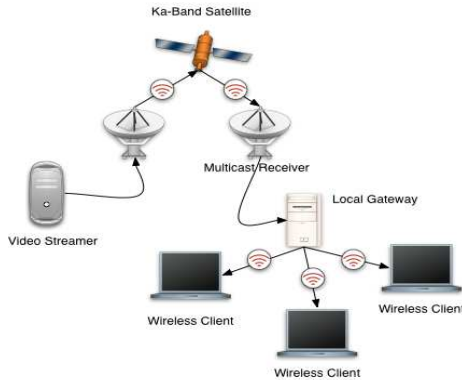


Fig. 2.18. The test-bed network topology.

The mobile devices are IBM Thinkpad R40e laptops (Celeron 2.0 Ghz with 256 Mb Ram running Debian Linux with a 2.6.8 kernel), and they are equipped with CNet CNWLC-811 IEEE 802.11b wireless cards. The indoor environment is depicted in Fig. 2.19

The dashed lines in Figure 2.19 represent the shortest radio paths between the local gateway and the client devices A and B (black stars). The rooms are at the first floor of the building of the CNR ISTI Institute in Pisa; they are delimited by thin walls.

2.2.2 Experimental Results

Notice that IEEE 802.11 includes the use of automatic repeat request (ARQ) [5] only in unicast mode. We implemented two software modules, an encoder

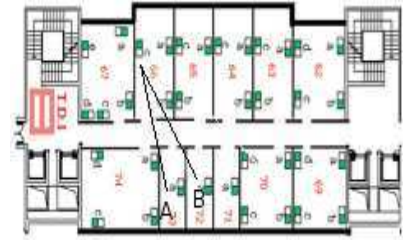


Fig. 2.19. Plant of the building.

and a decoder, written in C language, by using Rizzo's library [18]. The encoder works at the transport layer by fetching blocks of k information packets from the video stream and then transmitting $k+l$ UDP packets (k of information + l of redundancy) towards the receiving host. At the receiving host, the decoder fetches k of the $k+l$ packets per block and recovers the information, provided that no more than l packets are lost in a single block of packets. The receiver then feeds the VLC 0.8.1 decoder with the received stream to the VLC 0.8.1 decoder with the received stream. VLC uses a packet size of 1316 bytes, which is a block of seven 7 MPEG-4 frames. The encoder adds a preamble of 4 bytes for the sequence number, which is then cancelled by the decoder. The overall length of the 802.11 MSDU is then equal to $8+20+8+4+1316$ bytes, keeping into account the UDP, IP, and SNAP/LLC headers.

Packet error rate

The MPEG stream carries an Xvid version of the Pirates of Caribbean movie, with a frame rate of 25 frames per second at 576320 pixels, and an average data stream of 939 kb/s. Our experiments show that the satellite channel is error free (thus the only problem is the intrinsic satellite delay), while the wireless channel is error prone. Thus, the error recovery aspect must be addressed in the wireless environment. By default, 802.11 devices use an internal algorithm for changing the transmission signal rate in order to adapt to varying channel conditions. Since our aim is to verify the performance of different coding schemes, we fixed the signal rate, by disabling the internal auto rate-change algorithm. We used two data bit rates: 11 and 5.5 Mb/s. Lower transmission rates were not considered because the stream throughput would have exceeded the available information rate of the wireless channel. We analyze the channel between the local gateway and the A node (see Fig. 2.19), and between the local gateway and the B node (see Fig. 2.19), respectively. In the first case, which is the worst case (due to the distance between the gateway and the

client A), the experiment in uncoded mode (no FZC) shows that packet loss can be reduced from 13% to about 6% by changing the transmission rate from 11 to 5.5 Mb/s. In this case, the channel occupancy increases by 56%. A similar redundancy is required when using an FZC coding ratio of 150/100; however, in the latter case, we measured a much better performance, with a packet loss rate of 0.8%. Better performance yet can be obtained by using an FZC with 120/100 coding ratio, which increases channel occupancy by only 20%.

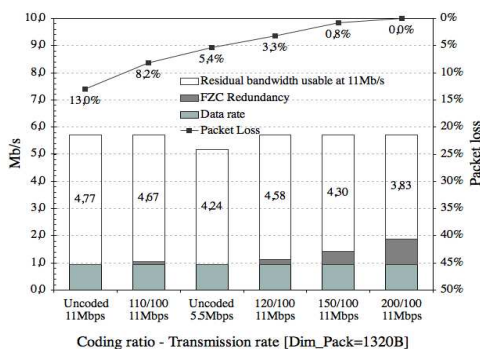


Fig. 2.20. Redundancy and error correction performance vs. coding ratio for client A.

When the B node is considered, the experiment in uncoded case (no FZC) shows that packet loss can be reduced from 5.9% to about 0.4% by changing the transmission rate from 11 to 5.5 Mb/s. However, if we use an FZC coding ratio of 110/100, we measured a much better performance (only 0.3% of packet loss) by increasing the channel occupancy by only 10%. Choosing a coding ratio of 120/100, all packet losses (about 6%) can be recovered by increasing the channel occupancy by 20%.

All measurements are summarized in Figures 2.20 and 2.21, where the residual bandwidth is defined as the bandwidth left available on the channel for use by other communications performed at 11 Mb/s. Notice the case of 5.5 Mb/s where, while no FZC redundancy is introduced, the occupied channel

share is 56% wider than the corresponding 11 Mb/s case, and the residual bandwidth is reduced accordingly.

Generally speaking, there is a tradeoff between redundancy and error correction performance; these results show that the usage of FZC is convenient with respect to changing the signal rate.

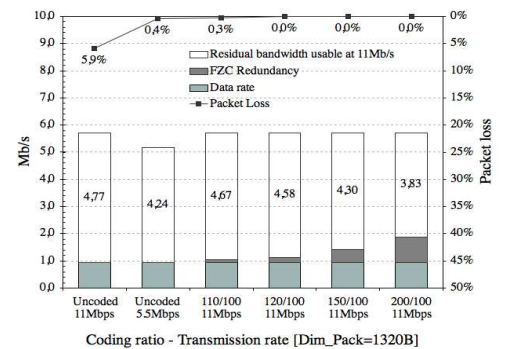


Fig. 2.21. Redundancy and error correction performance vs. coding ratio for the client B.

Packet delivery delay

A streaming application delivers time-based information, i.e. user data that has an intrinsic time component. By using erasure codes we introduce the packet delivery delay. In fact, when h packets in a block are lost, we must wait for all k packets of information plus h of redundancy. Delivery delay is an important parameter that must be evaluated like the packet loss. Our experiments show that the mean delivery delay for the node A is about 50 ms, and it is less than the delivery delay for the node B (48 ms). This is due to the fact that node A has a greater number of packet losses than node B. The maximum packet delivery delay is evaluated as the time necessary to recover all the information when a number of packet equal to the redundancy packets is lost. These experiments show that the limits imposed by ITU-T Recommendation G.114 [18] are preserved. Tables 2.3 and 2.4 show the packet delivery delay for clients A and B, respectively.

Table 2.3. Maximum, mean and variance of delivery delay for client A.

Coding ratio	Max [ms]	Mean [ms]	Var. [ms]
110/100	105.6	52.149	0.769
120/100	115.2	54.99	0.792
130/100	124.8	52.637	0.805
200/100	192	53.805	1.675

Table 2.4. Maximum, mean and variance of delivery delay for client B.

Coding ratio	Max [ms]	Mean [ms]	Var. [ms]
110/100	105.6	48.522	0.796
120/100	115.2	48.639	0.824
130/100	124.8	47.992	0.715
200/100	192	53.585	1.681

Mean opinion Score (MOS)

The MOS is the most widely known video quality metric. MOS is a subjective score, ranging from 5 (Excellent) down to 0 (Unacceptable). Thirty persons have answered to three quality questions (overall, video, and audio quality) for each coding ratio of the video received by client A; mean opinion scores have been calculated. The results for each quality question are shown in Figure 2.22. It can be seen that the coding ratio is important for opinions on the quality; this is true for all three questions. Not surprisingly, the best video quality is obtained by using the 200/100 coding ratio. When the coding ratio decreases from 200/100 to the uncoded case, the quality ratings become progressively poorer.

Table 2.5. Acceptability of received video by client A.

Uncoded 11M	110/100 11M	Uncoded 5.5M	120/100 11M	130/100 11M	150/100 11M	200/100 11M
7.7%	15.4%	26.9%	34.6%	100.0%	100.0%	100.0%

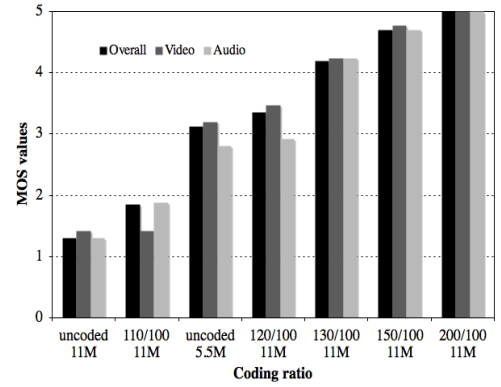


Fig. 2.22. MOS of received video by client A.

Acceptability opinions for each test were based on a binary choice: acceptable or not acceptable. Figure 2.23 display the percentage of people who report who report 'acceptable' options for each coding ratio. Table 2.5 clearly shows that the video quality is acceptable when using a coding ratio greater than 130/100. Video applications are sensitive to packet losses and, even if a few packets are lost, the video streaming performance can be considered unacceptable: with 3.3% of packet loss (coding ratio of 120/100), only 30% of subjects found the performance acceptable. Some samples of the proposed video for the MOS are depicted in Fig. 2.23.



Fig. 2.23. Samples of the streamed video trailer at different coding and bit rates.

References

1. S. Corson, J. Macker, char92Mobile Ad hoc Networking (MANET): Routing Protocol Performance Issues and Evaluation Considerationschar34, RFC 2501, January 1999.
2. C. Elia and E. Colzi. char92Skyplex: Distributed Up-link for Digital Television via Satellitechar34, IEEE Transactions on Broadcasting, Vol. 42, No. 4, December 1996
3. E. Feltrin, E. Weller, E. Martin, K. Zamani. char92Design, Implementation and Performances Analysis of an On Board Processor – Based Satellite Networkchar34, IEEE Communications Society, pages 3321-3325, 2004
4. EN 301 192 v1.2.1, Digital Video Broadcasting (DVB): Specification for data broadcasting, June 1999
5. http://www.eutelsat.com/fr/satellites/pdf/dealers/annex_d_skyplex.pdf.
6. IEEE 802.11. Information Technology Telecommunications and Information Exchange between Systems Local and Metropolitan Area Networks Specific Requirements Part 11: Wireless LAN Medium Access Control (MAC) and Physical Layer (PHY) Specifications. ANSI/IEEE Std. 802.11, ISO/IEC 8802-11, first edition, 2001.
7. IEEE 802.11. Supplement to IEEE Standard for Information Technology Telecommunications and Information Exchange between Systems Local and Metropolitan Area Networks Specific Requirements Part 11: Wireless LAN Medium Access Control (MAC) and Physical Layer (PHY) Specifications: Higher-Speed Physical Layer Extension in the 2.4 GHz Band. IEEE Std 802.11b-1999, 1999.
8. J. Bolot. char92Characterising end-to-end packet delay and loss in the internetchar34. J. of High-Speed Networks, pages 305-323, December 1993.
9. N. Celandroni, E. Ferro and F. Potort. char92Experimental results of a demand-assignment thin route TDMA systemchar34, International Journal of Satellite Communications, Vol. 14, pages 113-126, February 1996.
10. H. Schulzrinne, S. Casner, R. Frederick, V. Jacobson, char92RTP: A Transport Protocol for Real-Time Applicationschar34, RFC1889, January 1996
11. VLC homepage: <http://www.videolan.org/>.

12. L. Rizzo and L. Vicisano. char92RMDP: an FEC-based reliable multicast protocol for wireless environmentschar34. Mobile Computer and Communication Review, 2(2), April 1998
13. Zorzi, M. char92Performance of FEC and ARQ Error control in bursty channels under delay constraintschar34, VTC'98, Ottawa, Canada, May 1998
14. L. Rizzo, char92Effective erasure codes for reliable computer communication protocolschar34, ACM Computer Communication Review, April 1997.
15. T. P. Chen and T. Chen, char92Fine-Grained Rate Shaping for Video Streaming over Wireless Networkschar34, IEEE International Conference on Acoustics, Speech and Signal Processing (ICASSP-03), Hong Kong, 2003
16. V. Stankovic, R. Hamzaoui and Z. Xiong, char92Live Video Streaming over Packet Networks and Wireless Channelschar34, Packet Video 2003, Nantes, France, 2003.
17. E. Feltrin, E. Weller, E. Martin, K. Zamani, char92Implementation of a satellite network based on Skyplex technology in Ka bandchar34, Ninth Ka and Broad-band Communications Conference, Ischia, Italy, November 2003.
18. Luigi Rizzo's page on FEC at <http://info.iet.unipi.it/luigi/fec.html>.

3

The multipath fading channel

3.1 The environment

In wireless mobile communications, the electromagnetic waves often do not directly reach the receiver due to obstacles that block the line of sight path. A signal travels from transmitter to receiver over a multiple-reflection path; this phenomenon is called multipath propagation and causes fluctuations in the receiver signal's amplitude and phase. The sum of the signals can be constructive or destructive. A typical scenario of mobile radio communications is shown in Fig. 3.1, where the three main mechanisms that impact the signal propagation are depicted.

These well-known mechanisms are reflection, diffraction, and scattering [2], which constitute the main reasons for signal attenuation (fading). The type of fading experienced by a signal propagating through a mobile radio channel depends on the nature of the transmitted signal, as well as the characteristics of the channel. Different transmitted signals undergo different types of fading, according to the relationship among the signal parameters (such as path loss, bandwidth, symbol period, etc.), and the channel parameters (such as RMS delay spread and Doppler spread).

Reflection. When a radio wave bumps against a smooth surface, whose dimension is large compared with the signal wavelength, the radio wave is partially reflected, partially absorbed, and partially transmitted. While, in fact, the reflected wave is the result of multiple reflections against the wall, the reflection is usually represented as a single reflection wave. When a wave that travels in a first medium impacts with a second medium that is a perfect dielectric, part of the energy is transmitted into the second medium and part comes back to the first medium, without any energy absorption loss. If the second medium is a perfect conductor, then all incident energy is reflected back into the first medium, without any energy loss. The electric field intensity of the reflected and transmitted waves is derived from the incident wave by means of a reflection coefficient (Γ). The reflection coefficient is a function of the material's properties, the wave's polarization, the angle of incidence,

34 3 The multipath fading channel

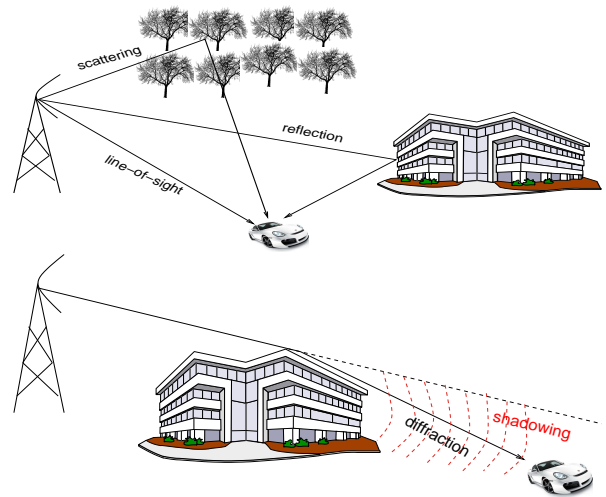


Fig. 3.1. A typical scenario of mobile radio communications

and the wave's frequency. **Diffraction.** When a building whose dimensions are larger than the signal wavelength obstructs a path between transmitter and receiver, new secondary waves are generated. This phenomenon is often called *shadowing*, because the diffracted field can reach the receiver even when shadowed by an impenetrable obstruction (no line of sight). Diffraction describes the modifications of propagating waves when obstructed. This phenomenon allows radio waves to propagate around the bending of the earth and behind obstructions. Most of the radio-wave energy is within the so called "First Fresnel Zone", i.e., the inner 60% of the Fresnel zone. The Fresnel zone for a radio beam is an elliptical area with foci located in the sender and the receiver. Objects in the Fresnel zone cause diffraction and hence reduce the signal energy. Hence, if the inner part contacts the ground (or other objects) the energy loss is significant. The *Fresnel zones* represent successive regions where the path length difference of the secondary waves with respect to the LOS path is a multiple of $\lambda/2$, being λ the wavelength. The Fresnel zones explain the concept of diffraction-loss as a function of the path difference around an obstruction. Estimating the signal attenuation caused by diffraction of radio waves over buildings is essential in predicting the field strength that arrives

at the receiver. When a single object, as a hill or a building, causes shadowing, the attenuation due to diffraction can be seen as the attenuation caused by the Knife-edge [2]. In other words, the obstruction can be treated as a knife-edge. The Knife-edge diffraction model is well described in [3]. *Scattering*. It happens when a radio wave bumps against a rough surface whose dimensions are equal to or smaller than the signal wavelength. In the urban area, typical obstacles that cause scattering are lampposts, street signs, and foliage. In mobile radio environment the signal level is often unlike what is predicted by reflection and diffraction models. This happens because the signal bumps against a rough surface, and the reflected energy spreads in all directions due to scattering. Objects, such as lamppost or trees, tend to scatter energy in all directions. In a radio channel, the knowledge of the location of the object that causes scattering can be used to predict the scattered signal strengths. A good approximation for scattering is given by the *radar cross section (RCS) model*. The *RCS* is defined as the ratio between the power density of the signal, scattered in the direction of the receiver, and the power density of the radio wave incident upon the scattering object, expressed in square meters. For rural and macro cellular areas, some of the models for scattering that have shown the best performance are those that use *bistatic radar techniques* [4][5], which can be used to calculate the received power due to scattering. Another negative influence on the characteristics of the radio channels is the *Doppler effect* due to the motion of the mobile station. The Doppler effect causes a frequency shift of each of the partial waves. The Doppler frequency of the incident wave is given by the relation

$$f = f_{max} \cos \alpha \quad (3.1)$$

where

$$f_{max} = \frac{v}{c_0} f_0 \quad (3.2)$$

is the maximum Doppler frequency or shift, which depends on the speed of the vehicle (v), the speed of the light (c_0), and the carried frequency (f_0). α is the angle of arrival of the incident wave (Fig. 3.2).

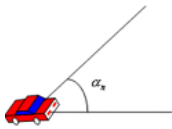


Fig. 3.2. Angle of arrival of the n^{th} incident wave

3.2 Fading types

Reflection, diffraction, and scattering have a great impact on the signal power, and they constitute the main reasons for signal attenuation (fading). The interaction between the waves derived by reflection, diffraction and scattering cause multipath fading at a specific location. Fading can be categorized into two main types: *large-scale fading* and *small-scale fading*. Large-scale fading is due to motion in a large area, and can be characterized by the distance between the mobile units. Small-scale fading is due to small changes in position (as small as the half-wavelength) or to changes in the environment (surrounding objects, people crossing the line of sight between transmitter and receiver, opening/closing of doors, etc.). Figure 3.3 is an overview of the fading types. Its explanation will constitute the core of next section.

In order to understand the main differences between large-scale and small-scale fading, let us consider a received signal $s(t)$ that is the convolution between the transmitted signal $r(t)$ and the impulse response of the channel $h_c(t)$:

$$r(t) = s(t) \otimes h_c(t) \quad (3.3)$$

The received signal can be seen as the product of two random variables [1]

$$r(t) = m(t) \cdot r_0(t) \quad (3.4)$$

where $m(t)$ is called *large-scale fading component*, and $r_0(t)$ is the *small-scale fading component*.

$m(t)$ is the *local mean* of the received signal, usually characterised by a log-normal *probability density function*, which means that the magnitude measured in decibel has a Gaussian probability density function. $r_0(t)$ is sometime referred to as a *multipath* or *Rayleigh fading*, because it follows a Rayleigh distribution. Figure 3.4 highlights these two effects.

3.3 Large-scale fading

Large-scale fading propagation models are used to predict the mean signal strength for an arbitrary transmitter-receiver (T-R) separation distance (large-scale models).

The free space propagation model

This is an ideal propagation model used to compute the received signal strength when there is a direct line of sight between a transmitter and a receiver unit, at distance d between them. The power received in free space is given by the Friis transmission equation 3.5, where P_t is the transmitted power, G_t is the transmitter antenna's gain, G_r is the receiver antenna's gain,

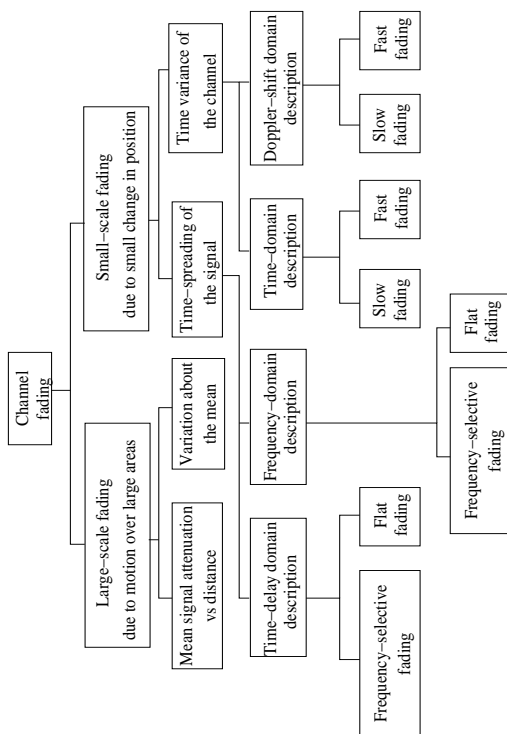


Fig. 3.3. Channel fading types

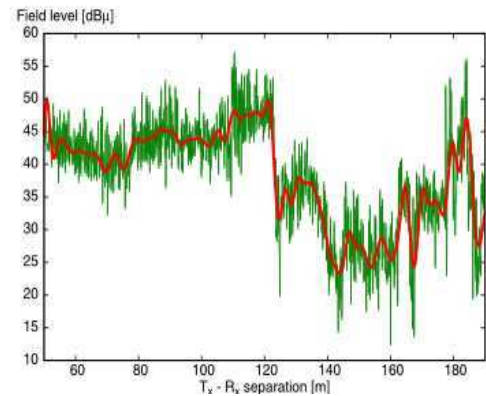


Fig. 3.4. Small-scale fading (grey line) and large-scale fading (black line)

L is the system loss factor (for example filter losses, antenna losses etc...) and $\left(\frac{4\pi d}{\lambda}\right)^2$ is called *path loss* or *free space loss* (L_{fs}).

$$P_r(d) = \frac{P_t G_t G_r \lambda^2}{(4\pi)^2 d^2 L} \quad (3.5)$$

The antenna gain is given by

$$G = \frac{4\pi A_e}{\lambda^2} \quad (3.6)$$

where A_e is the effective size of the antenna. Formula 3.5, expressed in dB is:

$$L_{fs}|_{dBm} = 10 \log \left(\frac{P_t G_t G_r}{P_r L} \right) = 20 \log \left(\frac{4\pi d}{\lambda} \right) \quad (3.7)$$

From now on we assume $L = 1$. The path loss is defined as the difference between the effective transmitted power and the received power, which includes the effects of the antenna gains.

The Log-normal shadowing model

Theoretical and measurement-based models indicate that the average received signal power decreases with the distance raised to some exponent. In the free-space model, the exponent is 2, that is, the received power decreases as the

square of distance. In the *log-normal path loss propagation model* the average path loss for an arbitrary T-R couple is expressed as a function of the distance d by using a *path loss exponent*, independently of the presence of a direct line of sight between the transmitter and the receiver units.

$$\bar{L}_p(d) \propto \left(\frac{d}{d_0}\right)^n \quad (3.8)$$

where n is the path loss exponent that indicates the rate at which the path loss increases with the distance, and d_0 called *free space close-in reference distance* [2]. It is important to select a value of d_0 that is appropriate for the propagation environment. In large cellular systems, 1 Km and 1 mile reference distances are commonly used, whereas in microcellular systems much smaller distances are used. The reference distance should always be in the far field of the antenna ($d_0 > 2D^2/\lambda$, where D is the largest antenna dimension), so that near-field effects are not considered in the reference path loss. The value of n depends on the specific propagation environment. Table 3.1 shows the values of the path loss exponent n for different environments [2].

Table 3.1. Path loss exponents for different environments.

Environment	Path Loss Exponent, n
Free space	2
Urban area cellular radio	2.7 to 3.5
Shadowed urban cellular radio	3 to 5
In buildin, line of sight	1.6 to 1.8
Obstructed in building	1.6 to 1.8
Obstructed in factories	1.6 to 1.8

The path loss expressed in dB is:

$$\bar{L}_p(d) \Big|_{dB} = L_{fs}(d_0) \Big|_{dB} + 10n \log\left(\frac{d}{d_0}\right) \quad (3.9)$$

In 3.9 the first part is the path loss at reference distance d_0 , and the second part is due to the particular environment where the measure occurs. Measurements have shown that the path loss $L_p(d)$ is a random variable which has a log-normal distribution around a mean value $\bar{L}_p(d)$ [6]. The path loss $L_p(d)$ (in dB) can be expressed in terms of the mean $\bar{L}_p(d)$ plus a random variable X_σ , which has a zero-mean and a Gaussian distribution [2].

$$L_p(d) \Big|_{dB} = L_{fs}(d_0) \Big|_{dB} + 10n \log\left(\frac{d}{d_0}\right) + X_\sigma \Big|_{dB} \quad (3.10)$$

Formula 3.10 is a *log-normal shadowing* and describes the random shadowing effect which occurs in a large number of measurements of the received

power in a large-scale model at the same distance d between transmitter and receiver but with different propagation paths. Figure 3.5 shows typical path losses measured in German cities [7].

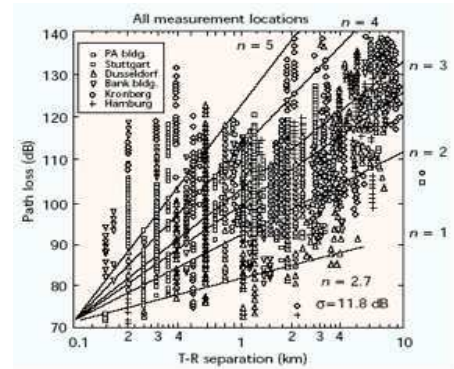


Fig. 3.5. Path loss vs. distance measured in several German cities [7]

3.4 Small-scale fading

The small scale fading is used to describe short-term, rapid amplitude fluctuations of the received signal during a short period of time. This fading is caused by interference between two or more multipath components that arrive at the receiver while the mobile travels a short distance (a few wavelengths) or over a short period of time. These waves combine vectorially at the receiver, and the resulting signal can rapidly vary in amplitude and phase.

Different channel conditions can produce different types of small-scale fading. The type of fading experienced by the mobile depends on the following factors:

Multipath propagation

The presence in the channel of a reflective surface and object that cause scattering creates a variation in amplitude, phase, and time delay. The random phase and amplitude of the different multipath components cause fluctuation in the signal strength.

Speed of the mobile

The relative motion between the transmitter and the receiver causes a random frequency modulation, because of the effect of different Doppler shifts on each of the multipath components.

Speed of surrounding objects

The surrounding environment is not important in a wireless channel only because it changes the multipath components, but also because of varying Doppler shifts for all multipath components.

Bandwidth of the signal

If the transmitted signal bandwidth is greater than the flat-fading bandwidth of the multipath channel, the signal at the receiver antenna is distorted.

There are two different causes of small-scale fading:

- The time spreading of the signal
- The time-variant behaviour of the channel due to motion of the mobile unit

These two aspects are analyzed respectively in sections A and B. Section C draws the conclusions.

Small-scale fading effects due to multipath Time Delay Spread

Time dispersion due to multipath causes the transmitted signal to undergo either flat or frequency selective fading. These two types of fading are analyzed in subsections A.1 and A.2 respectively.

Time delay spread: Flat Fading

Small-scale fading is defined as being flat or non-selective if the received multipath components of a symbol don't extend beyond the symbol's time duration. In other words, a channel is said to be subject to flat fading when all the received multipath components of a symbol arrive within the symbol's time duration. In a flat-fading channel ISI (inter-symbol interference) is absent; therefore such a radio channel has a constant gain and a linear phase response over a bandwidth which is greater than the bandwidth of the transmitted signal (3.6).

In a flat-fading channel the spectral characteristics of the transmitted signal are preserved at the receiver, and the channel does not cause any distortion due to the time dispersion. However, the strength of the received signal changes with time due to slow gain fluctuations caused by multipath. Flat-fading channels are also known as amplitude varying channels and are sometimes referred to as narrowband channels, as the bandwidth of the applied signal is narrow with respect to the channel bandwidth. In a flat-fading channel, the following hold true:

$$B_s \ll B_c \text{ or } T_s \gg \sigma_\tau \quad (3.11)$$

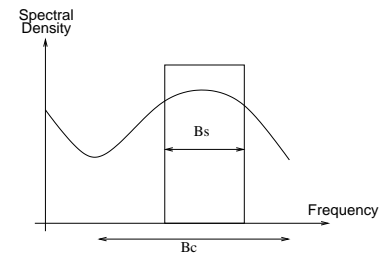


Fig. 3.6. Flat-fading case: B_s is the signal bandwidth, and B_c is the coherence bandwidth

where B_s is the bandwidth of the transmitted signal, B_c is the *coherence bandwidth* of the channel, T_s is the symbol's period, and σ_τ is the *rms delay spread* of the channel. These parameters are described in the section at the end of the chapter. Figure 3.7 shows how the gain varies for the received signal, but its spectrum is preserved. In the flat-fading channel, the symbol's duration time is much larger than the multipath time delay spread of the channel.

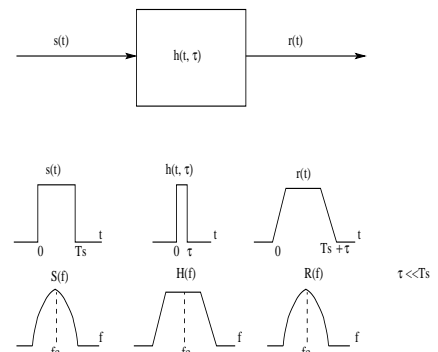


Fig. 3.7. Flat-fading channel characteristics

Time delay spread: Frequency-Selective Fading

If, opposite to the flat fading case illustrated in the previous subsection, the channel has a constant gain and a linear phase response over a bandwidth that is much smaller than the bandwidth of the transmitted signal, this channel causes *frequency selective fading* on the received signal. Under these conditions the channel impulse response has a delay spread which is greater than the symbol period. When this occurs, the received signal includes multiple versions of the same symbol, each attenuated (faded) and delayed. As a consequence, the received signal is distorted, that is, the channel produces ISI (inter-symbol interference). In the frequency domain, this means that certain frequency components in the received signal spectrum have higher gain than others (Fig. 3.8). For frequency selective fading, the spectrum of the received signal has a bandwidth that is greater than the coherence bandwidth B_c ; in other words, the channel becomes frequency selective when the gain is different for different frequency components of the signal.

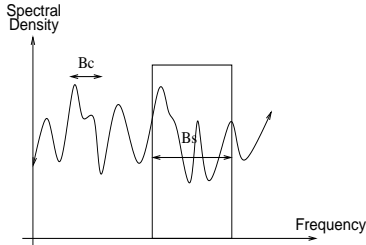


Fig. 3.8. Frequency selective fading case: B_s is the signal bandwidth, and B_c is the coherence bandwidth

To summarize, a signal undergoes frequency selective fading if

$$B_s > B_c \text{ or } T_s < \sigma_\tau \tag{3.12}$$

Figure 3.9 illustrates the characteristics of frequency selective fading channel. The spectrum $S(f)$ of the transmitted signal has a bandwidth greater than the coherence bandwidth B_C of the channel; in the time domain, the transmitted symbol is much smaller than the multipath time delay spread, which causes time dispersion.

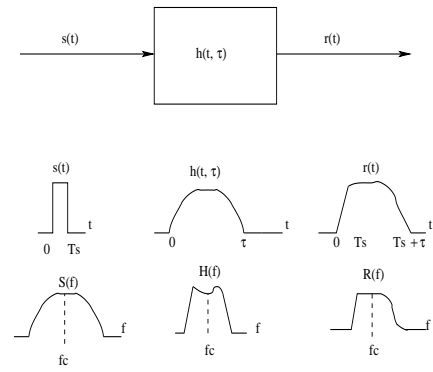


Fig. 3.9. Frequency selective fading channel characteristics

Small-scale fading effects due to Doppler Spread

While the multipath effects described in the previous section, depend on the static geometric character of the environment surrounding the transmitter and the receiver, the Doppler spread is caused by movements in the environment. In a fast fading channel, the channel impulse response changes rapidly within the symbol duration. If the coherence time (see section at the end of this chapter) is shorter than the symbol of the transmitted signal, then the signal undergoes fast fading. In the frequency domain, signal distortion due to fast fading increases with increasing Doppler spread relative to the bandwidth of the transmitted signal. Therefore, the signal undergoes fast fading if

$$T_s > T_c \text{ or } B_s < B_D \tag{3.13}$$

where T_c and B_D are the coherence time and the Doppler bandwidth (the width of the Doppler power spectrum), respectively (see section at the end of this chapter). Note that in the case of a frequency-selective, fast fading channel, the amplitude, the phase and the time delay of each of the multipath components are different for each component.

In a slow fading channel, the channel impulse response changes at a rate much slower than the transmitted signal. In this case, the channel can be assumed static over several symbol intervals. In the frequency domain the Doppler spread is much less than the bandwidth of the signal. To summarize, a signal undergoes slow fading if

$$T_s \ll T_c \text{ or } B_s \gg B_D \tag{3.14}$$

A classic example of fast fading channel was the Morse code signaling used in the HF frequency band, which exhibited a very low data rate.

3.5 Conclusion

In the small-scale fading two different dimensions are distinguished: multipath time delay spread and Doppler spread, as depicted in Figure 3.10 (where BW stands for “bandwidth”). Fading based on multipath time delay spread can be *flat fading* or *frequency selective fading*. Flat fading is present if the bandwidth of the signal is smaller than the bandwidth B_C of the channel, or equivalently if the delay spread is smaller than the symbol period. Frequency selective fading is present otherwise. Fading based on Doppler spread can be *fast fading* or *slow fading*. Fast fading is present if the coherence time T_C is smaller than the symbol period, or equivalently if the channel variation is faster than the baseband signal variation. Slow fading is present otherwise.

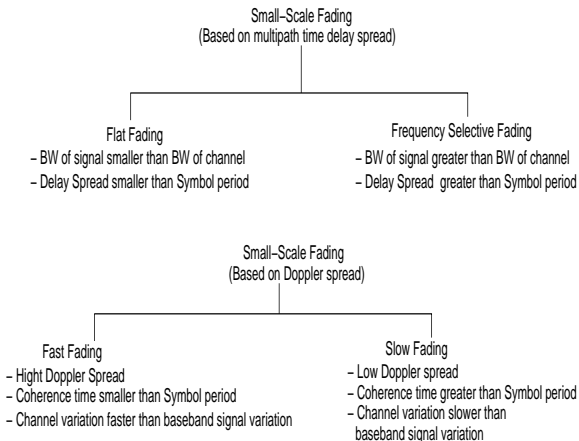


Fig. 3.10. Type of small fading

The relationship between the various multipath parameters and the type of fading experienced by the signal are summarized in Figure 3.11, where four regions are distinguished.

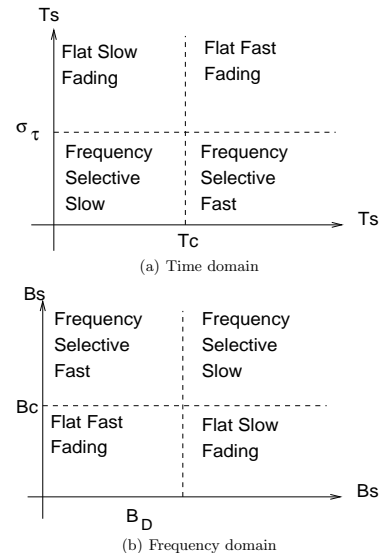


Fig. 3.11. Type of small-scale fading types of experienced by a signal from the viewpoint of (a) symbol period, (b) baseband signal bandwidth.

It is important not to confuse the terms *fast* and *slow fading* with the terms *large-scale* and *small-scale fading*. It should be emphasized that fast and slow fading deal with the relationship between the time rate of change in the channel and the transmitted signal, and not with propagation path loss models (large-scale or small-scale fading). The IEEE802.11 standard specifies the physical layer that must be used in Wireless LAN in 2.4 GHz Industrial-Scientific-Medical band, and then fixes the symbol period ($T_s=100$ ns). In Table 3.2, different types of *rms delay spread* for indoor radio channels are distinguished (in the order of nanoseconds). Therefore with these values of

rms delay spread and symbol period, the channel is flat because the delay spread is greater than the symbol period ($T_s > \sigma_\tau$). Since the value of the coherence time is estimated calculating the maximum Doppler frequency, we must choose the velocity of the mobile nodes, for example 100 Km/h and 2 m/s. With these velocities the maximum shift frequency is given by

$$f_{max} = \frac{v}{c_0} f_0 = \begin{cases} 224Hz & v = 100\text{Km/h} \\ 16Hz & v = 2\text{m/s} \end{cases}$$

the coherence time, that are inversely proportional to the Doppler spread is given by

$$T_C \approx \frac{1}{f_{max}} = \begin{cases} 4.46\text{ms} & v = 100\text{Km/h} \\ 62.5\text{ms} & v = 2\text{m/s} \end{cases}$$

Since the coherence time is greater than the symbol period ($T_s \ll T_C$), the channel would manifest slow fading effects. Analogous reasons can be made for the IEEE802.11g standard where the symbol's period T_s is 4ms, in this case the channel would manifest flat and slow fading effect.

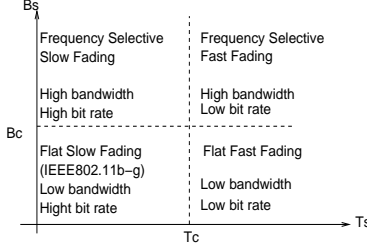


Fig. 3.12. Types of small-scale fading for the IEEE802.11 signal

Figure 3.12 shows the above description, as we can see, for an high bandwidth relative to coherence bandwidth the transmitted signal undergoes frequency selective, while for low bit rate relative to coherence time the signal undergoes fast fading.

3.6 Parameters of the mobile multipath channel

3.6.1 Time dispersion

The *mean excess delay*, *rms delay spread*, and the *maximum excess delay spread* (X dB) are parameters that can be calculated from the power profile.

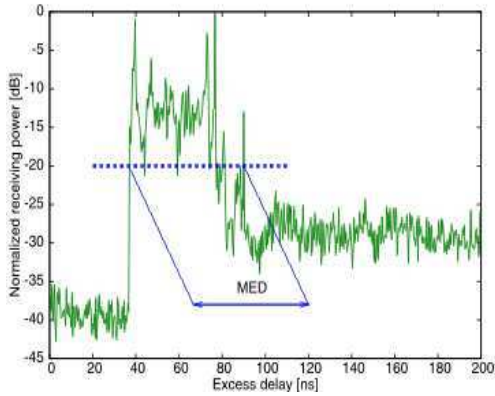


Fig. 3.13. Maximum excess delay

3.6.2 Coherence bandwidth

Analogous to the delay spread parameters in the time domain, the coherence bandwidth is used to characterize the channel in the frequency domain. The *coherence bandwidth* is a statistical measure of the frequency range where the channel can be considered "flat". In this frequency range two components pass with highly correlated gain and linear phase. Two sinusoids with frequency separation greater than B_C are affected quite differently by the channel. If the coherence bandwidth is defined as the frequency interval over which the autocorrelation of the channel's complex frequency transfer function is above 0.9, then the coherence bandwidth is approximately [16]

$$B_C \approx \frac{1}{50\sigma_\tau} \quad (3.18)$$

Most commonly, the coherence bandwidth is defined as the bandwidth over which the correlation function is at least 0.5; in this case we have [2]

$$B_C \approx \frac{1}{5\sigma_\tau} \quad (3.19)$$

An exact relationship between coherence bandwidth and rms delay spread does not exist. A simple exercise for clarification about flat and selective fading is derived in the last subsection of this section.

The *mean excess delay* is the first moment of the power delay profile, and is defined as

$$\bar{\tau} = \frac{\sum_k a_k^2 \tau_k}{\sum_k a_k^2} = \frac{\sum_k P(\tau_k) \tau_k}{\sum_k P(\tau_k)} \quad (3.15)$$

where a_k is the amplitude of the k th-component which arrives at the receiver, and $P(\tau_k)$ is the power of the k th-component. The *rms delay spread* is the square root of the second moment of the power delay profile, and is defined as

$$\sigma_\tau = \sqrt{\overline{\tau^2} - (\bar{\tau})^2} \quad (3.16)$$

where

$$\overline{\tau^2} = \frac{\sum_k a_k^2 \tau_k^2}{\sum_k a_k^2} = \frac{\sum_k P(\tau_k) \tau_k^2}{\sum_k P(\tau_k)} \quad (3.17)$$

Typical values of *rms delay spread* are shown in Table 3.2, which shows different values for indoor radio channels.

Table 3.2. Typical values of mean delay spread and maximum delay spread.

Mean delay spread [ns]	Maximum delay spread [ns]	Reference	Remarks
40	120	[8]	Large building
40	95	[9]	Office building
40	150	[10]	Office building
60	200	[11]	Shopping center Laboratory
106	270		
19	30	[12]	Office building: simple room only
20	65	[13]	Office
30	75		Cantine
105	170		Shopping center
30	56	[14]	Office building
25	30	[15]	Office building: single room only

The *maximum excess delay* is defined as the time delay during which the multipath energy falls to X dB below the maximum (Fig. 3.13).

It is important to underline that the values $\bar{\tau}$, σ_τ and σ_τ depend on the choice of noise threshold. The *noise threshold* is the threshold used to differentiate between the noise and the received multipath components. If the noise threshold is set too low, the noise is seen like a multipath component, and $\bar{\tau}$, σ_τ and σ_τ increase.

3.6.3 Doppler spread and coherence time

While the delay spread and coherence bandwidth are parameters which describe the time dispersion nature in the channel due to its geometric, static characteristics, the Doppler spread and coherence time parameters describe the time varying nature of the channel in the small-scale region, caused by the relative movements between transmitter and receiver. To understand how Doppler spread can cause frequency dispersion at the receiver, we see how a channel behaves when a pure sinusoidal at frequency f_C is transmitted. The received signal has spectral components in the range $f_C + f_D$ to $f_C - f_D$, where f_D is the Doppler shift. The coherence time T_C is the time domain dual of the Doppler spread; it is a measure of the time during which the channel can be assumed non to vary.

In the Clark model, Doppler spread and coherence time are defined as being inversely proportional each other:

$$T_C = \frac{1}{f_{max}} \quad (3.20)$$

where f_{max} is the maximum Doppler shift (equation 2). Using a different model, in [17] the coherence time is defined as the time over which the autocorrelation of the transfer function is above 0.5; then the coherence time is approximately defined as

$$T_C \approx \frac{9}{16\pi f_{max}} \quad (3.21)$$

References

1. Lee, W.C.Y., "Elements of cellular mobile radio system," IEEE Trans. Vehicular Technol., V-35(2), 48-56, May 1986.
2. Rappaport, T.S., "Wireless Communications," Prentice-Hall; Upper Saddle River, New Jersey, Chs. 3 and 4, 1996.
3. Mokhtari H, Lazaridis P (1999) "Comparative study of lateral profile knife-edge diffraction and ray tracing techniques using GTD in urban environment," IEEE Trans on Vehicular Technology, vol 48, no 1, pp 255-261
4. Leberz, M, et.al. "A versatile wave propagation model for the VHF/UHF range considering three-dimensional terrain," IEEE Trans. on Ant. and Prop. 40(10), pp. 1121-1131, Oct. 1992.
5. Tameh, E K, et.al. "A 3-D integrated macro and microcellular propagation model, based on the use of photogrammetric terrain and building data," In Proceedings of IEEE VTC'97, vol. 3, 1997, pp. 1957-1961, Phoenix, USA, 1997.
6. Cox, D.C., Murray, R., and Norris, A., "800MHz Attenuation measured in and around suburban houses," Bell Laboratory Technical Journal, 67(6), 921-954, Jul.-Aug. 1984.
7. Scott Y. Seidel, Theodore S. Rappaport, Sanjiv Jain, Michael L. Lord, Rajendra Singh, 'Path Loss, Scattering, and Multipath Delay Statistics in Four European Cities for Digital Cellular and Microcellular Radiotelephone', IEEE Transactions on vehicular technology, Vol 40, No. 4, November 1991.
8. D.M.J. Devasirvatham, 'Multi-Frequency Propagation Measurements and Models in a Large Metropolitan Commercial Building for Personal Communications', IEEE PIMRC '91, September 23-25, London, pp. 98-103.
9. D.M.J. Devasirvatham, 'Time Delay Spread Measurements at 850 MHz and 1.7 GHz inside a Metropolitan Office Building', Electronics Letters, February 2, 1989, pp. 194-196.
10. D.M.J. Devasirvatham, M.J. Krain and D.A. Rappaport, 'Radio Propagation Measurements at 850 MHz, 1.7 GHz and 4 GHz inside two dissimilar office buildings', Electronics Letters, vol. 26, no. 7, March 29, 1990, pp. 445-447.
11. I.T. Johnson and E. Gurdenelli, 'Measurements of Wideband Channel Characteristics in Cells Within Man Made Structures of Area Less Than 0.2 km²', COST 231 TD(90)083.
12. J. Lahteenmaki, 'Indoor Measurements and Simulation of Propagation at 1.7 GHz', COST 231 TD(90)084.
13. P.C. Anderson, O.J.M. Houen, K. Kladaakis, K.T. Peterson, H. Fredskild and I. Zarnoczay, 'Delay Spread Measurements at 2 GHz', COST 231 TD(91)029.
14. R.J.C. Bultitude, S.A. Mahmoud and W.A. Sullivan, 'A Comparison of Indoor Radio Propagation Characteristics at 910 MHz and 1.75 GHz', IEEE Journal on Selected Areas in Communications, vol. 7, no. 1, January 1989, pp. 20-30.
15. P. Nobles and F. Halsall, 'Delay Spread and Received Power Measurements Within a Building at 2 GHz, 5 GHz and 17 GHz', IEE Tenth International Conference on Antennas and Propagation, Edinburgh, April 14-17, 1997.
16. Lee, W.C.Y., Mobile Cellular Telecommunications System, McGraw Hill Publications, New York, 1989
17. Steele, r. ed., Mobile Radio communications, IEEE Press, 1994.

4

Propagation models

4.1 Outdoor path-loss models

Path-loss is a measure of the average attenuation suffered by a transmitted signal when it arrives at a receiver, after traversing a path of several wavelengths. Model for characterizing the path-loss can be classified in two main groups: statistical models, based on the characterization of the received signal, and deterministic models, based on physical parameters that describe the environment (terrain profile, position of buildings, used construction materials, and so on). The former models are easier to implement but also less sensitive to the geometry of the environment. The latter models are more complex, require more computational effort, but they are much more accurate. Other models exist, derived from measurement campaign for different situations. When propagation is considered in an outdoor environment, three main areas are taken into account: urban, suburban, and rural areas. The terrain profile, the presence of trees, buildings, moving cars, wind, and other possible obstacles have a great impact on the model characteristics. The outdoor mobile radio channel differ from the indoor radio channel mainly due to the distance covered by the signal, which is smaller in an indoor environment, and to the variability of the environment, which is much greater in an outdoor environment. Moreover, the variation in the fading rate and the type of interference have a strong impact in the characterizing the difference between the two types of signals. The delay spread in the indoor radio channel is typically smaller than the one in the outdoor channel; moreover, movements inside a building are often smaller than movements of vehicles in an urban area. Therefore, the change in channel characteristics is slower in time. The interference types are different because the propagation within the buildings is strongly influenced by local features, such as construction materials and type of building. The field of indoor radio propagation is relatively new, with the first wave of research occurring in the early 1980. Cox [1] at AT&T Bell Laboratories and Alexander [2] at British Telecom were the first to carefully study indoor path-loss in and around a large number of houses and office

54 4 Propagation models

buildings. From them on work has been done on indoor propagation and on the impact of the building structures [3][4][5][6]. In general, indoor channels may be classified either as LOS or obstructed, with varying degrees of clutter [7]. Some of the recently emerged indoor path-loss models are the Log-distance path loss model and the attenuation factor model, described by Seidel in [6].

4.1.1 Most popular statistical outdoor path-loss models

When the radio communications take place over irregular terrain, the terrain profile, with the presence of trees, buildings and other obstacles, changes the estimation of the path loss. Many models exist that are adequate to predict the path loss, and the following methods widely vary in their approach and accuracy.

The Longley-Rice model [8][9] is applicable to point-to-point communication systems in the frequency range from 40 MHz to 100 GHz, over different kinds of terrain. This model is particularly useful in predicting propagation losses over irregular terrain for which knife-edge diffraction losses are significant. The Longley-Rice model is also available as a computer program [10] of the Institute for Telecommunication Sciences is a statistical / semi empirical model of tropospheric radio propagation for low and high-altitude scenarios, respectively, in the frequency range of 0.02-20 GHz. This program is restricted to frequencies above 20 MHz because "sky" and "ground" wave propagation paths, which can be dominant propagation paths at frequencies less than 20 MHz, are not included in this program. This program is restricted to frequencies less than 20 GHz because the empirical database does not include absorption and refractivity of the atmosphere or ground at wavelengths shorter than 1 cm.

This program uses an empirical database to statistically weigh knife-edge diffraction losses with losses from multipath interference and smooth-spherical earth diffraction.

The program may be used either with terrain profiles that are representative of median terrain characteristics for a given area (the area- prediction mode) or with detailed terrain profiles for actual paths (the point-to-point mode).

There have been many modifications and corrections to the Longley-Rice model since its original publications. One important modification deals with radio propagation in urban areas, and this is particularly relevant to mobile radio. This modification introduces an excess term as an allowance for the additional attenuation due to urban clutter near the receiving antenna. This extra term, called the urban factor (UF), has been derived by comparing the predictions in the original Longley-Rice model with those obtained by Okumura.

One shortcoming of the Longley-Rice model is that it does not provide a way of determining corrections due to environmental factors in the immediate

vicinity of the mobile receiver, or to consider correction factors in order to account for the effects of buildings and foliage.

In 1965 Okumura carried out extensive measurements around Tokyo in the frequency range from 150 MHz to 2 GHz and published the results of his measurements as curves [11], given the median attenuation relative to the free space L_F , in an urban area, with a base station height h_t of 200 meters and a mobile antenna height h_r of 3 meters. These curves were plotted as a function of the frequency and the distance from the base station. The Okumura's model is used for finding out path loss for distances from 1 to 100 Km. The model is described by:

$$L = L_F + A_{mu}(f, d) - G(h_t) - G(h_r) - G_{AREA} \quad (4.1)$$

where L is the average propagation loss in dB, $A_{mu}(f, d)$ is the median attenuation relative to free space, L_F the free space propagation loss, $G(h_t)$ is the base station antenna height gain factor, $G(h_r)$ is the mobile antenna gain factor, and G_{AREA} is the gain due to the type of environment. Okumura's model is entirely based on measured data, and does not provide any analytical explanation.

The Hata model (1980) is an empirical formulation of the curves provided by Okumura, approximated through analytical formulations [12]. Hata presents the urban area path loss and provides a correction factor to the formula for applying it to other situations. The formula for the median path loss in urban areas is given by

$$L(\text{urban}) = 69.55 + 26.16 \log f_C - 13.82 \log h_t - a(h_r) + \dots \\ \dots + (44.9 + 6.55 \log h_t) \log d \quad (4.2)$$

where the path loss is expressed in dB, f_C is the frequency in the range 150-15000 MHz, h_t is the effective transmitter height ranging from 30 to 200 meters, h_r is the effective receiver antenna height ranging from 1 to 10 meters, d is the distance between transmitter and receiver in Km, and $a(h_r)$ is the correction factor for the effective receiver antenna height, which depends on the environment. For a small or medium city, the correction factor is given by

$$a(h_r) = (1.1 \log f_C - 0.7) * h_r - (1.56 \log f_C - 0.8) \quad (4.3)$$

while, for a large city, it is given by

$$a(h_r) = \begin{cases} 8.29(\log 1.54 h_r)^2 - 1.1 & \text{for } f_C \leq 200 \text{ MHz} \\ 3.2(\log 11.75 h_r)^2 - 4.97 & \text{for } f_C \geq 400 \text{ MHz} \end{cases}$$

The European CO-operation for Scientific and Technical research (EURO-COST) formed the COST-231 working committee to develop an extended version of the Hata model. COST-231 proposed the following formula to extend Hata's model to 2 GHz [13].

where $a(h_r)$ is defined in equations 4.3 and 4.4, and

$$C_M = \begin{cases} 0 \text{ dB} \\ 3 \text{ dB} \end{cases}$$

where the value of 0 is for medium-sized city and suburban areas, and 3 for metropolitan centers. The COST-231 extension of the Hata model is restricted to the following ranges of parameters:

$$f : 1500 \text{ MHz to } 2000 \text{ MHz} \\ h_t : 30 \text{ m to } 200 \text{ m} \\ h_r : 1 \text{ m to } 10 \text{ m} \\ d : 1 \text{ Km to } 20 \text{ Km}$$

The Walfisch and Bertoni model [14] and [15] considers the impact of rooftops and building heights by using diffraction in order to predict average signal strengths at street level. The model considers the path loss, S , to be a product of three factors:

$$S = L_0 L_{rts} L_{ms} \quad (4.4)$$

where L_0 represents the free space path loss between isotropic antennas, at a distance R :

$$L_0 = \left(\frac{4\pi R}{\lambda} \right)^2 \quad (4.5)$$

The path loss, expressed in dB, is given by

$$S|_{\text{dB}} = L_0 + L_{rts} + L_{ms} \quad (4.6)$$

where L_{rts} represents the *rooftop to street diffraction and scatter loss*, and L_{ms} indicates the multi-screen diffraction loss due to rows of buildings [1].

This model was considered for ITU-R (International Telecommunication Union - Radio communications) use in the IMT-2000 (International Mobile Telecommunications-2000) standards activities [17, 18]. studies found that path loss characteristics in LOS (line of sight) environment are dominated by interference between the direct path and the ground-reflected path [2], as in the two-ray model, in the following referred to as *2RM* (see Fig. 4.1) [2, 20]. 2RM assumes that only two paths exist between the transmitter and the receiver: the LOS, and a ground reflected propagation path. The model is based on geometric optics, and it is commonly used to predict the large-scale signal strength for mobile radio channels [30]. This model is valid under the condition that $d \gg \sqrt{h_t h_r}$ [32]; the meaning of h_t and h_r is explained in Fig. 4.1, which describes the model.

The 2RM is described by equation :

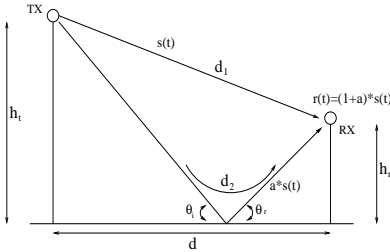


Fig. 4.1. 2-ray ground reflection model.

$$L_d|_{\text{dB}} = 10 \log_{10} \left(\frac{(\lambda)^2 G_t G_r}{(4\pi)^2 L} \cdot \left| \frac{1}{\Gamma} + \Gamma \frac{e^{j\theta_\Delta}}{d_2} \right|^2 \right), \quad (4.7)$$

$$\text{where } d_1 = \sqrt{(h_t - h_r)^2 + d^2}, \quad d_2 = \sqrt{(h_t + h_r)^2 + d^2}.$$

Γ is the reflection coefficient, which for non-conductive, non-ferromagnetic materials is a real number between -1 and 1, different for parallel (horizontal) and perpendicular (vertical) polarisations:

$$\Gamma_{\text{hor}} = \frac{\epsilon_r \sin(\theta_i) - k}{\epsilon_r \sin(\theta_i) + k} \quad \Gamma_{\text{ver}} = \frac{\sin(\theta_i) - k}{\sin(\theta_i) + k}$$

$$\text{where } k = \sqrt{\epsilon_r - \cos^2(\theta_i)}$$

Typical values for the ground relative permittivity ϵ_r are 4, 15, 25, while polarisation of the radio wave may change significantly due to reflection or scattering process [32]. G_t , G_r are the antenna gains of the transmitter and the receiver respectively, L is the system loss. θ_Δ is the phase difference due to the difference of the direct and reflected path lengths, and d is distance between transmitter and receiver. This model has been used for LOS propagation both in rural [2] and in urban environments [3, 22, 28]. In [3] the authors presented measurements in an urban area of Dresden, Germany and found that in LOS environment, the guiding effect reduces with increasing distance due to scattering from vehicular traffic, building and street irregularities which are expected to be significant attenuation mechanisms, particularly for rays which are reflected from walls. Hence, the attenuation effect due to obstacles increasingly compensates the guiding effect with large distance. In [22] and [29] the authors showed the results of a radio propagation study carried out in central Tokyo, Japan and provided clear evidence that the radio propagation follows the characteristics predicted by a theoretical two path model. This

model is characterised by a *break point* that separates the different properties of propagation in near and far regions relative to the transmitter; before the break point, the mean attenuation is close to the free-space path loss $1/d^2$, while after that point it decreases as $1/d^4$.

A good approximation of this behaviour is the *double regression model* suggested by [22]. The authors propose a model with two slopes for approximating the 2RM. In particular, they described the existence of a transition region where the break point b can be placed:

$$\frac{\pi h_t h_r}{\lambda} < b < \frac{4\pi h_t h_r}{\lambda}, \quad (4.8)$$

where h_t is the transmitter antenna height, h_r is the receiver antenna height, and λ is the wavelength of the radio signal. The *two-ray CMU Monarch model* used in ns-2 [4] adopts the double regression model, with the break point set to $4\pi h_t h_r / \lambda$.

For the wideband model, Feuerstein used a 20 MHz-pulsed transmitter at 1900 MHz to measure the path loss, outage, and delay spread in typical micro-cellular system. Using base station antenna heights (h_t) of 3.7 m, 8.5 m, and 13.3 m, and a mobile receiver with antenna height (h_r) of 1.7 m above ground, statistics for path loss, multipath, and coverage area were inferred from extensive measurements in LOS and obstructed (OBS) environments [30]. This work revealed that a 2-Ray ground reflection model is a good estimate for path loss in LOS, and a simple log-distance path loss model holds well for OBS environments.

Table 4.1 summarizes the characteristics of the considered outdoor propagation models. In [31] a comparison is made among various models of path loss.

4.1.2 Most popular outdoor path-loss deterministic models

Deterministic models for path-loss are based on the theory of electromagnetic wave propagation, and on a collection of many details relevant the environment. An overview of these methods is not in the scope of this paper; we just list some of the most popular/recent ones.

- Ray-Tracing, which is a technique based on geometrical optics that can easily used as an approximate method for estimating levels of high frequency electromagnetic fields [33, 34]. Two types of Ray-Tracing methods are used: the image method, and the Brute-Force Ray Tracing method.
- FDTD (Finite Difference Time Domain) method [35, 36]
- moment-method model [37]
- artificial neural-network model [38, 39]
- vector parabolic-equation model [40]
- fast far-field approximation model [41]
- the waveguide model [42]
- the Boltzmann model [43]

Table 4.1. Characteristics of the considered outdoor propagation models.

Models	Frequency range	Characteristics
Longley-Rice	40MHz-100GHz	- Path loss is predicted by using the path geometry of the terrain profile. - Geometric optics techniques are used to predict signal strengths within the radio horizon. - Diffraction losses over isolated obstacles are estimated by using the Fresnel-Kirchoff knife-edge model.
Okumura	150MHz-2GHz	- One of the most widely used models for signal prediction in urban areas. - Okumura published the results of his extensive measurement campaign as curves, given the median attenuation relative to the free space with a base station antenna height of 200 meters and a mobile antenna height of 3 meters.
Hata	150MHz-1.5GHz	- Empirical formulation of the curves provided by Okumura, approximated through analytical formulations. - Hata presents the urban area path loss and supplies a correction factor for applying his formula to other situations.
Extention to Hata	1.5GHz-2GHz	- COST-231 proposed a formula to extend Hata's model to 2 GHz.
Walfisch-Bertoni		- This model considers the impact of rooftops and building heights by using diffraction in order to predict average signal strengths at street level.
2RM		- Only two paths exist between transmitter and receiver.
Double regression		- Model with two slopes: -20 dB/dec before the break point, -40 dB/dec after that.
Wideband	1.9 GHz	- 2RM is a good estimate for path loss in LOS log-distance path loss model performs well for OBS environments.

4.1.3 State of Art of the path loss models

In [44] the authors present empirical path-loss formulas for microcells in low-rise and high-rise environments; they are derived from measurements con-

ducted in the San Francisco Bay area. Applicability of path-loss formulas is specified in terms of the restricted range of formula parameters. It was shown from the formula expressions that the slope indexes of Hata model and the single non-LOS formula showed good agreement with elevated antenna heights in a typical low-rise environment. In [45] authors summarize their 22 multiple-input multiple-output (MIMO) fixed wireless outdoor propagation measurements at 2.48 GHz conducted in the suburban residential areas of San Jose, California. They report on various channel characteristics such as path loss, Ricean K-factor, cross-polarization-discrimination (XPD), and channel capacity. They present simple models for these characteristics, focusing on excess loss dependency and, derived from that, the variation with distance. Also, they introduce an idea for a generalized MIMO channel model based on these modelled channel characteristics and the correlation properties between them. Hashim and Stavrou in [46] demonstrated that movement of vegetation structures introduces an adverse environment for high frequency radiowave propagation. They examined a series of vegetation scattering measurement campaigns during various wind conditions. The measurements were divided into controlled and outdoor environments. The controlled environment measurements were conducted in an anechoic chamber at 0.9, 2, 12 and 17 GHz. The outdoor measurements were carried out at 1.8 GHz and involved in recording of a transmitted signal originating from an existing digital cellular system (DCS-1800) base station. Analysis demonstrates that the received signal behaviour is highly wind-dependent, especially when the environment is changing from calm to a windy condition. The signal fast-fading is found to be Rician distributed, and an empirical model of the k-factor variation over wind speed is also presented. In [47] the authors describe the type of signals that occur in various environments and the modelling of the propagation parameters. Some key parameters and the relevant measurements are discussed in the different wireless environments treated.

4.2 Indoor Propagation Models

There is a great interest in characterizing the radio communications channel inside a building. The indoor channel differs from the outdoor channel because of the variation in the fading rate and the type of interference. The delay spread in the indoor radio channel is typically smaller than the delay spread in the outdoor channel; moreover, the movement inside a building is often smaller than the movement of vehicles in an urban area. Therefore, the change in channel characteristics is slower in time. The interference types are different because the propagation within the buildings is strongly influenced by local features, such as the construction materials, and the building type.

4.2.1 Log-distance Path Loss Model

In indoor environments the average large-scale path loss is expressed as a function of Transmitter-Receiver separation and path loss exponent n . Variations in environmental clutter at different locations having the same T-R separation distance is not accounted for in equation 3.9. This leads to measured signals which are vastly different than the average value predicted by 3.9. To account for the variations described above the equation 3.9 is modified as in 3.10. Notice that this equation is identical in form to the log-normal shadowing model. Typical values for various buildings are provided in [32].

4.2.2 Attenuation Factor Model

An in-building propagation model that includes the effect of building type as well as the variation caused by obstacles two additional terms are added to equation 3.9, resulting in [6, 7, 24, 25, 26, 27]

$$L_p(d) \Big|_{dB} = L_{fs}(d_0) \Big|_{dB} + 10n \log \left(\frac{d}{d_0} \right) + \sum_{q=1}^Q FAF(q) + \sum_{p=1}^P WAF(p) \quad (4.9)$$

where $FAF(q)$ and $WAF(p)$ are the floor and the wall attenuation factors, respectively. In [48, 49] are listed the FAF values for two buildings.

It has been observed that the propagation path loss as a function of the distance also has two distinct regions for indoor environments [50], as described in Equation 4.9. When electromagnetic radiation is incident on a wall or a floor in an oblique fashion, less power will be transmitted through the wall than would occur at normal incidence. Reference [27] modifies the $WAF(p)$ term to $WAF(p)/\cos \phi_p$ and $FAF(q)$ term to the term to $FAF(q)/\cos \phi_q$, where $WAF(p)$ and $FAF(q)$ are the values of the attenuation factors at normal incidence, and ϕ_p and ϕ_q are angles of incidence of the signal on the walls and floors, respectively. A diffraction term was also added to the formula in [27]. When the base station is out of the building, the path loss in the building was given in reference [51]. The empirical or statistical models described in this section are simple to implement, and are widely used when the accuracy of the data is not a critical requirement.

4.2.3 Deterministic models

In-building propagation is a highly complex process, as it occurs within environments possessing a variety of geometric and electromagnetic properties. Due to multiple interactions with walls, furniture, equipment, and people, received signals exhibit fading characteristics in space and spreading in time [4]. For site-specific calculations, deterministic approaches based on physical

models that take into account all or most of the environment's details constitute a reliable choice. In this framework, ray-tracing algorithms have been used extensively to perform indoor wireless studies [52, 53, 54]. On the other hand, there also exist some applications of the finite-difference time-domain (FDTD) method [55] for similar purposes. For example, the impact of different wall models on several channel parameters was pointed out via FDTD simulations in [56]. Moreover, FDTD results related to window were incorporated in a ray-tracing algorithm in [33], while [5] introduced a hybrid ray-tracing FDTD technique for accurate site-specific calculations.

References

1. Cox, D.C., Murray, R. R., and Norris, A.W., "Measurements of 800MHz radio transmission into buildings with metallic walls" Bell System technical journal, Vol. 62, No. 9, pp. 2695 - 2717, November 1983.
2. Alexander, S. T., "Radio propagation within buildings at 900 MHz" Electronics letters, Vol. 18, No. 21, pp. 913-914, 1982.
3. Moltdar, D., "Review on radio propagation into and within buildings" IEEE Proceedings, Vol. 138, No. 1, pp. 61-73, February 1991.
4. Hashemi, H., "The indoor radio propagation channel" Proceedings of the IEEE, Vol. 81, No. 7, pp. 943-968, July 1993.
5. Seidel, S.Y., et al., "The impact of surrounding buildings on propagation for wireless in-building personal communications system design", IEEE Vehicular technology conference, Denver, pp. 814-818, May 1992.
6. Seidel, S.Y., and Rappaport, T.S., "914 MHz path loss prediction models for indoor wireless communications in multi-floored buildings" IEEE Transaction on antenna and propagation, Vol. 40, No. 2, pp. 207-217, February 1992.
7. Rappaport, T.S., "Characterization of UHF Multipath radio channels in factory buildings" IEEE Transactions on antenna and propagation, Vol. 37, No. 8, pp. 1058-1069, August 1989.
8. Rice, P.L., Longley, A. G., Norton, K. A., and Baris, A. P., "Transmission loss predictions for tropospheric communication circuits" NBS Tech Note 101; two volumes; issued May 7, 1965; revised May 1, 1966; revised January 1967
9. Longley, A. G., and Rice, P.L., "Prediction of tropospheric radio transmission loss over irregular terrain; A computer method" ESSA Technical Report, ERL 79-ITS 67, 1968
10. Longley, A. G., "Radio propagation in Urban Areas" OT Reort, pp. 78-144, April 1978.
11. Okumura Y., Ohmori E., Kawano T., Fukuda K., "Field strength and its variability in VHF and UHF land-mobile service." Review of the Electrical Communications Laboratory, Vol. 16, pp. 825-873, September 1968.
12. M. Hata. "Empirical formula for propagation loss in land mobile radio services." IEEE Transactions on vehicular technology, Vol. 29, pp.317-325, 1980.
13. European cooperation in the field of scientific and technical research EURO-COST 231, "Urban transmission loss models for mobile radio in the 900 and 1800 MHz bands" revision 2, The Hague, September 1991.

References 65

32. Rappaport, T.S., "Wireless Communications," Prentice-Hall; 2th ed. Upper Saddle River, New Jersey, Chs. 3 and 4, 1996.
33. Zhijun Zhang; Sorensen, R.K.; Zhengqing Yun; Iskander, M.F.; Harvey, J.F. "A ray-tracing approach for indoor/outdoor propagation through window structures" IEEE Transactions on Antennas and Propagation, Volume 50, Issue 5, May 2002 Page(s):742 - 748
34. Remley, K.A.; Anderson, H.R.; Weissnar, A. "Improving the accuracy of ray-tracing techniques for indoor propagation modeling" IEEE Transactions on Vehicular Technology Volume 49, Issue 6, Nov. 2000 Page(s):2350 - 2358
35. Schuster, J.W.; Wu, K.C.; Ohs, R.R.; Luebbers, R.J. "Application of moving window FDTD to predicting path loss over forest covered irregular terrain" IEEE Antennas and Propagation Society International Symposium, 2004, Volume 2, 20-25 June 2004 Page(s):1607 - 1610
36. Luebbers, R.; Schuster, J.; Wu, K. "Full wave propagation model based on moving window FDTD" IEEE Military Communications Conference, 2003. MILCOM 2003 Volume 2, 13-16 Oct. 2003 Page(s):1397 - 1401.
37. Borjeson, H.; De Backer, B. "Angular dependency of line-of-sight building transmission loss at 1.8 GHz" The Ninth IEEE International Symposium on Personal, Indoor and Mobile Radio Communications, 1998, Volume 1, 8-11 Sept. 1998 Page(s):466 - 470.
38. Neskovic, A.; Neskovic, N.; Paunovic, D. "A field strength prediction model based on artificial neural networks" 9th Mediterranean Electrotechnical Conference, 1998. MELECON 98, Volume 1, 18-20 May 1998 Page(s):420 - 424.
39. Ostlin, E.; Zepernick, H.-J.; Suzuki, H. "Macrocell radio wave propagation prediction using an artificial neural network" IEEE 60th Vehicular Technology Conference, 2004. VTC2004-Fall, Volume 1, 26-29 Sept. 2004 Page(s):57 - 61.
40. Janaswamy, R. "Path loss predictions in the presence of buildings on flat terrain: a 3-D vector parabolic equation approach" IEEE Transactions on Antennas and Propagation, Volume 51, Issue 8, Aug. 2003 Page(s):1716 - 1728
41. Brennan, C.; Cullen, P.J. "Tabulated interaction method for UHF terrain propagation problems" IEEE Transactions on Antennas and Propagation, Volume 46, Issue 5, May 1998 Page(s):738 - 739
42. Whitman, G.M.; Kyu-Sung Kim; Niver, E. "A theoretical model for radio signal attenuation inside buildings", IEEE Transactions on Vehicular Technology, Volume 44, Issue 3, Aug. 1995 Page(s):621 - 629
43. Chopard, B.; Luthi, P.O.; Wagen, J.-F. "Lattice Boltzmann method for wave propagation in urban microcells" IEE Proceedings Microwaves, Antennas and Propagation, Volume 144, Issue 4, Aug. 1997 Page(s):251 - 255.
44. Har, D., Xia, H. H., Bertoni, H. L., "Path-loss prediction model for microcellular," IEEE Transaction on Vehicular Technology, Sept. 1999, Vol. 48, issue 5, pp. 1453-1462.
45. Soma, P., Baum, D. S., Erceg, V., Krishnamoorthy, R., Paulraj, A. J., "Analysis and modeling of multiple-input multiple-output (MIMO) radio channel based on outdoor measurements conducted at 2.5GHz for fixed BWA applications," IEEE International Conference on Communications, 2002, Vol. 1, pp. 272-276, New York, May 28 April, 2002.
46. Hashim, M. H., Stavrou, S., "Measurements and modelling of wind influence on radiowave propagation through vegetation," IEEE Transaction on Wireless Communications, 2006, Vol. 5, issue 5, pp. 1055-1064.

64 References

14. Walfisch, J., and Bertoni, H. L., "A theoretical model of UHF propagation in urban environments" IEEE transactions on antennas and propagation, Vol. AP-36, pp. 1788-1796, October, 1988.
15. Maciel, L. R., Bertoni, H. L., and Xia, H. H., "Unified approach to prediction of propagation over buildings for all ranges of base station antenna height" IEEE transactions on vehicular technology, Vol. 42, No. 1, pp. 41-45, February 1993.
16. Xia, H. , and Bertoni, H. L. "Diffraction of cylindrical and plane waves by an array of absorbing half screens" IEEE Transaction on Antenna and Propagation, Vol. 40, No. 2, pp. 170-177, February 1992.
17. Recommendation M.1455: "Key characteristics for the international mobile telecommunications 2000 (IMT-2000) RADIO INTERFACES".
18. Recommendation M.1225: "Guidelines for evaluation of radio transmission technologies for IMT-2000".
19. Rustako, A. J. et al. "Radiopropagation at microwave frequencies for line-of-sight microcellular mobile and personal communication," IEEE Transaction on Vehicular Technology, Vol. 40, pp. 203-210, February 1991.
20. Xia, H. H., Bertoni, H. L., Maciel, L. R., Lindsay-Stewart, A., Rowe, R. "Radio propagation characteristics for line-of-sight microcellular and personal communication," IEEE Transactions on Antennas Propagation, Vol. 41, pp. 1439-1447, Oct. 1993.
21. R. Jakoby and U. Liebenow, "Modeling of radiowave propagation in microcells" In proc. ICAP'95 Apr. 1995.
22. E.Green and M. Hata, "Microcellular propagation measurements in a urban environment", In proc. PIMRC, Sept. 1991.
23. Broch, J., Maltz, D. A., Johnson, D. B., Hu, Y. C., and Jetcheva, J., "A performance comparison of multi-hop wireless ad hoc network routing protocols," in Mobile Computing and Networking, 1998, pp. 85-97.
24. Pahlavan, K. Ganesh, R. Hotaling, T., "Multipath propagation measurements on manufacturing floors at 910MHz" Electronics Letters, 25, 3, February 1989, pp. 225-227.
25. D. A. Haand, "Indoor Wide Band Radio Wave Propagation and Models at 1.3 GHz and 4.0 GHz," Electronics Letters, vol. 26, no. 21, pp. 1800-1802.
26. D. M. J. Davasirvatham, "A Comparison of Time Delay Spread and Signal Level Measurements within Two Dissimilar Office Buildings," IEEE Transactions on Antennas and Propagation, AP-35, 3, March 1987, pp. 319-324.
27. K. Cheung, J. Sau, and R.D.Murch, "A new empirical model indoor propagation prediction," IEEE Trans. Vehic. Tech., VT-47, 3, August 1998, pp. 996-1001.
28. D. M. J. Devasirvatham, "Radio propagation studies in a small city for universal portable communications", In proc. of the IEEE VTC'88, 18-21 May 1988.
29. E.Green. "Measurements and model for the radio characterization of microcells", In proc. IEEE ICCS'90 Nov. 1990, Singapore.
30. Feuerstein, M. J., Blackard, K. L., Rappaport, T. S., Seidel, S. Y., and Xia, H. H., "Path loss delay spread and outage models as functions of antenna height for microcellular system design," IEEE Transactions on Vehicular Technology, Vol. 43, No. 3, pp. 487-498, August 1994.
31. Sarkar T.K., Zhong Ji, Kyungjung K., Medouri A., Salazar-Palm M., "A survey of various propagation models for mobile communication," HYPERLINK <http://ieeexplore.ieee.org/xpl/RecentIssue.jsp?punumber=74> Antennas and Propagation Magazine, IEEE , June 2003 , Volume: 45, Issue: 3 , page(s): 51 - 82.

66 References

47. Andersen, J. B., Rappaport, T. S., Yoshida, S., "Propagation measurements and models for wireless communications channels," IEEE Communications Magazine, 1995, Vol. 33, issue 1, pp. 42-49.
48. T. S. Rappaport and S. Sandhu, "Radio-Wave Propagation for Emerging Wireless Personal-Communication Systems," IEEE Antennas and Propagation Magazine, 36, 5, October 1994, pp. 14-24.
49. A. Saleh and R. Valenzuela, "A statistical model for indoor multipath propagation," IEEE Journal on Selected Areas Communications, vol. SAC-5, pp. 128-137, Feb. 1987.
50. Bertoni, J. L. Dailing, J. Qian, and H. D. Lee, "Mechanism governing UHF propagation on single floors in modern office buildings," IEEE Transaction on Antennas and Propagation, AP-41, 4, 1992, pp. 496-504.
51. S.Ruiz, Y.Samper, J.Prez, R.Agust, J.Olmos, "Software tool for optimising indoor/outdoor coverage in a construction site," Electronics Letters, 34, 22, October 1998, pp. 2100-2001.
52. C.-F. Yang, B.-C. Wu, and C.-J. Ko, "A ray-tracing method for modeling indoor wave propagation and penetration," IEEE Trans. Antennas Prop- agat., vol. 46, no. 3, pp. 907919, Jun. 1998.
53. R. P. Torres, S. Loreda, L. Valle, and M. Domingo, "An accurate and efficient method based on ray-tracing for the prediction of local flat-fading statistics in picocell radio channels," IEEE J. Sel. Areas Commun., vol. 19, no. 1, pp. 170178, Feb. 2001.
54. P. Bernardi, R. Cicchetti, and O. Testa, "An accurate UTD model for the analysis of complex indoor radio environments in microwave WLAN systems," IEEE Trans. Antennas Propag., vol. 52, no. 6, pp. 15091520, Jun. 2004.
55. A. Taflov, Computational Electrodynamics: The Finite-Difference Time-Domain Method. Norwood, MA: Artech House, 1995.
56. Z. Yun, M. F. Iskander, and Z. Zhang, "Complex-wall effect on propagation characteristics and MIMO capacities for an indoor wireless communication environment," IEEE Trans. Antennas Propag., vol. 52, no. 6, pp. 914922, Apr. 2004.
57. Y. Wang, S. Safavi-Naeini, and S. K. Chaudhuri, "A hybrid technique based on combining ray tracing and FDTD methods for site-specific modeling of indoor radio wave propagation," IEEE Trans. Antennas Propag., vol. 48, no. 5, pp. 743754, May 2000.

Frame error models

Frame loss is a key factor determining the quality of multimedia applications such as audio/video conferencing and Internet telephony. Understanding these error characteristics is important for many purposes, e.g., for simulation-based performance evaluation of wireless multimedia applications or for exploiting knowledge about these error characteristics within a protocol that dynamically adapts its behaviour, e.g., the packet size and speed rate. In either case, a compact representation of the error characteristics, an *error model*, is required. Such models can be developed on an physical layer, describing the behaviour of the received signal strength and/or the interference power, or they can be applied to the data link layer, describing the sequence of frame that the receiver delivers to higher protocol layers. The advantage of frame error models is that they describe exactly the errors that higher protocol layers (such as transport or application layer) undergo.

While no generally accepted model exists for describing the loss process in Wi-Fi networks, there are some proposals, which we review here. In addition, some simplifications are common in the simulation community. In the following, we review the most common models in actual use. Moreover, since we are dealing with frame loss statistics, a particular instance of a frame loss process can be written as a sequence of zeros, meaning that no loss has occurred and the frame has gone through the channel unharmed, and ones, meaning that the frame has not been received correctly. Given this convention, we describe the main statistical properties of the models subsequently mentions. We also describe how to compute the parameter of each model to fit a measured instance of a frame loss process. All models are discrete stationary random processes of a variable $x_n \in \{0, 1\}$.

We use the common symbols μ for the mean $E\{x\}$, σ^2 for the variance $E\{(x - \mu)^2\}$, $r(k)$ for the autocorrelation function $E\{x_n x_{n+k}\}/E\{x^2\}$. We also give expressions for two commonly used statistics: the error gap length distribution and the block error probabilities.

An *error gap* is a sequence of zeros (correctly received frames) delimited by ones (lost frames). The *gap length* U is defined as the number of zeros in

a gap plus one, so a gap is made from a delimiting one, $U - 1$ zeros, and one more delimiting one. The *error gap distribution* $u(n)$ is defined as $Pr\{U \geq n\}$.

An *error burst* is a sequence of ones (lost frames) delimited by zeros (correctly received frames). The *error burst distribution* $b(n)$ is defined as $Pr\{B \geq n\}$.

The *block error probability* $P(m, n)$ is defined as the probability that exactly m errors occur in a block of n consecutive frames.

5.1 Bernoullian

The simplest model for frame loss in a communication network is the Bernoullian process. With this model, each frame has a fixed probability p of being lost or corrupted; the loss probabilities for each frame are i.i.d. (independent and identically distributed) random variables. Given a number N of transmitted frames, the number X of lost frames follows a binomial distribution:

$$P\{X = x\} = \binom{N}{x} p^x (1-p)^{N-x} \quad (5.1)$$

which, for big N , can be approximated to Poisson distribution with mean and variance both equal to Np , needing just a single parameter, this is the simplest significant model. Being p the probability that a given frame lost, this process has mean $\mu = p$, variance $\sigma^2 = \mu(1-\mu) = p(1-p)$ and autocorrelation function null for all lags greater than 0.

Since the most prominent feature of this process is its mean, the obvious way to fit it to an observed trace is to set p equal to the mean of the observed process.

However, it is possible to fit the process to the distribution using other statistics, such as the error gap distribution and the block error probability [1].

The error gap distribution of a Bernoullian process is $u(n) = p(1-p)^{n-1}$, that is, a geometric distribution with mean equal to $1/p$, while the error burst distribution is $b(n) = p^{n-1}(1-p)$, that is, a geometric distribution with mean equal to $1/(1-p)$.

The error block probability is, for a given block length n , a binomial distribution with mean equal to pn .

5.2 Two state Markov model

The first step towards a more complex model is to introduce some correlation among the loss probabilities of consecutive frames, thus dropping the assumption of i.i.d. loss probabilities for different frames. We suppose that the channel can be in one of two states, S_1 and S_2 where frames are always

5.3 Two-state Markov-modulated Bernoullian process 69

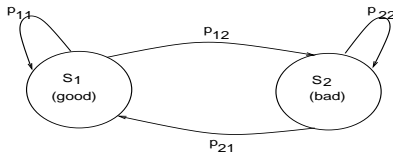


Fig. 5.1. Channel model based on a two-state Markov chain.

received (good state) or always lost (bad state). We model this description as a discrete two-state Markov chain, shown in Figure 5.1.

We call p and q the state transition probabilities p_{12} and p_{21} , respectively, so we have $p_{11} = 1 - p$ and $p_{22} = 1 - q$. This is a two-parameter model: one more than the simple Bernoullian model, the price for introducing correlation.

With the notation used previously, p is the probability of exiting the good state and q the probability of exiting the bad state; the stationary probability of being in the good state is $Pg = q/(p+q)$, while that of being in the bad state is $Pb = p/(p+q)$. This process has mean $\mu = Pb = p/(p+q)$, variance $\sigma^2 = \mu(1-\mu) = pq/(p+q)^2$ and autocorrelation function $r(n) = Pb + (1-Pb)(1-p-q)^n$.

The mean duration of the good and bad states are $1/p$ and $1/q$, respectively; this means that the channel exhibits error bursts of consecutive ones, whose mean length is $1/q$, that are separated by gaps of consecutive zeros whose mean length is $1/p$. Both burst and gap lengths have geometric distribution.

The error gap distribution of a bistable process is $u(n) = 1$ for $n = 1$ and $p(1-p)^{n-2}$ for $n > 1$ and $b(n) = q(1-q)^{n-1}$.

5.3 Two-state Markov-modulated Bernoullian process

The concept of having a good and a bad state in a communication channel was proposed by Gilbert [2] by assigning a null loss probability to the good state and a $1-h$ loss probability to the bad state. As a consequence, the channel is governed by a Bernoulli process while in the bad state. Later on, Elliott [3], complicated the model by defining the good state as having a $1-k$ loss probability, thus using a Bernoulli process for both the good and the bad states. Gilbert's model needs the three p , q and h parameters, while Elliott's needs one more, namely k .

The stationary state probabilities are the same as in the bistable case. The error probability is $1-k$ when in good state, $1-h$ when in the bad state. This process has mean $\mu = (1-k)Pg + (1-h)Pb$ and variance $\sigma^2 = \mu(1-\mu)$, where $k = 1$ in the Gilbert model. The autocorrelation function for $n > 0$ for the Gilbert model is $r(n) = (1-h)[Pb + (1-Pb)(1-p-q)^n]$, while for

70 5 Frame error models

the more general Gilbert-Elliott model (GE) is $r(n) = \mu + [pq(h-k)^2/\mu(p+q)^2](1-p-q)^n$. The mean duration of the good and bad states are the same as in the bistable case, but the error burst distribution is $b(n) = (1-q)^{n-1}(1-h)^{n-1}[q(1-q)h]$ in the Gilbert model.

Gilbert derived the relationship between the transition probabilities (p and q), h , and the error gap distribution. Following the development in [2], the error gap distribution can be written in the former:

$$u(n) = AJ^n + (1-A)L^n \quad (5.2)$$

By using the values of A , J , and L which best match the error gap distribution, the model parameter q and p and h can be derive as

$$\begin{aligned} h &= \frac{JL}{J-A(J-L)} \\ p &= \frac{(1-L)(1-J)}{1-h} \\ q &= A(J-L) + (1-J) \left(\frac{L-h}{1-h} \right) \end{aligned}$$

Figures 5.2 and 5.3 show the error gap and error bursts distributions, respectively.

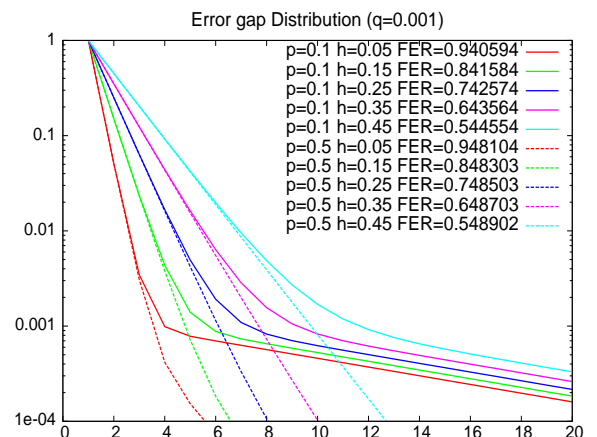


Fig. 5.2. Error gap distribution for the Gilbert model.

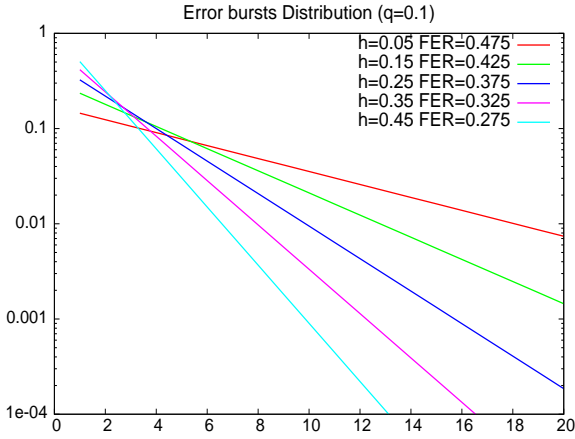


Fig. 5.3. Error bursts distribution for the Gilbert model.

The block error probabilities are found using a set of recurrence relations [3].

$$P(m, n) = \frac{q}{p+q} + S_1(m, n) \frac{p}{p+q} - S_2(m, n) \quad (5.3)$$

where $S_1(m, n)$ and $S_2(m, n)$ are given in recurrent form by

$$\begin{aligned} S_1(m, n) &= S_1(m, n-1)(1-p) + S_2(m, n-1)p \\ S_2(m, n) &= S_2(m, n-1)(1-q)h + S_1(m-1, n-1)(1-q)(1-h) + \dots \\ &\quad + S_1(m, n-1)qh + S_1(m-1, n-1)q(1-h) \end{aligned} \quad (5.4)$$

The initial conditions used in computing the above values for Gilbert's model are

$$\begin{aligned} S_1(0, 1) &= 1 \\ S_1(1, 1) &= 0 \\ S_2(0, 1) &= h \\ S_2(1, 1) &= 1-h \end{aligned}$$

$$S_1(m, n) = S_2(m, n) = 0 \text{ when } m < 0 \text{ or } m > n.$$

These studies on the validity of the model mainly aim at showing how well the model represents the received fading envelope, not at describing bit or frame losses in the channel. Furthermore, these and other validation studies have assumed that the underlying communications channel is not frequency selective, which is only valid for narrowband channels. Additionally, in the characterization of these models, it has been assumed that fairly simple modulation schemes, such as BPSK or DPSK, are used [15]. These assumptions are not valid for wideband channels like those used by 802.11 devices, where complex modulation schemes are present. Moreover, no experimental validation has been done on how appropriate these models are when used to represent frame losses in 802.11 channels.

In the context of wireless link layer modelling, Konrad et al in [16] and [17] outline the inadequacy of the two-state Markov chain and present a Markov-based Trace Analysis (MTA) model algorithm for GSM wireless channels. Ji et al in [18] compare the performance of the MTA model, the full-state k-order model, the hidden Markov model, and the extended ON/OFF model in capturing GSM frame losses.

In [19] the authors use the WaveLAN physical device. The transmission is via direct-sequence spread spectrum using the lowest ISM bands, 902-928 MHz. Starting from measures they derive that while the two-state Markov model may be adequate for some applications, the higher accuracy of the improved model justifies its complexity for others. Similar studies are conducted in [20], where the authors measure throughput, packet loss rates, range, and patterns of errors within packets. They conclude that the reliable range of WaveLAN is about 40 meters. Beyond this limit, its behaviour becomes unstable: the relative placement of sender and receiver becomes extremely important, with movements of even a single meter in an unexpected direction making an enormous difference in the success of packet capture. This event is the same that we have verified in our 802.11b measurement campaigns, as we will show in the following sections.

In order to model the indoor 802.11a wireless channel, in [21] the authors test five different models: Gilbert, Gilbert-Elliott, and the 3-4-5 state hidden Markov models. They show that higher-order state hidden Markov models provide a better fit to measured data than the traditional two-state Gilbert models.

Carvalho et al in [22] proposed a novel wireless indoor network model (logarithmic series distribution) for 802.11g and compare it with GE by performing the chi-square goodness-of-fit test. The proposed model is shown to be more accurate than the GE in particular but very representative IEEE802.11g scenario. The model has two parameters: one is a function of the source packet rate; and the order is almost constant. Measures have been performed in an indoor environment with an infrastructure network. They conclude that their model is 63.9% superior to GE.

Khayam [23] and Radha [24] conducted an investigation at the IEEE802.11b link layer in order to facilitate the design of effective cross-layer error control

Another approach is to determine the values of the transition probabilities and h , which provide the closest fit for the block error probabilities.

In the GE model the error gap distribution is modelled the same way as in the Gilbert model. While there will be some minor differences in the error gap distribution due to the addition of the parameter k , it is assumed that the value of k is close to one, and will have only a minor effect on the distribution values. Its effect on the error gap distribution is therefore ignored. The values generated for $P(m, n)$, however, must include the effect of the parameter k . Note that GE's model reduces to Gilbert's model if $k = 1$. The block error probability for the GE model is given by 5.3, the recurrent form of $S_2(m, n)$ is given by 5.4, but the recurrent form of $S_1(m, n)$ is

$$\begin{aligned} S_1(m, n) &= S_1(m, n-1)(1-p)k + S_1(m-1, n-1)(1-p)(1-k) + \dots \\ &\quad + S_2(m, n-1)pk + S_2(m-1, n-1)p(1-k). \end{aligned} \quad (5.5)$$

The following approaches are used in determining the model parameters, starting from the data measure.

1. Using the transition probabilities obtained from the Gilbert best fit to the error gap distribution, find the value of k that provides a best fit to the $P(m, n)$ data.
2. Find parameter values of p , q , h , and k that best fit the block error data.

5.4 State of Art on the utilization of frame loss models

The GE model has extensively been used to assist in the design of communication system [4, 5]. In [6] and [7] performance of different version of TCP were evaluated in the presence of GE channel. In [8, 9] and [10], the GE model is used to evaluate the channel codes, while in [11] the impact of the loss burst length on the end-to-end FEC over multi-hop GE wireless channels are analyzed and presented. One of the major mistakes in literature about the GE wireless model is that does not differ from the 2-state Markov model. Note that when $p+q=1$, the model turns into a Bernoulli model.

The validity of Markov models has been widely studied. These studies focus in verifying the legitimacy of fundamental assumptions and the statistical characteristics of the model. In particular, Wang and Chang [12] show under what conditions the Markov assumption of Rayleigh fading is adequate, while Tan and Beaulieu [13] extend this idea and suggest that a better approach is to analyze the autocorrelation function of the model. Authors in [14] suppose a flat fading channel modelled as a Gaussian random process. With this type of channel they consider the power threshold as a binary process that describes block (hundred of bits) successes and failures. They show that for slow fading the first order Markov approximation is adequate; on the contrary, in fast fading, an i.i.d. model provides a suitable losses' description.

schemes for the support of real-time services. The authors found that the non-LOS indoor wireless channel is characterized by byte-level error patterns that are not memoryless, thus showing that simplistic models are inadequate for that type of environment, for which they propose a hierarchical Markov model (hMM). The same authors in [25] demonstrate that the traditional two-state Markov chain provides a very suitable model for 802.11b packet loss process. They also show that the two-state, the hierarchical and the hidden Markov models are not adequate for modelling the bit errors.

In [5] the authors investigate the performance of IEEE 802.11b ad hoc networks. They present a channel model for an 802.11 network derived from measurements done in an outdoor environment, by considering different traffic types (i.e., TCP and UDP traffics), at a data rate of 2 Mbps. Their experimental results indicate that transmission ranges are much shorter than assumed in simulation studies. In addition, they also observed a dependency of transmission range on transmission speed and mobile device's height. The channel model they derive for 802.11 networks indicates that virtual carrier sensing is not necessary and the RTS/CTS mechanism only introduces additional overhead. This model is used to identify new hidden stations or capture phenomenon that are not solved by current 802.11 mechanisms. The dependency between the data rate and the transmission range was investigated by measuring the packet loss rate experienced by two communicating stations whose network interfaces transmit at a constant (preset) data rate. Specifically, four sets of measurements were performed, corresponding to the different data rates: 1, 2, 5.5, and 11 Mbps.

References

1. Paolo Barsocchi, Gabriele Oliveri, and Francesco Potort. "Packet loss in TCP hybrid wireless networks". In: proceedings of the Advanced Satellite Mobile Systems Conference (ASMS), Hersching (DE), May 2006.
2. E.N. Gilbert, "Capacity of a burst-noise channel," *The Bell System Technical Journal*, 1960.
3. E. O. Elliott, "Estimates of error rates for codes on burst-noise channels," *Bell Systems Technical Journal*, vol. 42, pp. 1977-1997, September 1963.
4. M. Zorzi and Ramesh R. Rao, "On the Statistics of block errors in bursty channel," *IEEE Transaction Communications*, vol. 45, no. 7, June 1997.
5. H. S. Wang, "On Verifying the first-order Markovian assumption for Rayleigh fading channel model," in *In Proc. ICUCP'94*, Sep. 1994.
6. M. Zorzi, A. Chockalingam and Ramesh R. Rao, "Throughput Analysis of TCP on Channels with Memory," *IEEE Journal on Selected Areas in Communications*, vol. 18, no. 7, July 2000.
7. M. Rossi, R. Vicenzi, M. Zorzi, "Accurate Analysis of TCP on Channels with Memory and Finite Round-Trip Delay," *IEEE Journal on Selected Areas in Communications*, vol. 3, no. 2, March 2004.
8. J. E. Yee and E. J. Weldon, "Evaluation of the performance of error-correcting codes on a Gilbert channel," *IEEE Transactions Communications*, vol. 43, no. 8, Nov. 1989.
9. M. Mushkin and I. Bar-David, "Capacity and coding for the Gilbert-Elliott channels," *IEEE Transaction on Information Theory*, vol. 35, Nov. 1989.
10. J. Garcia-Frias and J. Villaseñor, "Turbo decoding of Gilbert-Elliott channels," *IEEE Transactions Communications*, vol. 50, no. 3, Mar. 2002.
11. Mingquan Wu and Hayder Radha, "Network-Embedded FEC (NEF) Performance for Multi-Hop Wireless Channels with Memory," in *IEEE International Conference on Communications (ICC)*, May 2005.
12. H. S. Wang, N. Moayeri, "On Verifying the Firsts-Order Markovian Assumption for a Rayleigh Fading Channel Model," *IEEE Transactions on Vehicular Technology*, vol. 45, no. 2, May 1996.
13. C. C. Tan, N. C. Beaulieu, "On First-Order Markov Modeling for the Rayleigh Fading Channel," *IEEE Transactions on Communications*, vol. 48, no. 12, Dec. 2000.
14. M. Zorzi, R. R. Rao, L. B. Milstein, "On the accuracy of a first-order Markov model for data block transmission on fading channels," *IEEE International Conference on Universal Personal Communications*, November 1995.
15. H. S. Wang, N. Moayeri, "Finite-State Markov Channel - A useful Model for Radio Communications Channels," *IEEE Transactions on Vehicular Technology*, vol. 44, no. 1, Feb. 1995.
16. Almudena Konrad, Ben Y. Zhao, Antony D. Joseph, and Reiner Ludwig, "A markov-based channel model algorithm for wireless networks," in *Fourth ACM International Workshop on Modeling, Analysis and Simulation of Wireless and Mobile System (MSWiM)*, 2001, Rome, Italy.
17. A. Konrad, B. Y. Zhao, A. D. Joseph, and R. Ludwig, "A markov-based channel model algorithm for wireless networks," *Wireless Networks*, vol. 9, Sept. 2003, pp. 189-199.
18. Ping Ji, Benyuan Liu, Towsley, D., Kurose, J., "Modeling frame-level errors in GSM wireless channels," in *IEEE Global Telecommunications Conference*, 2002. *GLOBECOM'02.*, vol. 3, 17-21 Nov. 2002.
19. B. Noble, G. Nguyen, Q.R. Katz and M. Satyanarayanan, "A Trace-based Approach for Modeling Wireless Channel Behaviour," in *Winter Simulation Conference '96*, 1996.
20. D. Duchamp, N. Reynolds, "Measured Performance of a wireless LAN," in *17th IEEE Conference on Local Computer Networks*, Sept. 1992.
21. Hartwell, J. A., Fapojuwo, A. O., "Modeling and characterization of frame loss process in IEEE 802.11 wireless local area networks," in *IEEE 60th Vehicular Technology Conference VTC2004*, Sep. 2004. [16]
22. L. Carvalho, J. Angeja, A. Navarro, "A New Packet Loss Model of the IEEE 802.11g Wireless Network for Multimedia Communications," *IEEE Transactions on Consumer Electronics*, vol. 51, Aug. 2005, pp. 809 - 814.
23. Syed A. Khayam, Shirish S. Karande, Hayder Radha, and Dmitri Loguinov, "Performance Analysis and Modeling of Errors and Losses over 802.11b LANs for High-Bitrate Real-Time Multimedia," *Signal Processing: Image Communication*, vol. 18, Aug. 2003.
24. Shirish S. Karande, Syed A. Khayam, Michael Krappel, and Hayder Radha, "Analysis and Modeling of Errors at the 802.11b Link-Layer," in *IEEE International Conference on Multimedia and Expo (ICME)*, July 2003.
25. Syed A. Khayam and Hayder Radha, "Markov-based modeling of wireless local area networks," in *WSWiM*, 2003.
26. Anastasi G., Borgia E., Conti M., Gregori E., "Wi-Fi in ad-hoc mode: a measurement study", *Proceedings of the Second IEEE Annual Conference on Pervasive Computing and Communications (PERCOM'04)*, Orlando, FL, USA, 14-17 March 2004, pp. 145-154.

6

Measurement campaign

We started in 2005 a wide measurement campaign on frame losses over WLANs with the aim of defining wireless channel indoor and outdoor models more matching the reality than those available in the literature. This section describes the test-bed used for the measurement campaign.

Only a few researchers have tackled the expensive task of measuring WLANs [1] to understand performance anomalies and the implications of installation choices. However, accurate WLAN measurements have proven to be more elusive than those in wired LANs due to the characteristics of the wireless medium. For instance, measurements over a single wireless hop, such as in an 802.11 infrastructure network, can provide different results depending upon the hop distance, cross and contending traffic, the building structure and even human motion within a measurement test-bed. In general, capturing aspects of WLAN performance requires more than collecting measurement data at any one layer in the protocol stack, and proper investigation is needed at all layers. As far as the MAC layer is considered, a complete frame loss model needs to consider a frame error model, an ARQ (Automatic Repeat reQuest) model and a multi-rate switching model that implements a dynamic rate switching algorithm.

We want examine how ad hoc point-to-point Wi-Fi behaves at the frame level, with both ARQ and dynamic rate switching disabled. As far as we know no results have been published of analogous measurement campaigns.

In fact, measurement campaigns have usually been conducted on complex network setups [6], or in simple scenarios where ARQ algorithm was always used, hiding the underlying frame error process details [5, 7].

An additional peculiarity of our measurement process is that transmission is not greedy, but instead individual frames are sent at precisely controlled time intervals, thus allowing a precise timing characterisation of the frame error process.

One aim of this measurement campaign is to explore a relationship between transmission range, transmission rate and height of transmitter and receiver from ground. In order to do that, we relied on measurements of the

78 6 Measurement campaign

received power level as seen by the network card. Few experimenters have adopted this procedure, such as [7], but to our knowledge no published results are available at the frame level. In order to collect detailed information about frame transmission on wireless channel, researchers need to use tested procedures: description and validation of such a procedure with associated software is an additional contribution of this chapter.

6.1 The measurement methodology

In order to perform reliable measurements at the frame level on a WiFi channel in the absence of collisions, we use two laptops equipped with the Debian GNU/Linux operating system. Standard drivers are used for the wireless network cards. The cards are put in ad hoc mode, so that it is not necessary to depend on an access point, and no management overhead is present apart from the periodic beacon. Important settings for IEEE 802.11b network cards are the fragmentation threshold, which we disabled in our measurements, the RTS/CTS threshold, which we also disabled, the retransmission limit, and the transmission rate. We were interested in channel-level measurements, so we disabled retransmissions, and we disabled the adaptive rate switching, in order to make measurements at different transmission rates in controlled conditions.

During this doctoral thesis we wrote a software transmitter (Send) and a receiver (Receive) able to collect statistics about frame losses and power levels by using the built-in signal level of only received frames. The transmitter sends frames at precisely controlled time intervals, with known length and contents; the receiver checks the sequence number inside the frames and keeps a trace of the lost ones. Both the transmitter and the receiver log a timestamp and the power level for each frame, together with other statistics useful for assessing the procedure reliability. The tools discussed in this chapter are released with a free software copyright license and are available for download at <http://wnlab.isti.cnr.it/paolo/measurements/Software.html>.

The novelty of this measurement campaign is that we simply used the built-in signal level monitor available in the wireless boards, instead of using expensive hardware such as logic status analyzer, etc....

6.1.1 Timing considerations

Depending on the type of measurements, it may be necessary to accurately synchronize the clocks of the sender and receiver. For example, when evaluating packet delay due to collisions and frame retransmissions, it is important that the clocks of the transmitter and the receiver be synchronized. We used the Network Time Protocol (NTP, [8]) to synchronize the clocks of the laptops before starting the measurements and to evaluate the frequency error and consequently the time difference at the end of a measurement. We found out that just a 15 minutes' time of warmup after boot was enough to let the

clock of the laptops stabilize with a residual error of less than 1 ppm, which amounts to a few milliseconds after a hour long measurement. Also, the clock jitter we could measure is always in the order of few μ s, that is, the same order of magnitude of errors introduced by the Linux kernel.

One use of precisely synchronized clocks is to evaluate the processing delays of the transmitter and receiver. A strict upper bound for this statistics is the one-way delay of packets, which we measured to always be less than 1 ms. Since 1 ms is the clock resolution on the kernel we used, the delay is less than the timing error due to the clock granularity.

As far as timing is concerned, then, we conclude that processing delays are negligible and that clocks are accurate as long as the laptops are warmed up for 15 minutes after boot and then synchronized with NTP. As far as the precision of sending times is concerned, we refer the reader to Fig. 6.1, where we report the difference, measured at the receiver, between the interpacket intervals and the expected fixed value that we used during validation.

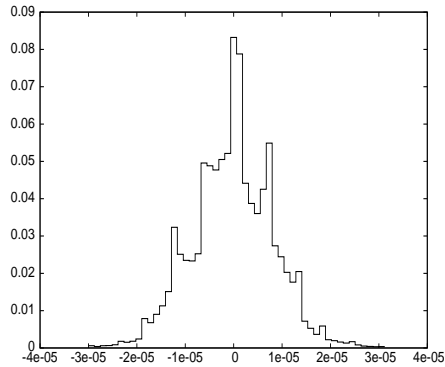


Fig. 6.1. Error of packet intervals at the receiver.

6.1.2 Software

Send is the transmitter program, which sends frames at precisely controlled time intervals, with the format shown in Fig. 6.2.

Send uses every care in order to be as precise as possible and use few system resources. It uses Linux's quasi-real time scheduler, it locks pages into

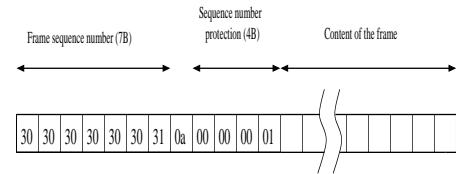


Fig. 6.2. Transmitted frame.

memory after growing the stack, in order to avoid page faults, it can use Posix high resolution timers if the appropriate kernel patch is installed and is written for speed.

Receive is the receiver program, a frame sniffer built upon the PCAP [9], a free library which provides a high level interface to packet capture systems on different operating systems. All packets on the network, even those addressed to other hosts, are accessible through this mechanism. *Receive* knows the format of frames sent by *Send*, and uses this knowledge to trace lost frames, by analyzing sequence numbers placed by *Send* into the frames. It is also possible to use a modified card driver that does not discard frames received with a bad CRC with *Receive*, which is then able to log bit corruptions by comparing expected with received bits, but this possibility has not been used in the validation measurements.

Receive shows packet losses, packet corruptions (only with a modified network driver) and mean signal strength in real time using graphical output on a text console. It collects data for each received frame and stores it into two separate files, one for information regarding bit corruptions and one for received frames, for each of which it reports information's like arrival time, frame length, sequence number, signal level and so on.

References

1. M. Yarvis, K. Papagiannaki, and W. S. Conner, "Characterization of 802.11 Wireless Networks in the Home," in proc. of 1st workshop on Wireless Network Measurements (WiNMee), Apr. 2005, riva del Garda, Italy.
2. D. Aguayo, J. Bicket, S. Biswas, G. Judd, and R. Morris, "Link-level measurements from 802.11b mesh network," in SIGCOMM '04, Vol. 34, no. 4, New York, NY, USA; October 2004, pp. 121-132.
3. Anastasi G., Borgia E., Conti M., Gregori E., "Wi-Fi in ad-hoc mode: a measurement study", Proceedings of the Second IEEE Annual Conference on Pervasive Computing and Communications (PERCOM'04), Orlando, FL, USA, 14-17 March 2004, pp. 145-154.
4. D. Dhoutaut and I. Guerin-Lassous, "Experiments with 802.11d in ad hoc configurations," in 14th IEEE International Symposium on Personal Indoor and Mobile Radio Communications. Beijing, China, Sept. 2003, pp. 1618-1622.
5. D. L. Mills "Internet time synchronization: the network time protocol" IEEE Transaction on Communications 39 (Oct. 1991), 1482-1493.
6. <http://www.tcpdump.org>

A fundamental issue often disregarded in MANET simulation is how to model the packet loss process as seen by the application and routing software.

Only a few researchers have tackled the expensive task of measuring WLANs [10]. The procedure that we used for the measurements is chosen in such a way that the characteristics of the channel are measured, rather than the specifics of the network cards or the protocol. Most importantly, retransmissions are disabled, speed is fixed, ad hoc mode is used, and frames are sent at precisely controlled time instants. As a consequence, our results are useful for a wide range of simulation applications. We are not aware of any published experimental results that relate frame errors with signal strength and distance in controlled conditions.

Most MANET simulations assume a Wi-Fi rural network scenario, where packet loss is the outcome of a three-stage process. The lowest-level stage is the frame error process, that is, the statistical description of the occurrences of a transmitted IEEE 802.11 frame being received in error and discarded, or not received at all. Next comes the ARQ (automatic repeat request) stage described by the MAC layer, whereby the transmitter considers a frame as lost if it does not receive an ACK. In this case, it retransmits the frame up to a configurable number of times, typically set to 7. On top of this, Wi-Fi interfaces implement multi-rate switching, by choosing among the available modulations and codings in order to better exploit the instantaneous channel conditions. What applications running on a Wi-Fi network see is the outcome of all three stages. In this chapter, we propose a simple yet effective model for the frame error process, which is based on extensive measurements in a rural area using laptops with standard Wi-Fi interfaces.

In this chapter we examine how ad hoc point-to-point Wi-Fi behaves at the frame level, with both ARQ and dynamic rate switching disabled. As far as we know no results have been published of analogous measurement campaigns. In fact, measurement campaigns have usually been conducted on complex network setups [6], or in simple scenarios where ARQ algorithm was always used, hiding the underlying frame error process details [5, 7], or else by

to create a backbone between sensor networks and terrestrial networks. Other applications can be for rescue teams working in the open, or more generally for public protection and disaster recovery (PPDR) situations.

We performed our outdoor rural measurement campaign using two IBM Thinkpad R40e laptops (Celeron 2 GHz with 256 MB ram running Debian Linux with a 2.6.8 kernel), equipped with CNet CNWLC-811 IEEE 802.11b wireless cards and standard drivers. The cards were put in ad hoc mode, so that it was not necessary to depend on an access point, and no management overhead was present except for the periodic beacon.

We disabled fragmentation, RTS/CTS, retransmissions (ARQ) and dynamic rate switching. We used different fixed speeds of 1, 2, 5.5 and 11 Mb/s, with frame lengths of 500, 1000 and 1500 data bytes, at transmitter-receiver distances up to 350 m.

By disabling ARQ, the MAC layer transmits each packet only once, rather than trying to retransmit a frame up to 7 times after a loss. This means that we sampled the channel at a constant rate of 200 frames per second, thus accurately measuring the frame error process in the time domain. We performed over 200 simulation runs, each 200 000 frames long, in three different outdoor rural locations.

7.2 Two-ray propagation model

Previous studies found that path loss characteristics in LOS (line of sight) environment are dominated by interference between the direct path and the ground-reflected path [2], as in the two-ray model, in the following referred to as 2RM. This model is characterised by a *break point* that separates the different properties of propagation in near and far regions relative to the transmitter; before the break point, the mean attenuation is close to the free-space path loss $1/d^2$, while after that point it decreases as $1/d^4$.

The *double regression* model suggested in [13] approximates 2RM using two slopes meeting at the break point b , whose position is to be chosen within a transition region:

$$\frac{\pi h_t h_r}{\lambda} < b < \frac{4\pi h_t h_r}{\lambda}, \quad (7.1)$$

where h_t is the transmitter antenna height, h_r is the receiver antenna height, and λ is the wavelength of the radio signal. The *two-ray CMU Monarch* model used in ns-2 [4] adopts a double regression model, with the break point set to

$$4\pi \frac{h_t h_r}{\lambda}. \quad (7.2)$$

For frequencies in the hundreds of MHz, such as those considered in [13], 2RM has a trend that is well-approximated by a double regression model. However, in the case of Wi-Fi, the double regression model is less suitable for approximating 2RM, as shown in Figure 7.1.

aggregating many diverse results that sum up different propagation effects [11, 12]. An additional peculiarity of our measurement process is that transmission is not greedy, but instead individual frames are sent at precisely controlled time intervals, which coupled with the lack of infrastructure transmissions and ARQ retransmissions allows a precise timing characterisation of the frame error process.

One aim of this chapter is to explore a relationship between transmission range, transmission rate and height of transmitter and receiver from ground. In order to do that, we relied on measurements of the received power level as seen by the network card. This procedure has been adopted by few experimenters, such as [7], but to our knowledge no published results are available with precise timings at the frame level. We find that a two-ray model is adequate to describe the relationship between distance and received power. In contrast with the so-called *two-ray CMU Monarch* model used in ns-2 [4], which is in fact an approximate double regression model, in our measures we observed that the received power does not monotonically decrease with distance, but has a significant “hole” where the direct signal and the ground-reflected signal interfere destructively.

The second aspect we explore in detail is the relationship between the received power level and the frame error process. We find that the frame error process is Bernoullian, and that the error probability closely follows the law for coherent PSK demodulation in AWGN (Additive White Gaussian Noise) channel. This contrasts with simple models where all packets are lost if the distance exceeds a given range.

Third, we observe a slow fading process, with bandwidth between 0.25 and 2.5 Hz, which may have a strong influence on the behaviour of dynamic rate switching algorithms. This effect is significantly different from the one implemented in the *shadowing CMU Monarch* model of ns-2, which ignores correlations between subsequent frame errors.

The proposed model should prove useful for simulations of mobile ad hoc rural networks, particularly for evaluating the effects of mobility. Because of its simplicity, it could be used as a benchmark scenario when evaluating results obtained in more challenging environments.

7.1 Measurement setup

The measurements have been carried out in a rural environment, such as a wide field not cultivated, partially covered with grass, with an unobstructed line of sight, without interferences due to other wireless networks, and without reflections due to walls, trees, lampposts or buildings. Some applications can be used in this type of environments; for instance, precision agriculture is one of the promising domains where wireless sensor networks could be exploited, by observing the microclimate within a field, so that plant-specific farming can ultimately be realized. In this context, the wireless networks can be used

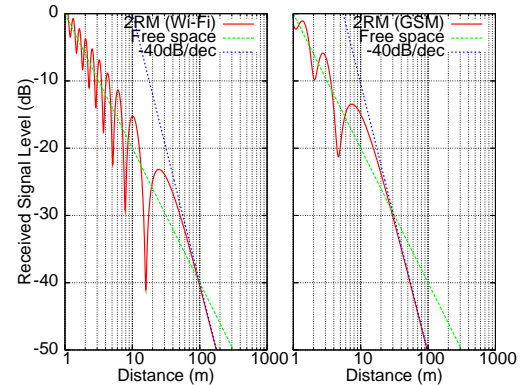


Fig. 7.1. Comparison between 2-ray propagation models at Wi-Fi and GSM frequencies for $h_t = h_r = 1$ m.

Given the above considerations, we propose to substitute the *two-ray CMU Monarch* propagation model used in ns-2 (in fact a double regression model) with 2RM for modelling the received power. The main reason is that 2RM correctly models the “hole” that we observed in our measurements at a distance of about 15 m.

Figure 7.2 shows the measured values superimposed over the *two-ray CMU Monarch* model and on the proposed 2RM. We computed the measured signal level in dB by fitting the observed values with a -40 dB/dec slope for distances greater than b , and estimating that a tick on the received signal level provided by the card represents 0.6 dB. Notice in Fig. 7.2 that 2RM accounts well for the measured values, and specifically it models the “hole” that we observed in the measurements. 2RM predicts that the received signal level has its last hole at a distance

$$d_h = 2h_t h_r / \lambda$$

from the transmitter, provided that $h_t, h_r \ll d$. With vertical polarisation, at the bottom of the last hole the power level is the same as that received at a distance

$$\sqrt{\pi \epsilon_r} d_h^3 / (h_t + h_r),$$

that is, approximately

$$-20 \log_{10}(\sqrt{\epsilon_r} d_h / (2(h_t + h_r))) \text{ dB}$$

lower than the signal level predicted by the *two-ray CMU Monarch* model.

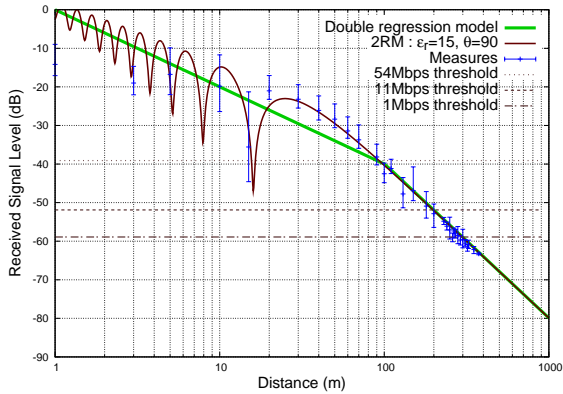


Fig. 7.2. Measured signal level, double regression model and two-ray model with sensitivity thresholds for $\Delta L = 0$. Error bars indicate 0.05, 0.50 and 0.95 quantiles of observed values.

In our case, with nodes at 1 m height from the ground, 2RM predicts a hole at 16 m where the received power with vertical polarisation and an estimated relative permittivity ϵ_r of 15, is the same as that received at 160 m; the error with respect to the double regression model is about 24 dB at that point. This is an important observation, because it means that, with vertical polarisation, connection can be lost at very short distances if the transmission range of the card is less than about 160 m. While, in our measurement, we observed transmission ranges of about 200 m at 11 Mb/s, any reduction in the transmission range will make the effect of the hole apparent and break connectivity.

A transmission range reduction may be consequent to one or more different effects, such as a less sensitive receiver, a speed higher than 11 Mb/s, a non-direct antenna orientation, a mismatch between transmitting and receiving antenna polarisation, or scattering due to obstacles close to the transceivers. Such effects are probably very frequent; one example are the transmission ranges observed in [5], which vary from 30 m to 120 m at different speeds compared to the ranges we measured, which vary from 190 m to 340 m. Another example is the horizontal radiation pattern measured in [14] for two D-Link DWL 650 PCMCIA cards; shown in Fig. 7.3: signal strength varia-

tions in excess of 10 dB are possible, and variations of 3 dB are normal when changing the orientation by 20° . Since this can happen for both the transmitter and the receiver, one can get signal strength variations in excess of 20 dB due to the horizontal radiation pattern alone; considering the vertical radiation pattern would increase these numbers. As a consequence, rural area simulations for mobile networks (MANETs) should consider transceivers whose performance a) is generally less than the declared one, b) is generally variable to keep the changing orientation into account, and c) may show a hole in the transmission range at about 15 m for transceivers at 1 m height from the ground, especially for speeds greater than 11 Mb/s.

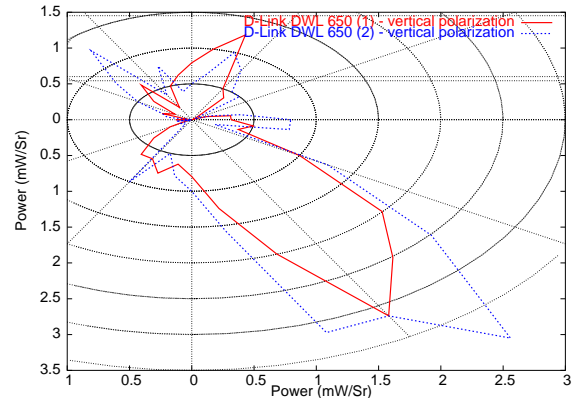


Fig. 7.3. Horizontal radiation pattern for two PCMCIA cards (vertical polarisation).

The 2RM in Figure 7.2 is the signal strength at a distance d , relative to the signal strength at 1 m; it is expressed in dB by

$$L_d = 10 \log_{10} \left| \frac{1}{d} + \Gamma \frac{e^{j2\pi \frac{\delta_d}{\lambda}}}{d + \delta} \right|^2, \quad (7.3)$$

$$\text{where } \delta_d = \sqrt{(h_t + h_r)^2 + d^2} - \sqrt{(h_t - h_r)^2 + d^2}$$

is the path difference between the direct and the reflected rays. Γ is the reflection coefficient, which for non-conductive, non-ferromagnetic materials

is a real number between -1 and 1, different for parallel (horizontal) and perpendicular (vertical) polarisations:

$$\Gamma_{hor} = \frac{\epsilon_r \sin(\theta) - k}{\epsilon_r \sin(\theta) + k}, \quad \Gamma_{ver} = \frac{\sin(\theta) - k}{\sin(\theta) + k}$$

$$\text{where } k = \sqrt{\epsilon_r - \cos^2(\theta)}, \quad \theta = \arccos \frac{d}{\sqrt{(h_t + h_r)^2 + d^2}}.$$

Typical values for the ground relative permittivity ϵ_r are 4, 15, 25, while polarisation of the radio wave may change significantly due to reflection or scattering process [15].

The most commonly used type of antennas are vertically or horizontally polarised [16]. In the following, we consider vertical polarisation because it is more widespread and because it is the case where the hole is deeper, making it a worst case scenario.

7.2.1 Slow fading

The received power level is modulated by a slow fading process with bandwidth in the range from 0.25 to 2.5 Hz. We attribute this modulation to multi-path fading caused by scattering of the radio waves on terrain features imperceptibly moved by the gentle wind, such as moving grass (for the slow oscillations) and moving ground powder (for the faster ones).

The fading distribution is approximately bell shaped around the mean received power, with a ratio of mean power to standard deviation of about 5 dB. In practice, the size and speed of this fading process will have a significant impact on dynamic rate switching algorithms, so their design should take it into account.

7.3 Loss probability versus power level

In [11] a series of measurements is presented that were obtained while comparing simulation results with experimental ones in MANETs. While interesting and compatible with our own results, data are aggregated over many positions, and cannot be directly compared with our limited but precisely controlled scenario.

Our aim is to find a statistical relationship between frame errors and received power level. In Fig. 7.4 frame error and signal level are depicted for each distance at various transmission rates.

7.3.1 Frame error process

A facet that we want to investigate in this chapter is describing the statistical properties of frame error traces in IEEE802.11b in the rural LOS environment, and identify the characteristics that should be captured in a frame error model.

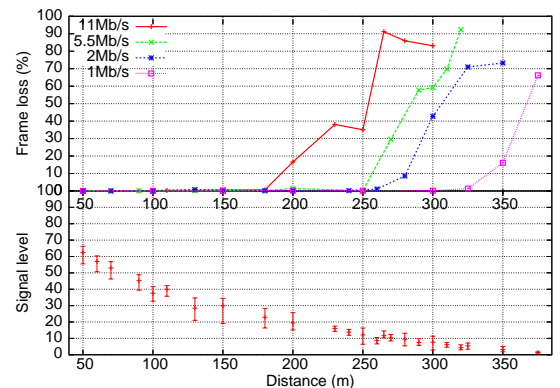


Fig. 7.4. Frame errors and signal levels for each transmission rate.

Let us define an error burst (burst for short) as a sequence of consecutive errored frames, marked by 1 in our traces, and an error-free burst (gap for short) as a sequence of consecutive correct frames, marked by 0 in our traces. Let Z_i denote a wide sense stationary sequence of random variables corresponding to the frame error trace. Let X_i , Y_i denote the length of bursts and gaps, respectively.

- Frame error rate (p). The frame error rate is given by:

$$p = \bar{X} / (\bar{X} + \bar{Y}) \quad (7.4)$$

where \bar{X} is the average burst length, and \bar{Y} the average gap length.

- Discrete probability mass function (pmf). The pmf of X and Y are defined as

$$f_X(x) = P\{X = x\}, \quad f_Y(y) = P\{Y = y\} \quad (7.5)$$

- Autocorrelation. The autocorrelation of a frame error trace is defined as

$$\rho_Z(h) = E[(Z_{i+h} - \bar{Z})(Z_i - \bar{Z})] / E[(Z_i - \bar{Z})^2] \quad (7.6)$$

where h is the lag and \bar{Z} is the mean of Z .

- Coefficient of variation (Cv). The Cv of bursts and gaps are defined as

$$Cv(X) = \sigma_X / \bar{X}, \quad Cv(Y) = \sigma_Y / \bar{Y} \quad (7.7)$$

where σ_X and σ_Y are the standard deviations of burst and gap lengths, respectively. This parameter is a measure of variability with respect to the geometric distribution (which has a coefficient of variation less than or equal to one).

7.4 Modelling frame errors as a Bernoulli process

We analyse the stationarity behaviour of the errored frame sequences by using the Mann-Kendall test. To this end we first split the traces in equal length segments, we compute the mean for each segment, and then we run the stationarity test. We found that, at 0.05 significance level, all the traces pass the stationarity test with a segment length of 1000 samples. The follow statistic will be referred at this segment length.

We examine now the autocorrelation function and the probability mass function associated with the burst and gap lengths.

The autocorrelation function shows that no correlation exists for all the lags evaluated inside each segment. Our samples are then stationary and uncorrelated for lags not longer than 1000 samples.

Figures 7.5 and 7.6 show the probability mass functions of bursts and gaps, with frame error rates categorised in 10% wide intervals.

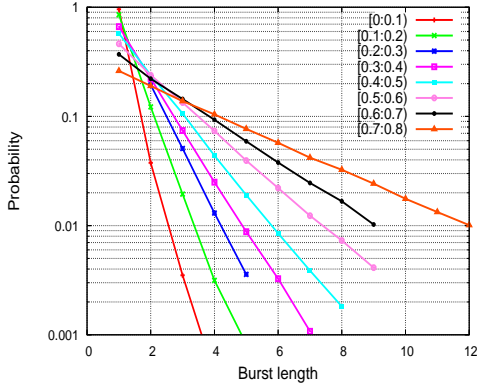


Fig. 7.5. Probability mass function of burst lengths.

Each line in Figure 7.5 represents the burst distribution calculated over intervals listed in the legend. The figures show that the burst and gap length distributions are well approximated by exponentially decaying functions.

All these characteristics are consistent with a Bernoulli error process, that is, samples of the frame error process are i.i.d. random variables with constant probability p of being equal to 1 (frame error) and $1-p$ probability of being 0 (frame correctly received) during short time intervals. Let's now check whether the coefficient of variation for the traces, defined in (7.7), is consistent with a Bernoulli process, for which:

$$\begin{aligned} C_v(X) &= \sigma_X / \bar{X} = \frac{\sqrt{p/(1-p)^2}}{1/(1-p)} = \sqrt{p} \\ C_v(Y) &= \sigma_Y / \bar{Y} = \sqrt{1-p}. \end{aligned} \quad (7.8)$$

For each segment, we computed the frame error rate p , $C_v(X)$, and $C_v(Y)$ then we compared the measured results with the analytical ones in (7.8). The overall means of the relative errors are 0.007 and 0.006 for $C_v(X)$ and $C_v(Y)$, respectively.

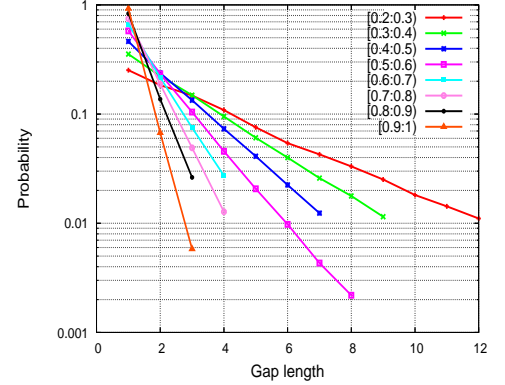


Fig. 7.6. Probability mass function of gaps lengths.

Since it is evident that the distribution of the burst and gap lengths decays linearly when a log-scale is used for the y-axis, suggesting that burst and gap lengths are geometrically distributed, we use the chi-square goodness-of-fit test (Figure 7.7) to provide one more systematic evidence that the distributions are

geometric. We compare the empirical distribution of the burst and gap lengths with an exponential distribution (which is the continuous-valued equivalent of the geometric distribution). The chi-square goodness-of-fit test is used to check whether to reject the null hypothesis that the burst and gap lengths are random variable with the given distribution. The data are divided into k bins and the test is defined as

$$\chi^2 = \sum_{i=1}^k (O_i - E_i)^2 / E_i \quad (7.9)$$

where O_i is the observed value for bin i and E_i is the expected value for bin i . We divided the whole trace in equal segment length, for lengths varying from 100 to 80000. We verified that the null hypothesis is not rejected 90% of times at significance level 5% with a segment length of 1000 samples.

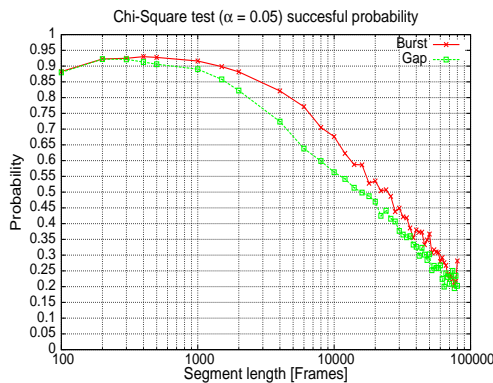


Fig. 7.7. Chi-square test results.

In summary, we can consider the observed frame error process as a Bernoullian process for time spans up to 5 s. For longer time spans, the Bernoulli process is modulated by a slowly-varying process.

7.4.1 AWGN model

We found out that modelling the propagation channel as a simple additive white Gaussian noise channel with perfect synchronisation provides a good

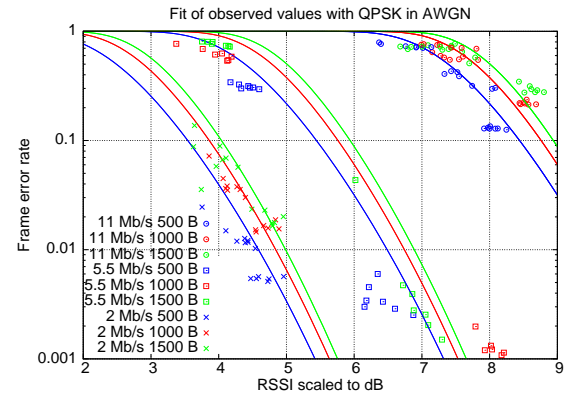


Fig. 7.8. Fit of Equation 7.10 with measured values.

fit with observed results, as shown in Figure 7.8, where observed frame error rate is plotted versus received signal strength indicator (RSSI) plus a constant value found by minimisation of squared log differences. Specifically, the law relating frame error probability p with received power is well approximated by

$$\begin{aligned} p &= 1 - [1 - \exp(R + g_p)]^{S l_p} [1 - \exp(R + g_d)]^{S l_d}, \\ &\text{with } \exp(x) = \frac{1}{2} \operatorname{erfc}(10^{\frac{x}{10}}), \end{aligned} \quad (7.10)$$

where l_p and l_d are the lengths in bytes of the PLCP header and of the MAC data part, respectively; g_p and g_d are the rate gains in dB for the PLCP header and the payload, respectively, which depend on the transmission rate; R is the ratio of chip energy over noise at the receiver in dB, relative to 11 Mb/s rate.

Header and data lengths are summarised in Table 7.1. Rate gains relative to the 11 Mb/s data rate are obtained from [17, 18, 19]; header lengths include 8 bytes of LLC+SNAP headers; g_p for rates of 2, 5.5 and 11 Mb/s are given for long (short) preambles.

7.4.2 Practical usage

As far as the value of R in (7.10) is concerned, it must account for the path loss computed using (7.3), plus an offset accounting for transmission power, antenna gain depending on orientation and type, internal noise of the receiver,

Table 7.1. Rate-dependent parameters in Equation 7.10.

Bit rate	l_p [byte]	l_d [byte]	g_p [dB]	g_d [dB]
1 Mb/s	6	36 + payload	+7.9	+7.9
2 Mb/s	6	36 + payload	+7.9 (+4.9)	+4.9
5.5 Mb/s	6	36 + payload	+7.9 (+4.9)	+3.0
11 Mb/s	6	36 + payload	+7.9 (+4.9)	0
6 Mb/s	3	38 + payload	+5	+5.0
9 Mb/s	3	38 + payload	+5	+3.5
12 Mb/s	3	38 + payload	+5	+1.9
18 Mb/s	3	38 + payload	+5	-0.6
24 Mb/s	3	38 + payload	+5	-3.8
36 Mb/s	3	38 + payload	+5	-7.1
48 Mb/s	3	38 + payload	+5	-11.5
54 Mb/s	3	38 + payload	+5	-12.8

and other possible sources of noise like scattering due to obstacles near the antennas. Let us define a reference scenario, consistent with our measurements and the receiver sensitivity as defined in IEEE 802.11. We consider two stations placed at 1 m height from ground that transmit a sequence of frames containing a 1024 bytes MPDU (MAC protocol data unit) at 11 Mb/s, with a frame error rate of 8% at 200 m. Given the frame length, the rate and the frame error rate, from (7.10) we obtain $R = 9.6$ dB.

2RM is practically coincident with the -40 dB/dec asymptote for distances greater than the break point defined in (7.2). 200 m is farther than the break point when the height from the ground of equal-height nodes is less than 1.4 m, which is consistent with our previous assumptions. We can thus approximate L_d given by (7.3) with

$$L_d = 20 \log_{10} \left(\frac{4\pi h_t h_r}{\lambda d^2} \right)$$

which, for $d = 200$ m, gives $L_d = -51.9$ dB. This gives us the relationship in dB $R = L_d + 61.5$.

More generally, the value of R in Equation (7.10) should be set to

$$R = L_d + 61.5 + \Delta L \quad (7.11)$$

where ΔL is a value in dB that accounts for different transmission power, receiver sensitivity, gain of transmitting and receiving antennas, long-term instability of the receiver and possibly near-field scattering. The value of ΔL observed in our experiments varies between -2.3 dB and +3.4 dB. We attribute this variability to small changes in antenna pointing from one measurement to the next, to slightly different positioning of the laptop on the small table we used, leading to different scattering in the vicinity of antennas, and to a slow oscillation of received power level that we can observe with a period of about 20 minutes, which may be the effect of thermal instability within the PCMCIA cards.

References

1. H. H. Xia, H. L. Bertoni, L. R. Maciel, A. Lindsay-Stewart, and R. Rowe, "Radio propagation characteristics for line-of-sight microcellular and personal communication," *IEEE Transactions on Antennas Propagation*, vol. 41, pp. 1439–1447, Oct. 1993.
2. A. J. Rustako, N. Amitay, G. J. Owens, and R. S. Roman, "Radio propagation at microwave frequencies for line-of-sight microcellular mobile and personal communications," *IEEE Transactions on Vehicular Technology*, vol. 40, no. 1, pp. 203–210, Feb. 1991.
3. R. Jakoby and U. Liebenow, "Modeling of radiowave propagation in microcells," in *proc. ICAP'95*, Apr. 1995.
4. J. Broch, D. A. Maltz, D. B. Johnson, Y.-C. Hu, and J. Jetcheva, "A performance comparison of multi-hop wireless ad hoc network routing protocols," in *Mobile Computing and Networking*, 1998, pp. 85–97.
5. G. Anastasi, E. Borgia, M. Conti, and E. Gregori, "Wi-Fi in ad hoc mode: a measurement study," in *proceedings of the IEEE International Conference on Pervasive Computing and Communications (PerCom)*, Mar. 2004, pp. 145–154.
6. D. Aguayo, J. Bicket, S. Biswas, G. Judd, and R. Morris, "Link-level measurements from an 802.11b mesh network," in *SIGCOMM '04: Proceedings of the 2004 conference on Applications, technologies, architectures*, vol. 34, no. 4, October 2004, pp. 121–132.
7. D. Dhoutaut and I. Guérin-Lassous, "Experiments with 802.11b in ad hoc configurations," in *14th IEEE International Symposium on Personal, Indoor and Mobile Radio Communications*, Beijing, China, Sept. 2003, pp. 1618–1622.
8. D. L. Mills, "Internet time synchronization: the network time protocol," *IEEE Transactions on Communications*, vol. 39, pp. 1482–1493, Oct. 1991.
9. "http://www.tcpcdump.org."
10. M. Yarvis, K. Papagiannaki, and W. S. Conner, "Characterization of 802.11 wireless networks in the home," in *proc. of 1st workshop on Wireless Network Measurements (WiNMe)*, Apr. 2005.
11. D. Kotz, C. Newport, R. S. Gray, J. Liu, Y. Yuan, and C. Elliott, "Experimental evaluation of wireless simulation assumptions," in *MSWiM '04: Proceedings of the 7th ACM international symposium on Modeling, analysis and simulation of wireless and mobile systems*, Venezia (IT), Oct. 2004, pp. 78–82.

7.5 Recommendations for simulation practitioners

The most commonly used propagation models in ns-2 suffer from significant inaccuracies. First, they neglect the received power "hole" that may prevent reception at about 15 m distance outdoor. Second, they do not consider slow power level random variations. Third, they use a threshold receiving power for deciding whether a frame is correctly received.

For a generic simulation we recommend using (7.10), using the parameters listed in Table 7.1 and a value for R computed as in Equations (7.11) and (7.3). For ϵ_r we recommend a value of 15, and the use of vertical polarisation, which is both commonly used and the worst case. A value of ΔL set to 0 dB means a range of 200 m at 11 Mb/s. If one wants to simulate a receiver with a better/worse sensitivity, ΔL should be increased/decreased by the corresponding dB value. Alternatively, if one wants to increase the range by a factor α , they should set $\Delta L = 40 \log_{10}(\alpha)$. A program for computing the packet loss probability using the described criteria is available at <http://wnet.isti.cnr.it/software/wifiper.m>.

A Gaussian fading process with 1 Hz bandwidth and -5 dB standard deviation power should be superimposed to the received power, especially for simulation involving still nodes and dynamic rate switching. As shown in [14], attenuations up to 10 dB for each antenna due to pointing are reasonable assumptions. This means that each node should define a suitable attenuation value with respect to each other by reducing ΔL for anything but a perfect pointing. For moving nodes, this attenuation should be made a time-varying random variable depending on the mobility model.

12. C. Reis, R. Mahajan, M. Rodrigo, D. Wetherall, and J. Zahorjan, "Measurement-based models of delivery and interference in static wireless networks," *SIGCOMM Comput. Commun. Rev.*, vol. 36, no. 4, pp. 51–62, 2006.
13. E. Green and M. Hata, "Microcellular propagation measurements in an urban environment," in *proc. PIMRC*, Sept. 1991.
14. C. Criminisi, "Caratterizzazione sperimentale del comportamento elettromagnetico di NIC 802.11b," Master's thesis, University of Palermo (IT), 2004.
15. T. S. Rappaport, *Wireless Communications*, 2nd ed. Upper Saddle River, NJ (US): Prentice-Hall, 2002.
16. C. Soras, M. Karaboikis, G. Tsachtsiris, and V. Makios, "Analysis and design of an inverted-F antenna printed on a PCMCIA card for the 2.4 GHz ISM band," *IEEE Antenna and Propagation Magazine*, vol. 44, Feb. 2002.
17. C. Heegard *et al.*, "High performance wireless ethernet," vol. 39, no. 11, pp. 64–73, Nov. 2001.
18. C. Heegard, "Range versus rate in IEEE 802.11g wireless local area networks," presented in September meeting IEEE 802.11 Task Group G, Sept. 2001. [Online]. Available: <http://www.nativei.com/heegard/papers/RvR.pdf>
19. W. Camey, "Ieee 802.11g: new draft standard clarifies future of wireless LAN," Texas Instruments, Tech. Rep., 2002, white paper.

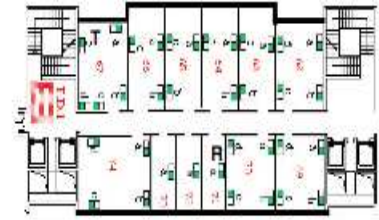


Fig. 8.1. Plant of the building where the measurements have been taken; T and R are the transmitter and receiver laptops used for the measurements.

Indoor

Indoor channels are highly dependent upon the placement of walls and partitions within the building. As placement of these walls and partitions dictates the signal path inside a building. In such cases, a model of the environment is a useful design tool in constructing a layout that leads to efficient communication strategies. To achieve this aim, a channel model of an indoor environment must be applied to various layout plans of offices which will lead to the characterization of design methodologies.

A channel model is useful in determining the mechanisms by which propagation in the indoor environment occurs, which in turn is useful in the development of a communication system. By examining the details of how a signal is propagated from the transmitter to the receiver for a number of experimental locations, a generic model may be developed that highlights the important characteristics of a given indoor environment. Generic models of indoor communications can then be applied to specific situations to describe the operation of a radio system, and may also be used to generate designs that are particularly suited to supporting radio communication systems.

In this chapter we describe a preliminary results of a measurement campaign carried out in the research institute ISTI in Pisa (IT). Figure 8.1 depicts the arrangement of the relevant area of the building, at the first floor, where thin concrete walls delimit the rooms. The dashed line represents the shortest radio path between the sender and the receiver (about 15 meters). Even if we carried out an extended measurements campaign, in this dissertation we present only one, because all data trace showed the same characteristics. The measurements are done with a flow of 1000-byte frames spaced by 50 ms, at a fixed 11Mb/s rate with fragmentation and retransmission disabled.

This chapter is subdivided in two main section; Section 8.1 address the main frame level statistics, while section 8.2 focuses on presents the results obtained at bit level.

8.1 Frame level statistics

Figures 8.2 8.3 and 8.4 show the trend of received frames (green line), lost frames (red line) and corrupted frames (blue line). Each points are obtained averaging 1200 frames. These Figures show that exist three different state characterized by a different variance, for instance the Figure 8.2 clearly represent this concept during Wednesday, Thursday and Sunday. The rapidly changing quality of the wireless channel is probably owing to persons during the working hours, but even it is due to portable computer, doors and so forth that, during the measures, change one's place. Generally speaking the presence of working persons may change the frame error rates partly because they cause an environment variation and therefore a change of fading and the multipath conditions.

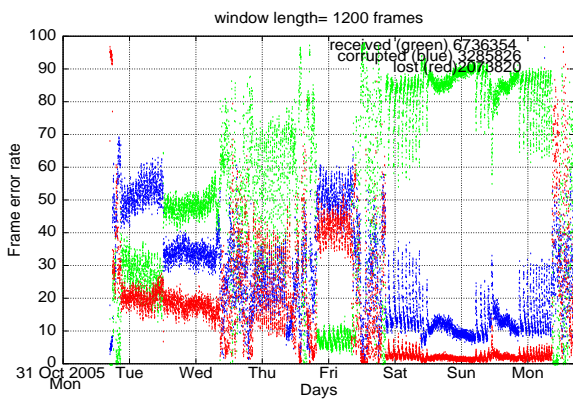


Fig. 8.2. Average of received, lost and corrupted frames during the first week.

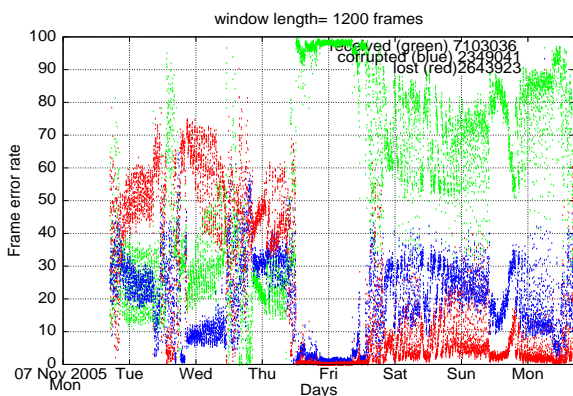


Fig. 8.3. Average of received, lost and corrupted frames during the second week.

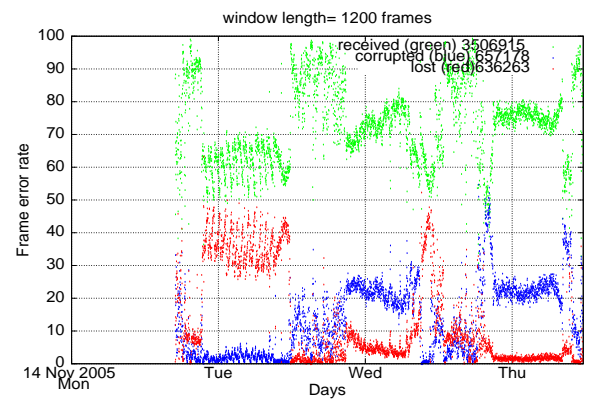


Fig. 8.4. Average of received, lost and corrupted frames during the third week.

Figures 8.5 and 8.6 show the probability mass functions of burst and gap, for the entire trace. Figure 8.5 shows that the burst length distribution is well approximated by a straight line function in log-log scale. While the gap length distribution in Figure 8.6 can not be approximate by it.

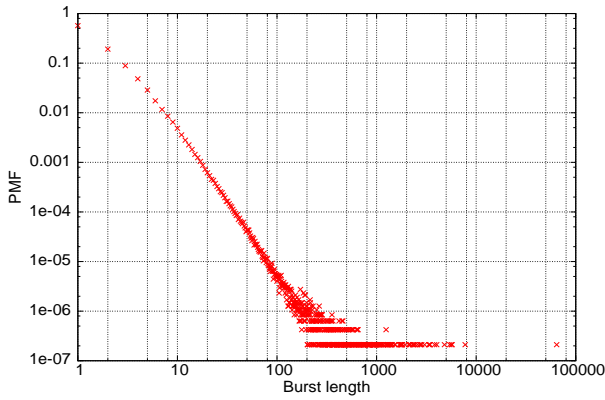


Fig. 8.5. Probability mass function of burst length at frame level.

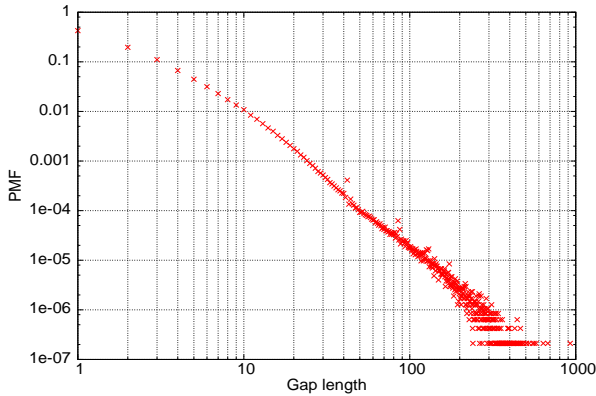


Fig. 8.6. Probability mass function of gap length at frame level.

8.2 Bit level statistics

In order to investigate the bit error statistics in the indoor environment we use a modified card driver that does not discard frames received with a bad CRC, and our receiver program which is then able to log bit corruptions by comparing expected with received bits.

Figure 8.7 shows the gap distribution, this distribution is probably due to the Complementary Code Keying standardized in IEEE802.11. In fact by analysing this distribution we verified that the gap distribution is obtained by adding 8 curves with the same amplitude but with a different phase.

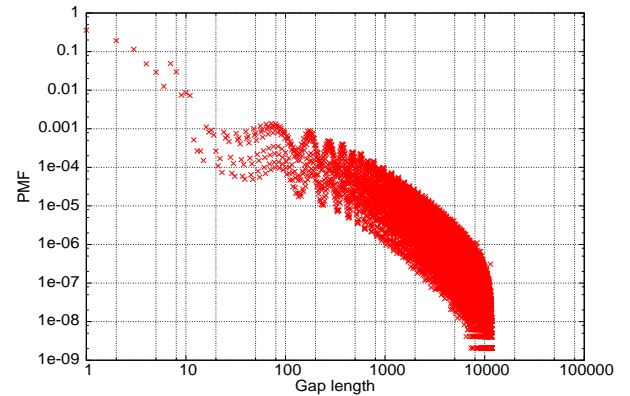


Fig. 8.7. Probability mass function of gap length at bit level.

Figure 8.8 shows the burst distribution at bit level, we can observe that the probability to have a burst length equal to 8 is 10^{-3} .

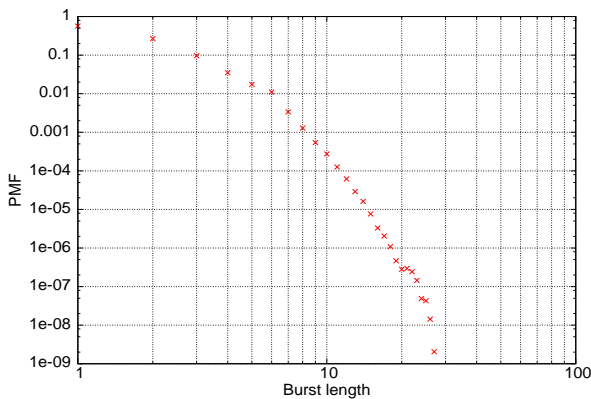


Fig. 8.8. Probability mass function of burst length at bit level.

An important statistic is the number of errored bits per frame. Because of fading and multipath conditions wireless channels have error rates that are typically around 10^{-2} ; however, most applications require that the error rates be significantly smaller (in most case 10^{-5} or less). In addition to the poor channel quality, the design of wireless frame system is complicated by the rapidly changing quality of the wireless channel. It is therefore crucial that appropriate error control protocols be developed that are well suitable to the application being supported. Many paper [2, 3, 4] describe a FEC technique in order to increase the performances in a multicast wireless networks, or an ARQ technique in a unicast wireless networks (already implemented in IEEE802.11). These mechanisms are often combined (Hybrid ARQ mechanisms) by using an acknowledgments to adjust the quality of redundancy of FEC codes [1]. In section 2.2 we have shown that the video quality is acceptable when using a frame redundancy greater than 30%. Figure 8.9 show that using a bit redundancy equal to 1.25% (100 bits in 1000 bytes) we can recovery 90% of frames corruption. By using this information, the gap and the burst distribution, we can evaluate what type of codes can be more appropriate in order to improve the quality of the communication channel.

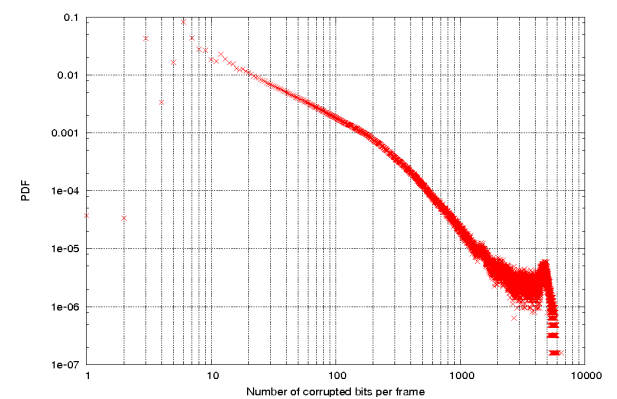


Fig. 8.9. Probability mass function of number of errored bits per frame

References

1. S. Lin and D. Costello, "Error Control Coding: Fundamentals and Applications," Prentice-Hall, Englewood Cliffs, NJ, 1983.
2. P. K. McKinley and S. Gaurav, "Experimental evaluation of forward error correction on multicast audio streams in wireless LANs," in Proceedings of ACM Multimedia 2000, (Los Angeles, California), pp. 416-418, November 2000.
3. J. Nonnenmacher, E. W. Biersack, and D. Towsley, "Parity-based loss recovery for reliable multicast transmission Networking," IEEE/ACM Transactions on, Volume: 6 Issue: 4, Aug. 1998 Page(s): 349-361.
4. P. Chumchu and A. Seneviratne, "Adaptive Packet Level Redundancy Mechanisms for Reliable Mobile Multicast: Proposed Architecture and Performance Analysis," in The First International Conference on Information Technology and Applications (ICITA 2002), 2002.

9

Packet loss model for TCP hybrid wireless networks

In this chapter, we concentrate on frame error models targeted to TCP-based applications, for which the combination of high, correlated packet loss and high latency may cause very bad performance. Since TCP interprets packet loss as a sign of congestion, thus slowing its pace to avoid worsening the network conditions, frame errors due to corruption causes decreased throughput, even in the absence of network congestion. Various techniques exist that tackle this problem [4], but no definitive answers yet. This is consequently a widely studied research topic, often by means of simulations, for a variety of reasons, related partly to the usual simulation advantages, such as repeatability, ease in changing the problem's parameters and statistical significance, and partly to the peculiarities of the environment, namely the fact that satellite links are expensive and not widely available, especially for high bit rates.

A complete packet error model requires three levels of operation: a frame error model at the raw channel level, an implementation of the Wi-Fi ARQ (automatic retransmission) mechanism, and an implementation of the vendor-dependent speed switching mechanism. The first level gives a synthetic statistical representation of the frame error process on the raw channel due to one of two effects: bad preamble acquisition and, for correctly acquired frames, bad CRC due to corrupted bits in the MAC protocol data unit. The second level implements the ARQ mechanism defined in the IEEE 802.11 standard, by which a transmitter retries sending a frame up to a configurable number of times – typically 7 – when it does not receive an acknowledgement for the frame sent. The third level implements an adaptive modulation and coding scheme, by which the sender may choose to switch to a different transmission speed when the perceived channel conditions change. This study tackles the first two levels out of the three that are required for a complete packet error model. It aims at choosing an adequate statistical model for the raw channel frame error by studying how TCP behaves on a fixed-speed channel with ARQ.

9.1 Link Characteristics

In the proposed hybrid scenario, two links with very different characteristics are traversed by the TCP flow. Each link, from the point of view of TCP, is defined by four characteristics:

- capacity, which is the available rate seen at the IP level;
- latency, that is the time a packet takes to traverse the link;
- buffer size, which is the size of the buffer that a router or bridge uses to store packets waiting to be sent on the link;
- segment error, which is a description of the process causing segment drops due to link errors.

9.1.1 Satellite link

As far as the capacity is concerned, we considered a 2 Mb/s link, which is a common commercial figure.

As far as the delay is concerned, the geostationary channel introduces a signal delay of around 250 ms, the exact number depending on the satellite's position with respect to the earth stations. To this, one should add the processing delays at the earth stations due to segmentation, interleaving, coding, and the reverse operations at the receiver's side. When TDMA schemes are used, there is delay due to the frame structure, and possibly delay due to dynamic allocation. Moreover, there are processing delays at the routers, so any latency not smaller than 300 ms is a reasonable assumption.

The routers at the earth stations have buffers on the incoming terrestrial interfaces, where traffic is stored prior to sending on the satellite link. This is necessary for TDMA systems, where packets must wait for the first opportunity to be transmitted, is used by dynamic allocation methods where the allocation can be based on traffic backlog at the earth stations, and is generally useful for absorbing traffic rate fluctuations. From the TCP point of view, moreover, the buffer has the important role of allowing complete utilisation of the link capacity. In fact, it can be shown that the channel can be fully used only if no errors are present and the buffer size is at least equal to $C \cdot RTT$, where C is the channel capacity and RTT is twice the link latency. We set the buffer in our experiments to exactly the said value, that is, 150 kB.

Geostationary satellite links are commonly depicted as AWGN channels, that is, affected by additive white Gaussian noise. In fact, given the extremely small antenna aperture, the high pointing precision and the absence of mobility, the only relevant noise at the receiver is the thermal noise, which gives rise to uncorrelated bit corruption and, in turn, to uncorrelated frame errors with constant probability; for this reason, in clear sky, we assume a Bernoullian channel, sometimes called a Poisson channel.

In this section, we neglect the issues related to signal fading due to variable atmospheric conditions, which would require a different treatment, and assume a satellite channel with a FER (Frame Error Rate) of 10^{-5} which, for our

purpose, is the same as errorless, because it is about the same FER which is caused by congestion [5]. This figure is consistent with measurements done on a recent Skyplex-based satellite system [6].

9.1.2 Wi-Fi link

Wi-Fi links comply with the IEEE 802.11 [1] standard, which has provisions for ACM (Automatic Coding and Modulation). ACM, which we call speed switching, is widely implemented in commercial Wi-Fi devices, but the algorithm for choosing which speed to adopt is not defined by the standard and still the subject of research. In this section we analyse the behaviour of TCP with different frame error traces at a fixed Wi-Fi nominal rate of 11 Mb/s. Our experiments show that real network cards behave as the standard dictates with very little error [3]. Computations based on the standard give a capacity of 5.3 Mb/s for a unidirectional flow of 1000-data byte packets, long preambles, no fragmentation and RTS/CTS disabled [7].

Our experiments show a latency produced by the driver and hardware around 1 ms, plus delays due to retransmissions greater than 50 ms in less than 0.1% of packets. From the TCP point of view, these delays are not significant, so we considered the latency of the Wi-Fi link as null.

The link buffer has no influence on the TCP dynamics, as long as it can keep few back-to-back segments, because the bottleneck is on the satellite link. Any buffer size greater than four packets' worth would yield the same results.

As far as the error model is concerned, this is the topic of Section 9.4. Measurement traces and synthetic traces were used, and an ad hoc error model was developed for ns-2 called Ttem (time trace error model). Using this error model, we were able to emulate a Wi-Fi channel affected by noise, where the state of the channel (good or bad) is described by a trace file containing a 0 for a good interval where no error happens and a 1 for a bad interval where a frame is corrupted; we made measurements at 5 ms long intervals. The Ttem error model keeps into account the IEEE 802.11 ARQ algorithm, but no speed switching. Ttem, as a patch to ns-2.29, is available at <http://wnet.isti.cnr.it/software/ttem> as free software, in order to make it possible for everyone to check, use and modify it.

9.2 Measurements environment

This section compares simulation done using real traces of frame errors on a raw (before ARQ) Wi-Fi channel with synthetic traces of frame errors produced by commonly used models.

We performed a comprehensive measurement campaign [2] using laptops with standard Wi-Fi interfaces configured in ad hoc mode, at different fixed

speeds of 1, 2, 5.5 and 11 Mb/s, fragmentation disabled, retransmission disabled, for different distances in different environments: open air, far from buildings, and office environment with varying numbers of thin walls between the laptops. We used custom software for sending the frames at precisely controlled time intervals and to receive them while registering the signal strength of received frames and the occurrences of lost frames, and we obtained traces of frame losses of various lengths and at different time resolutions.

The traces that are considered for this work are obtained in the research institute ISTI in Pisa (IT), an office building. Fig.9.1 depicts the arrangement of the relevant area of the building, at the first floor, where thin concrete walls delimit the rooms.

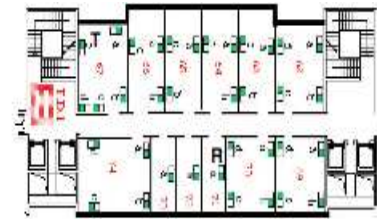


Fig. 9.1. Plant of the building where the measurements have been taken; T and R are the transmitter and receiver laptops used for the measurements.

The transmitter and receiver are two laptops equipped with a Debian GNU/Linux operating system. The transmitter sends a flow of 1000-byte unicast frames spaced by 5 ms, at a fixed 11 Mb/s rate with fragmentation and retransmission disabled. The receiver checks the sequence number inside the frames and keeps a trace of the lost ones. Since the channel occupancy of a frame is about 1.2 ms, this kind of measure traces the indoor channel conditions quite accurately.

9.3 Commonly used packet error models

The most common model used to model frame error on a Wi-Fi channel is the Bernoullian process, that is, an error process where each frame experiences the same fixed probability of being corrupted, and frame losses are independent from each other [7, 8]. The main attractiveness of this model is its simplicity and its mathematical tractability. Only one parameter is needed to define

it, usually the mean error probability p . A Bernoullian frame error model generates burst of consecutive frame errors (error bursts) whose length is geometrically distributed with mean equal to $1/(1-p)$. The distance between two bursts, that is, the gap length, is geometrically distributed as well, with mean equal to $1/p$.

A slightly more complex model defines the channel as being in one of two states, namely a good state where all frames are successfully received and a bad state where all frames are lost because of corruption [10, 11]. The mathematical modelling of this channel is done via a two-state Markov chain, usually referred to as a Gilbert or Gilbert-Elliott model. In fact, both the Gilbert model [12] and the Elliott model [13] are more complex, the first requiring three parameters and the second requiring four. This is why we refer to the simple good-bad model as a bistable model, where the probability of going from the good to the bad state is b and the probability of going from the bad to the good state is g . The stationary probabilities of being in the good and bad states are $P_g = g/(b+g)$ and $P_b = b/(b+g)$, respectively; P_b is also the mean frame error probability. The mean durations of the good and bad states are $1/b$ and $1/g$, respectively; this means that the channel exhibits error bursts of consecutive ones, whose mean length is $1/g$, which are separated by gaps of consecutive zeros whose mean length is $1/b$. Both burst and gap lengths have geometric distributions.

The models mentioned have no long-range memory: the Bernoullian process is memoryless, while the bistable process has memory limited to the previous state. As a consequence, both models have geometrically decaying correlations. However, the frame error traces we measured exhibit remarkably different statistics, which is the main ground for this investigation. As an example, we show a plot of the error gap distribution, a statistic originated with classical studies about bit-level models for telephone wires [12], and that may be significant in the context of TCP, where the length of error-free periods has a role as far as the goodput is concerned. The error gap distributions observed in the measured traces exhibit long polynomial tails, a peculiar trait that is not shared with commonly used models: both Bernoullian and bistable models produce error gap distributions with geometrically decaying tails, as depicted in Fig. 9.2 for the case of a Bernoullian synthetic trace.

9.4 TCP on synthetic versus measured packet loss

Even if the real traces exhibit significant statistical differences with respect to the Bernoullian and bistable models, choosing a model for simulation purposes need not be done on the basis of statistical similarity with the real process that is simulated, rather it should be done on the basis of how well the model behaves with respect to the intended purpose of the simulation. Therefore, it may well happen that a simple channel frame error model whose behaviour is

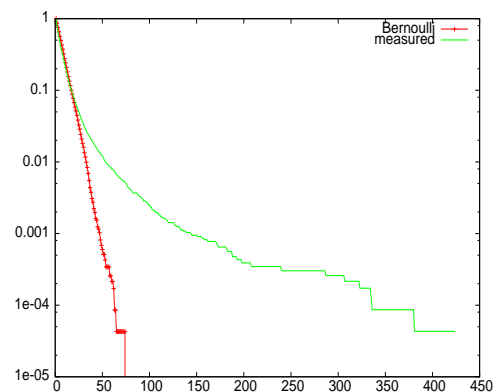


Fig. 9.2. Error gap length distributions for one observed frame error trace and a synthetically generated Bernoulli trace with the same average frame error rate.

apparently very different from the real packet error process is well suited for simulation in a given environment.

To this aim, we examined how well the two simple channel error models mentioned above perform, when used in modelling the behaviour of TCP in hybrid networks, by using the ns-2 simulator with the Ttem error model, which reads a trace of the channel state, applies the IEEE 802.11 ARQ algorithm and discards packets that cannot be received after a given number of retries, 7 in our case. The performance measure considered is the goodness of fit of a graph of single-connection TCP goodput versus mean frame error rate on the raw channel (before ARQ). We compare the goodput obtained with synthetic Bernoulli and bistable models to the goodput obtained using measured traces in the above-depicted indoor scenario.

First of all, we validate our simulation scenario by comparing Padhie's formula [14] with the results obtained with a synthetic Bernoulli trace. Padhie's formula quite accurately models the behaviour of a single TCP connection on a fixed-bandwidth link with uncorrelated segment losses due to either congestion or corruption, neglecting losses on the return channel and considering no link buffer. To compare the simulation's results with Padhie's formula, we run 10 instances of a single TCP connection for 2000 seconds, discarded the first 200 seconds to comply with Padhie's steady-state assumption, and considered the mean RTT, RTO and forward segment error rates of the 10 runs for frame error rates ranging from 2% to 30%. As shown in Figure 9.3, the median values

of the goodput over 10 ns-2 runs and Padhie's formula have a good agreement in the high error region, where the link buffer is mostly empty, while Padhie underestimates the goodput in the low error region, where the buffer influence becomes important.

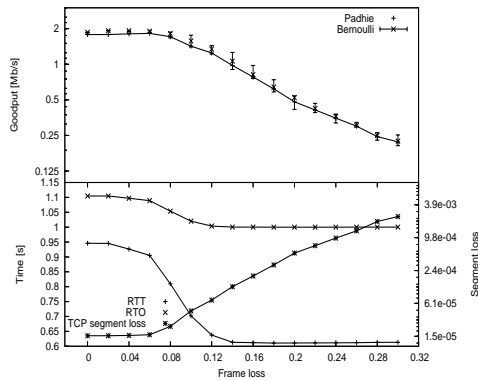


Fig. 9.3. Goodput as computed with Padhie's formula and with a trace with Bernoullian frame error.

We then made the comparison that is the aim of this section. Taking the steady-state TCP single-connection goodput as a performance measure, we see how well different statistical models fit the measured frame error traces. We consider four different models in addition to the real traces, as shown in Table 9.1.

Table 9.1 is worth some comments. When using a Bernoulli process, which is defined by a single parameter, fitting it to observed data means choosing a significant statistical parameter of the observed data. The choice of such a parameter is not obvious. In our case, the simplest choice of a parameter is the mean FER. However, there are some good reasons why choosing a different parameter could be wiser. One candidate as an alternative to the FER is the mean burst length, an important parameter with respect to ARQ performance: the longer the error bursts, the higher the probability that ARQ cannot recover a lost frame. Another candidate is the mean gap length, which is related to TCP performance. As it is observed in [15], TCP performance is higher for higher burstiness of the segment error process, because the congestion window

Table 9.1. Traces used in the simulation experiment.

(a)	Bernoulli process having the same frame error rate as the real traces
(b)	Bernoulli process having the same mean burst length as the real traces
(c)	Bernoulli process having the same mean gap length as the real traces
(d)	bistable process having the same frame error rate, mean burst length and mean gap length as the original traces
(e)	the real traces

has a higher probability of becoming big if gaps are long. In fact, the measured error process has both longer bursts and longer gaps than a Bernoulli process with the same FER.

In Fig. 9.4, the goodput is plotted versus the frame error rate of the real traces.

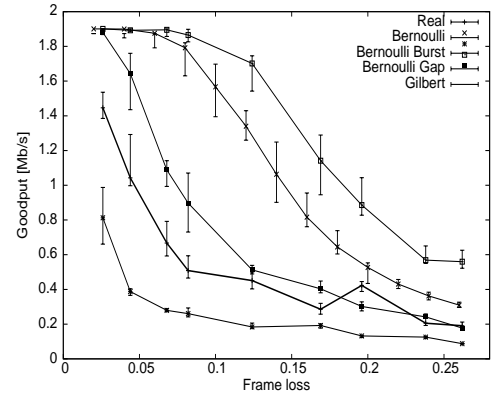


Fig. 9.4. TCP goodput versus frame error rate of real traces for different error models.

First of all, it is clear that (a), the simplest process, does not adequately model TCP's goodput at different frame error rates: the goodput with (a) is at least twice the one of (e); moreover, the behaviour is different, as (e)

is convex, while (a) is not. Using the mean burst length as the parameter of interest gives the same behaviour as the real traces, as it can be seen by comparing (b) with (e), but the values are very different. As discussed above, this observation is a hint that the behaviour of ARQ is dominant in the chosen performance measure, that is, the TCP goodput. Apparently, the gap length, on the other hand, is much less important, as using it as the parameter for tuning the Bernoulli process does not yield satisfactory results: the trace for the (c) case is the one farthest from (e). One reason could be that, as shown in Fig. 9.2, the distribution of gap lengths in the real process has a polynomial, rather than exponential, tail implying that a Bernoulli process with the same mean gap length as the real traces has a lower FER than that of the real traces.

We considered until now a model with a single parameter. With the bistable model, we have two parameters, hence a greater flexibility. The three statistics of mean frame error rate, mean burst length and mean gap length are related, so they are defined by only two parameters, which implies that they can be simultaneously fitted using the bistable model. In fact, the bistable model fits the chosen performance measure best: the plot of (d) is nearest to (e), while still a considerable distance away.

9.5 Conclusion

When choosing a model for the frame error rate process on a Wi-Fi channel, measurements coupled with simulation experiments using ns-2 show that none of the simplest models can be used to obtain an accurate estimate of the TCP goodput. Neither the Bernoulli process nor the good-bad bistable process with two parameters (sometimes referred to as Gilbert-Elliott process) are adequate when the main statistics of FER, mean burst length and mean gap length are considered.

This conclusion implies that more work is needed in this area, in order to provide researchers and simulation practitioners with reliable models for the frame error process at the channel level. The first direction of investigation should be directed to considering whether the simple Bernoulli or bistable processes could be used for TCP performance evaluation, by choosing parameters different from the FER and the mean burst or gap lengths. Should this turn out to be infeasible, the research should be directed to different, possibly more complex error models. Similar research methods should be used for estimating performance measure other than TCP's goodput, such as audio or video performance, ARQ performance or Wi-Fi channel capacity.

One thing that is conspicuously missing from the above analysis is the speed switching behaviour of the Wi-Fi interface. In order to model this behaviour, one would need channel measurements done at different speeds in different conditions in addition to choosing a speed switching algorithm, whose

behaviour would greatly influence the performance measure under study, and that could itself be the object of research.

One more extension of this work could be considering the frame error process caused by atmospheric fading on the satellite channel, in addition to the one relative to the Wi-Fi channel.

References

1. IEEE Std 802.15.1-2002 IEEE Std 802.15.1 IEEE Standard for Information technology - Telecommunications and information exchange between systems - Local and metropolitan area networks - Specific requirements Part 15.1: Wireless Medium Access Control (MAC) and Physical Layer (PHY) Specifications for Wireless Personal Area Networks (WPANs).
2. A. Annese, P. Barsocchi, N. Celandroni, and E. Ferro, "Performance evaluation of UDP multimedia traffic flows in satellite-WLAN integrated paths", proceedings of 11th Ka Band Utilization Conference, Rome, September 2005.
3. Gabriele Oligeri, "Misura e caratterizzazione di un canale Wi-Fi", <http://fly.isti.cnr.it/didattica/tesi/Oligeri-Finotti/Oligeri.pdf>.
4. M. Allman, S. Dawkins, D. Glover, J. Griner, T. Henderson, J. Heidemann, S. Ostermann, K. Scott, J. Semke, J. Touch and D. Tran, "Ongoing TCP research related to satellites", IETF, RFC 2760, February 2000.
5. N. Celandroni and F. Potort, "Maximising single connection TCP goodput by trading bandwidth for BER", International Journal of Communication Systems, Vol. 16, No. 1, pp. 63-79, February 2003. Special issue on Wireless Access to the Global Internet: Mobile Radio Networks and Satellite Systems.
6. D. Adami, S. Giordano, M. Pagano, and R. Secchi, "Modeling the Behavior of a DVB-RCS Satellite Network: an Empirical Validation", proceedings of the International Working Conference on Performance Modelling and Evaluation of Heterogeneous Networks, Ilkley (UK), July 2005.
7. J. Jun, P. Peddabachagari, M. Sichiitiu, "Theoretical Maximum Throughput of IEEE 802.11 and its Application", Second IEEE International Symposium on Network Computing and Application (NCA'03), Cambridge (US), April 2003.
8. Z. Tang, Z. Yang, J. He and Y. Liu, "Impact of bit errors on the performance of DCF for wireless LAN", proceedings of the IEEE conference on Communications, Circuits and Systems, vol. 1pp. 529-533, 2002.
9. P. Chatzimisios, A. C. Boucouvalas and V. Vitsas, "Performance analysis of IEEE 802.11 DCF in presence of transmission errors", proceedings of the IEEE International Conference on Communications (ICC 2004), vol. 7, pp. 3854-3858, June 2004.
10. Michele Zorzi, Ramesh R. Rao, and Laurence B. Milstein, "On the accuracy of a first-order Markov model for data transmission on fading channels", Proceedings of the International Conference on Universal Personal Communications, pp. 211-215, November 1995.
11. B. P. Crow, I. Widjaja, J. G. Kim and P.T. Sakai, "IEEE 802.11 wireless local area networks", IEEE Communications Magazine, vol. 35, no. 9, pp. 116-126, 1997.
12. E.N. Gilbert, "Capacity of a burst-noise channel", The Bell System Technical Journal, No. 39, pp. 1253-1265 September 1960.
13. E. O. Elliott, "Estimates of error rates for codes on bursty-noise channels", Bell System Tech. J., 42(9):1977, September 1963.
14. J. Padhie, V. Firoiu, D.F. Towsley, and J.F. Kurose, "Modeling TCP Reno performance: a simple model and its empirical validation", IEEE/ACM Trans. Networking, vol. 8, pp. 133-145, April 2000.
15. E. Altman, K. Avrachenkov, C. Barakat, "A stochastic model of TCP/IP with stationary random losses", Computer Communication Review, Vol.30, No.4, October 2000, pp. 231-242.